DESIGN AND DEVELOPMENT OF EFFICIENT METHODS FOR HISTOPATHOLOGICAL IMAGE ANALYSIS

A Thesis Submitted
In Partial Fulfillment of the Requirements for the
Degree of

DOCTOR OF PHILOSOPHY

in
Computer Science and Engineering
by

RAVI SHARMA
(2K17/PHDCO/08)

Under the Joint Supervision of

Dr. Kapil Sharma
Professor
Information Technology
Delhi Technological University

Dr. Manju Bala
Assoc. Professor
Computer Science
I.P. College of Women

Department of Computer Science and Engineering

DELHI TECHNOLOGICAL UNIVERSITY
(Formerly Delhi College of Engineering)
Shahbad Daulatpur, Main Bawana Road, Delhi-110042. India

May 2025

ACKNOWLEDGENTS

I express my deep gratitude to my supervisors, **Dr. Kapil Sharma** and **Dr. Manju Bala.** Their precise and lucid thoughts have helped me to manage many responsibilities comfortably. They not only encouraged me to work but also gave their guidance, experience, constructive thoughts, and took a keen interest throughout the work and preparation of the manuscript, which has made me worth that I claim to be now. Working with them made me more independent and liable, which I believe is the most important aspect in anyone's career. I am indebted to them more than they recognize. I sincerely thank **Dr. Manoj Kumar**, Head of the Department of Computer Science, for their support and guidance. Your leadership has been instrumental to my research journey. Also, I would like to express my sincere gratitude to **Prof. Pratik Sharma**, the Honorables Vice Chancellor of Delhi Technological University, for fostering an environment of academic excellence and research innovation. Your leadership and unwavering commitment to advancing scholarly pursuits have been a constant source of inspiration throughout my doctoral journey. I am truly grateful for the opportunities and support provided by your administration.

And above all, I am blessed by Lord Shri Salasar Balaji Maharaj for giving me the strength and perseverance to toil towards this accomplishment without any hardships.

Candidate's Signature

DELHI TECHNOLOGICAL UNIVERSITY
(Formerly Delhi College of Engineering)
Shahbad Daulatpur, Main Bawana Road, Delhi-42

CANDIDATE'S DECLARATION

I **Ravi Sharma** hereby certify that the work which is being presented in the thesis entitled **Design and Development of Efficient Methods for Histopathological Image Analysis** in partial fulfillment of the requirements for the award of the Degree of Doctor of Philosophy, submitted in the Department of **Computer Science and Engineering**, Delhi Technological University is an authentic record of my own work carried out during the period from **JULY 2017** to **MAY 2025** under the supervision of **Dr. Kapil Sharma and Dr. Manju Bala**.

The matter presented in the thesis has not been submitted by me for the award of any other degree of this or any other Institute.

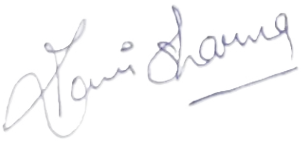

Candidate's Signature

DELHI TECHNOLOGICAL UNIVERSITY
(Formerly Delhi College of Engineering)
Shahbad Daulatpur, Main Bawana Road, Delhi-42

CERTIFICATE BY THE SUPERVISORS

Certified that **Ravi Sharma** (2K17/PHDCO/08) has carried out their search work presented in this thesis entitled **"Design and Development of Efficient Methods for Histopathological Image Analysis"** for the award of **Doctor of Philosophy** from Department of Computer Science and Engineering, Delhi Technological University, Delhi, under our supervision. The thesis embodies results of original work, and studies are carried out by the student himself, and the contents of the thesis do not form the basis for the award of any other degree to the candidate or to anybody else from this or any other University/Institution.

Signature
(Dr. Kapil Sharma)
(Professor)
(Delhi Technological University)

Signature
(Dr. Manju Bala)
(Associate Professor)
(I.P. College of Women)

Date:09/06/2025

ABSTRACT

Histopathological image classification is a vital component in disease diagnosis and treatment, particularly for cancer. This thesis focuses on designing efficient methods for segmentation, feature selection, and classification of histopathological images using enhanced metaheuristic algorithms.

An Enhanced Multi-Objective Grey Wolf Optimization (EMOGWO) algorithm was developed for segmentation, achieving a mean Dice coefficient of **0.964** and a segmentation accuracy of **96.4%** on H&E-stained ER+ breast cancer images. Compared with baseline methods (K-means-SC and MOGWO-SC), the proposed EMOGWO-SC improved boundary detection accuracy by **3.2%** and reduced computation time by **22%**.

For feature selection, an Improved Multi-Objective Whale Optimization Algorithm (IMOWOA) was proposed. IMOWOA selected an optimal subset of features, reducing feature dimensionality by **25–35%** while maintaining high discriminative power. When applied to multiple benchmark histopathological datasets such as BreakHis and BACH, the IMOWOA-based feature selection achieved an average classification accuracy of **98.1%**, outperforming existing techniques including DE, Jaya, and Adaptive Jaya by up to **4.5%**. The framework also reduced processing time by approximately **30%**.

Comprehensive statistical analysis using IGD, SP, MS, and t-tests confirmed that the improvements were significant at a 95% confidence level ($p < 0.05$). The overall framework demonstrates competitive accuracy, robustness, and computational efficiency, offering strong potential for computer-aided diagnostic applications.

Keywords: Histopathological image classification, EMOGWO, IMOWOA, Feature selection, Metaheuristic optimization.

LIST OF PUBLICATIONS

1. Ravi Sharma, Kapil Sharma, “An optimal nuclei segmentation method based on enhanced multi-objective GWO”, Complex and Intelligent Systems 2021, https://doi.org/10.1007/s-40747-021-00547-y (IF: 5.0) (Paper Published)

2. Ravi Sharma, Kapil Sharma, and Manju Bala “Analysis of Histopathological images: An Overview” in the 2022 International Conference on Computing, Communication, Security and Intelligent Systems (IC3SIS), 2022. (Published and Presented)

3. Ravi Sharma, Kapil Sharma, and Manju Bala “Generation of Histopathological Images Caption using CNN and LSTM” in the International Conference on Computing, Communication, Security and Systems 2023(Published and Presented)

4. Ravi Sharma, Kapil Sharma, Manju Bala “Efficient feature selection for histopathological image classification with improved multi-objective WOA” Sci Rep 14, 25163 (2024). https://doi.org/10.1038/s41598-024-75842-y. (IF:3.8) (Paper Published)

TABLE OF CONTENTS

LIST OF TABLES

LIST OF FIGURES

LIST OF ACRONYMS & ABBREVIATIONS (Alphabetically)

ACO	Ant Colony Optimization
BBO	Biogeography-based Optimization
BIRCH	Balanced Iterative Reducing and Clustering using Hierarchies
BOF	Bag-of-Features
BRIEF	Binary Robust Independent Elementary Features
CNN	Convolutional Neural Networks
CT	Connective Tissue
CURE	Clustering using Representatives
DE	Differential Evolution
DE-TCR	Enhanced Differential Evolution
DHCDC	Divisive Hierarchical Clustering with Diameter Criterion
DIVCLUST	Divisive clustering
DNN	Deep Neural Networks
EA	Evolutionary Algorithm
EBR	Edge Based Regions
ES	Evolutionary Strategy
ET	Epithelial Tissue
FAST	Features from Accelerated Segment Test
FCM	Fuzzy C-Means
FCS	Fuzzy C-Shells
FNR	False Negative Rate
FPR	False Positive Rate
FV	Fisher Vector
FWIoU	Frequency Weighted Intersection over Union

GMM	Gaussian Mixture Model
GNN	Gaussian Naive Bayes
GSA	Gravitational Search Algorithm
GWO	Grey Wolf Optimization
H&E	Hematoxylin and Eosin
HIA	Histopathological Images Analysis
HIC	Histopathological Images Classification
HOG	Histogram of Oriented Gradients
HV	Hard Voting
KCB	Kernel Codebook Encoding
LBG	Linde–Buzo–Gray Algorithm
LBP	Local Binary Pattern
LCC	Locality Coordinate Coding
LLC	Local constrained Linear Coding
LR	Logistic Regression
LSA	Localized Soft Assignment
LTC	Local Tangent-Based Coding
LVQ	Learning Vector Quantization
MIoU	Mean Intersection over Union
MM	Multi-Modal
MPA	Mean Pixel Accuracy
MT	Muscle Tissue
NS	Non Separable
NT	Nervous Tissue
OMP	Orthogonal Matching Pursuit
ORB	Oriented Fast and Rotated Brief
PA	Pixel Accuracy
PCA	Principal Component Analysis

PSO	Particle Swarm Optimization
RAM	Random Access Memory
RBM	Restricted Boltzmann Machines
RF	Random Forest
RGB	Red Green Blue
SA	Soft Assignment
SIFT	Scale-Invariant Feature Transform
SMO	Spider Monkey Optimization
SPC	Sparse Coding
SURF	Speeded Up Robust Features
SVC	Super Vector Coding
SVM	Support Vector Machine
TN	True Negative
TP	True Positive
VLAD	Vector of Locally Aggregated Descriptors
VQ	Vector Quantization
WOA	Whale Optimization Algorithm
WSI	Whole-Slide Image

CHAPTER 1

INTRODUCTION

This chapter introduces the domain of histopathological image analysis, emphasizing its importance in medical diagnostics. It outlines the motivation behind the study, highlights key challenges in automating the analysis process, and presents an overview of the thesis structure. Specifically, this research focuses on enhancing three critical stages of histopathological image analysis: nuclei segmentation, feature selection, and classification.

Image analysis plays a vital role in numerous fields, including robotics, computer vision, and especially medical imaging, where its importance is elevated due to its direct impact on public health. Within medical imaging, histopathological image analysis has emerged as one of the most significant and challenging areas, essential for accurate disease diagnosis and effective drug development. Histopathology refers to the microscopic examination of tissue sections to identify pathological conditions. This process is traditionally performed by expert pathologists in laboratories, relying on visual cues in stained tissue samples.

As biological tissues are inherently colorless, staining methods are applied to enhance cellular structures. The most widely used staining protocol is hematoxylin and eosin (H&E) staining, where hematoxylin stains cell nuclei blue and eosin imparts a pink or red hue to the cytoplasm. With the growing adoption of digital workflows, whole-slide image (WSI) scanners are now commonly used in pathology laboratories to produce high-resolution digitized tissue images for further analysis [1]. Automating histopathological image analysis enables consistent, efficient, and objective evaluation of disease-related features. This process typically involves multiple stages, including segmentation, feature extraction, feature selection, and classification. Figure 1.1 [2] illustrates two histopathological images showing healthy and inflamed tissues, respectively.

The digitization of tissue slides has significantly enhanced the accuracy of disease diagno-

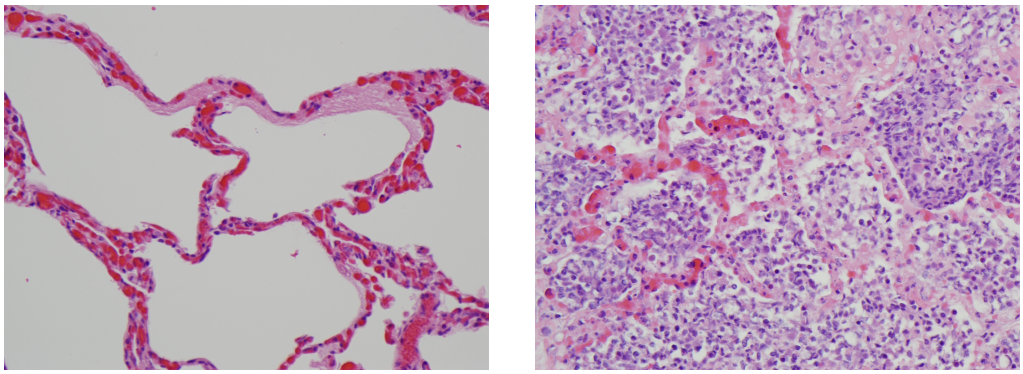

(a) Healthy tissue (b) Inflamed tissue

Figure 1.1: Histopathological images.

sis by enabling pathologists to examine images on digital platforms [2]. However, the manual interpretation of these large and complex images remains time-consuming, subjective, and dependent on the pathologist's expertise. This necessitates the development of automated methods to assist in histopathological image analysis and reduce diagnostic variability [3].

Automated histopathological image analysis typically involves four main stages: segmentation, feature extraction, feature selection, and image classification. The process begins with the segmentation of the image into different regions of interest, such as nuclei, cytoplasm, or background, to isolate key cellular structures indicative of disease. Next, a range of features such as shape, texture, and intensity are extracted from these segmented regions to quantitatively describe their characteristics. Following this, feature selection techniques are applied to identify the most relevant and discriminative features, reducing redundancy and enhancing system efficiency. Finally, robust image classification methods categorize the processed images into diagnostic classes, enabling reliable and scalable analysis of histopathological data.

The remaining chapter presents the motivation behind the study, major problems with manual analysis, challenges in automating histopathological image analysis and organization of the thesis.

1.1 Motivation

In recent years, rapid advancements in computational power and image analysis techniques have enabled the development of powerful machine-learning algorithms for medical image analysis. Moreover, the introduction of whole-slide scanners has allowed histopathological tissue slides

to be digitized, making them readily accessible for computational evaluation.

Despite technological progress, histopathological image analysis continues to rely heavily on y expert pathologists' manual interpretation, primarily due to the variability and complexity of the images. This process is time-consuming and prone to subjectivity, as diagnostic outcomes often depend on the experience and judgment of the individual. Automating this task can improve efficiency and consistency by incorporating machine intelligence to assist and support pathologists.

Automated identification of inflamed tissues can reduce inter-observer variability and enhance diagnostic accuracy. However, automating histopathological image analysis remains challenging due to morphological complexity and technical variations, including differences in organ structures, imaging devices, slide orientations, and staining methods [4]. Additionally, histopathological images often have much higher data density than other modalities, such as radiological imaging, which complicates feature descriptor design and affects classification performance [5].

1.2 Major Problems with Manual Analysis

Histopathological image analysis is essential for both disease diagnosis and pharmaceutical development. Despite the availability of modern diagnostic technologies, this analysis is still largely performed manually. Manual evaluation of high-resolution images demands significant time and effort from pathologists. The key issues associated with manual analysis are outlined below:

- **Scarcity of expert pathologists:** With advances in medical imaging, pathology laboratories now generate vast amounts of data daily. As a result, there is a growing global demand for skilled pathologists. For example, in Australia, the Australian Medical Workforce Advisory Committee has acknowledged a shortage of qualified professionals [6].

- **Variability and subjective observations [5] [7]:** Diagnostic conclusions can differ based on the experience and training of individual pathologists. Such variability may lead to inconsistent, delayed, or incorrect treatment decisions.

- **Morphological complexity of tissue structures [5]:** Histopathological images contain various morphological structures and complexities, such as the use of different staining

dyes, illumination variations at the time of capturing the images, different shapes and sizes of nuclei, and many more. These factors make consistent manual analysis extremely challenging..

- **Time-consuming and labor-intensive:** The manual analysis of a histopathological image requires at least three to four hours of sitting, and the evaluation of quantitative properties makes it a more complex task. Further, if the images are captured at a high magnification rate, then more time is needed by the pathologists to analyze the whole slide.

To overcome the shortcomings mentioned above, the automated analysis of histopathological images may be used. An automated image analysis system can provide meaningful data more accurately and in a timely manner for histopathological images. This reduces the workload on the pathologists and creates less human subjectivity. This process enhances the manual analysis process by generating reliable and fast results. Recent advancements in computer vision and image analysis open up various opportunities to design and develop an automated system for histopathological image analysis. These systems help make unbiased, efficient, and accurate analysis reports promptly and perform automated nuclei segmentation, feature extraction, feature selection and classification of different tissue types, which can be accessed widely as a tool for research.

Therefore, the development of automated histopathological image analysis methods has emerged as a significant research problem in medical imaging [5][2][8]. However, there are many problems associated with the development of such an automated system. The following section discusses the various challenges in the automation of histopathological image analysis.

1.3 Challenges

Though many histopathological image analysis methods are available in the literature which show quite promising results, there still exist some challenges which affect the accuracy of the system. This needs the attention of the researchers for improvements so that the expectations of the pathologists can be fulfilled.

1. **Variations in the color and illumination:** Histopathological images are the colorful tissue images after staining and captured by the whole slide scanners. The color provided

by staining methods may vary as it is a manual process, and similarly, there may be variations in the illumination light while capturing the images. These color and illumination variations may degrade the automated system's performance significantly [9].

2. **Different staining methods:** Most of the works for histopathological image analysis have been done on tissue section images stained with some chemicals like immunohistochemical (IHC), immunofluorescence (IF), and haematoxylin & eosin (H&E). These staining procedures are very costly and time-consuming. The use of multiple staining methods to prepare histopathological images makes the analysis difficult for automated methods [5] [10].

3. **Enormous density of data:** An additional obstacle in the automated histopathological image analysis is the huge density of the data as compared to other biomedical images like tomography, radiology, and other image modalities, which has to be contended by the automated methods. For example, the chest CT scan, captured on high resolution, consists of approximately 143 million pixels with $512 \times 512 \times 512$ spatial elements. On the other hand, the biopsy tissue of the prostate, captured at $40\times$ resolution by a whole slide image scanner, consists of approximately 235 million pixels with $15,000 \times 15,000$ elements. Moreover, for one patient study, there is a requirement of 10 to 20 biopsy samples which results in generating a huge amount of data of approximately 3 to 4 billion pixels. Therefore, unlike the automated methods proposed for radiology and other medical imaging, automated histopathological image analysis methods are usually built so that they have to perform efficiently and accurately on high density data.

4. **Multimodal data fusion:** Histopathology is generally used to study cancer in the patients, but the diagnosis and prognosis of cancer in patients are very hard. Two patients are going through the same treatment procedure with the same disease, it may result in different outcomes. The reason for this difference may be patient-specific or due to the lack of related information between the progression of the disease and clinical aspects. There is common consent between scientists and pathologists that understanding tumor visual morphology using automated image analysis methods, along with disease classification will result in better treatment and patient care. Therefore, multimodal data fusion has emerged as a relevant challenge for digital pathology labs for recommending patient treatments.

5. **Maintenance of image data:** A large amount of data is generated due to the advancements in digital imaging tools and image acquisition methods. The storage, registration, maintenance, and transmission of such a large volume of data is challenging. The spectral imaging data from the slide scanner makes the problem more complex.

1.4 Organization of the Thesis

For histopathology, computer vision, and biomedical scientists, the above-mentioned challenges will open various research problems and opportunities to develop new image analysis methods. Pathologists and computer scientists work together with microscopy and slide scanner vendors to build innovative and novel methods to solve various challenges of image analysis in digital pathology. Furthermore, in the last few years, histopathological digital images have rapidly increased over the internet, and there is a need to organize them properly to enhance researchers' retrieval and analysis processes. Hence, an automated system for histopathological image analysis can prove to be beneficial. Numerous automated techniques for histopathological image analysis have been reported in the literature. These techniques include graph-based algorithms, hashing, bag-of-features, and deep neural networks. Grey wolf optimization and whale optimization methods are widely used in image analysis, particularly for nuclei segmentation, feature selection and classification in histopathological images. However, there is a need for improvement in the different phases of wolf optimization and whale optimization methods. The fundamental goal of this thesis is to design and develop effective methods for histopathological image analysis. The main contribution of the thesis is four-fold. Its first goal is to create an effective nuclei segmentation technique based on clustering. The suggested approach uses a unique multi-objective grey wolf optimizer variation to discover the ideal cluster of centroids. Second, images of Estrogen Receptor-Positive (ER+) breast cancer stained with H&E have been employed to segment nuclei using the proposed EMOGWO. The segmentation accuracy of the suggested technique is empirically tested against K-means-SC and MOGWO-SC. Third, a new improved multi-objective whale optimization algorithm-based feature selection method has been proposed. The proposed algorithm is validated against three additional cutting-edge techniques, MOPSO, MOEA/D, and MOWOA. Fourth, the proposed IMOWOA-FS method is applied to real-world histopathological image datasets for classification using five widely-used classifiers—ZeroR, SVM, LDA, RF, and KNN. The classification results obtained

using IMOWOA-FS are compared against those achieved using three existing feature selection techniques: Differential Evolution (DE), Jaya Algorithm, and Adaptive Jaya Algorithm. The comparison is carried out across multiple evaluation metrics, including classification accuracy, number of selected features, and computational time, to demonstrate the effectiveness and generalizability of the proposed method. The complete workflow of the thesis is shown in Figure 1.2. The remaining material is arranged in the following chapters.

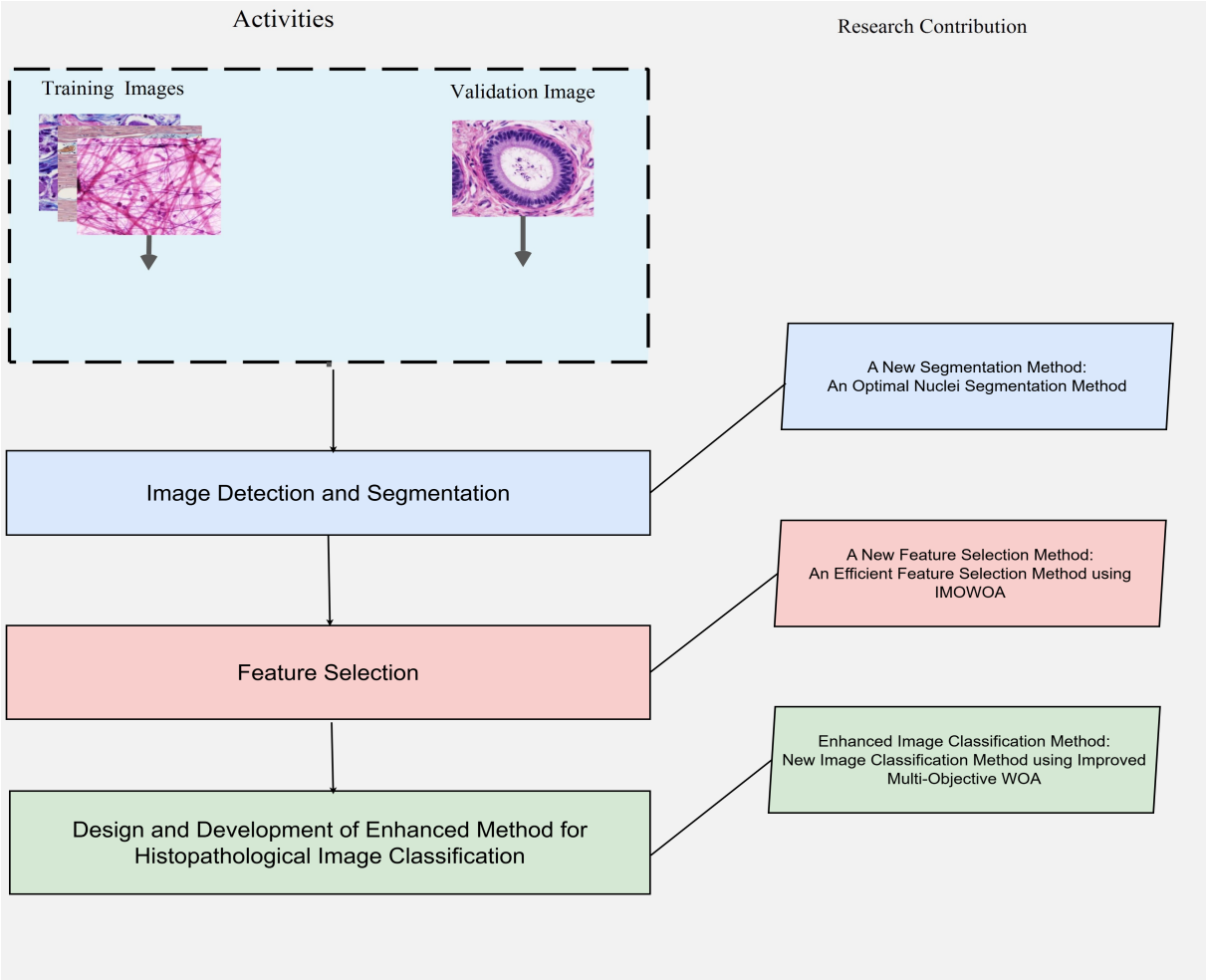

Figure 1.2: The workflow of the proposed research work.

Chapter 2 This chapter provides a comprehensive literature review covering each stage of histopathological image analysis, including segmentation, feature extraction, feature selection, and classification. Based on this review, existing research gaps are identified, and corresponding research objectives are formulated.

Chapter 3 This chapter introduces a novel nuclei segmentation technique based on Enhanced Multi-Objective Grey Wolf Optimization integrated with Superpixel Clustering (EMOGWO-SC). It elaborates on the proposed methodology and provides a comparative performance analysis against other state-of-the-art multi-objective optimization algorithms.

Chapter 4 This chapter proposes an Improved Multi-Objective Whale Optimization Algorithm (IMOWOA) for optimal feature selection in histopathological image analysis. The chapter describes the objective functions, algorithm enhancements, and experimental evaluation, highlighting the method's effectiveness in reducing feature dimensionality while maintaining or improving classification performance.

Chapter 5 This chapter applies the IMOWOA-based Feature Selection method (IMOWOA-FS) to classify histopathological images using selected features. The chapter evaluates classification performance across multiple datasets using various machine learning classifiers, and compares the results with those from existing feature selection techniques in terms of accuracy, efficiency, and feature reduction.

Chapter 6 This chapter concludes the thesis by summarizing the major research contributions and findings. It also outlines potential directions for future work, focusing on improving automated histopathological image analysis and extending the proposed methods to broader biomedical imaging challenges.

CHAPTER 2

LITERATURE REVIEW

This chapter presents a comprehensive review of existing techniques for histopathological image analysis, focusing on its key phases: segmentation, feature extraction, feature selection, and classification. It systematically examines the strengths and limitations of various approaches, leading to the identification of critical research gaps. Based on this analysis, the chapter concludes by outlining the research objectives addressed in this thesis.

2.1 Introduction

Histopathology images provide a detailed view of diseases and their effects on tissues. Under a microscope, these images can be examined to detect the presence of conditions such as cancer. Computer-Aided Diagnosis (CAD) plays a key role in histopathological image analysis, helping improve the accuracy and efficiency of disease detection. Digital image processing methods like preprocessing, segmentation, feature extraction, and classification are required to implement computer-assisted analysis systems. Along with disease grading, illness severity can be determined by automatically extracting quantitative measurements of disease characteristics from histopathological images. Numerous cancer detection and grading applications, including prostate, breast, renal cell, neuroblastoma, and lung cancer, have been studied using computer-aided histopathology. The histopathological images are examined using various segmentation, feature extraction, feature selection and classification methods.

An automated histopathological image classification system's general architecture is shown in Figure 2.1. It is primarily made up of two stages: the training and the validation phase. The initial stage is known as the training phase, during which a sample of histopathological images is chosen randomly from the database and transformed using an image representation

technique into feature vectors. The image labels for training are provided as input to the learning model or classifier. Using the same image representation technique, a histopathological image is chosen from the image database and transformed into a feature vector using the trained learning model. The trained learning model receives the produced feature vector and uses it to predict the image's label. Consequently, the image representation approach is crucial in the classification of histopathological images, and the system's accuracy largely depends on how well it performs. The histopathological image classification approaches may be categorized into three groups

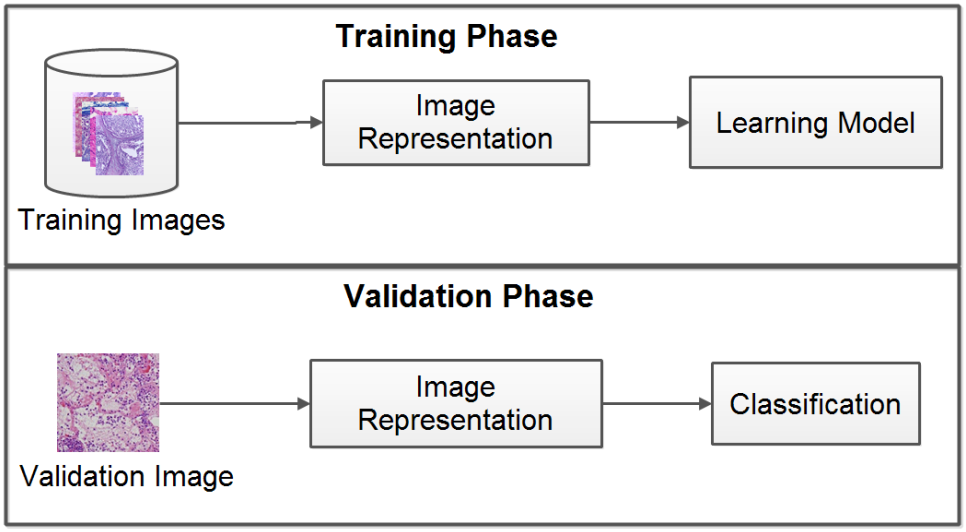

Figure 2.1: General workflow of an automated histopathological image classification method.

based on image representation techniques: statistical methods, learning-based approaches, and methods based on mid-level representations, as depicted in the Figure. 2.2.

2.2 Image Representation Techniques

Statistics-based image representation techniques, which rely on pixel-level processes, extract local or low-level features from histopathology images. Without requiring segmentation, the features offer great insights about the contents of the medical images for the categorization assignment. For instance, morphological characteristics have been utilized to identify vessel-like structures in medical images [11]. An image area that differs from its immediate vicinity is represented as a low-level feature [12]. "Handcrafted features" is another term for these qualities. Various customized feature extraction techniques are designed and applied to extract the handmade characteristics from the images [13]. Numerous features of cells and nuclei, such as size, shape, color, texture, and distribution of nuclei in tiny areas or patches, are recorded using sta-

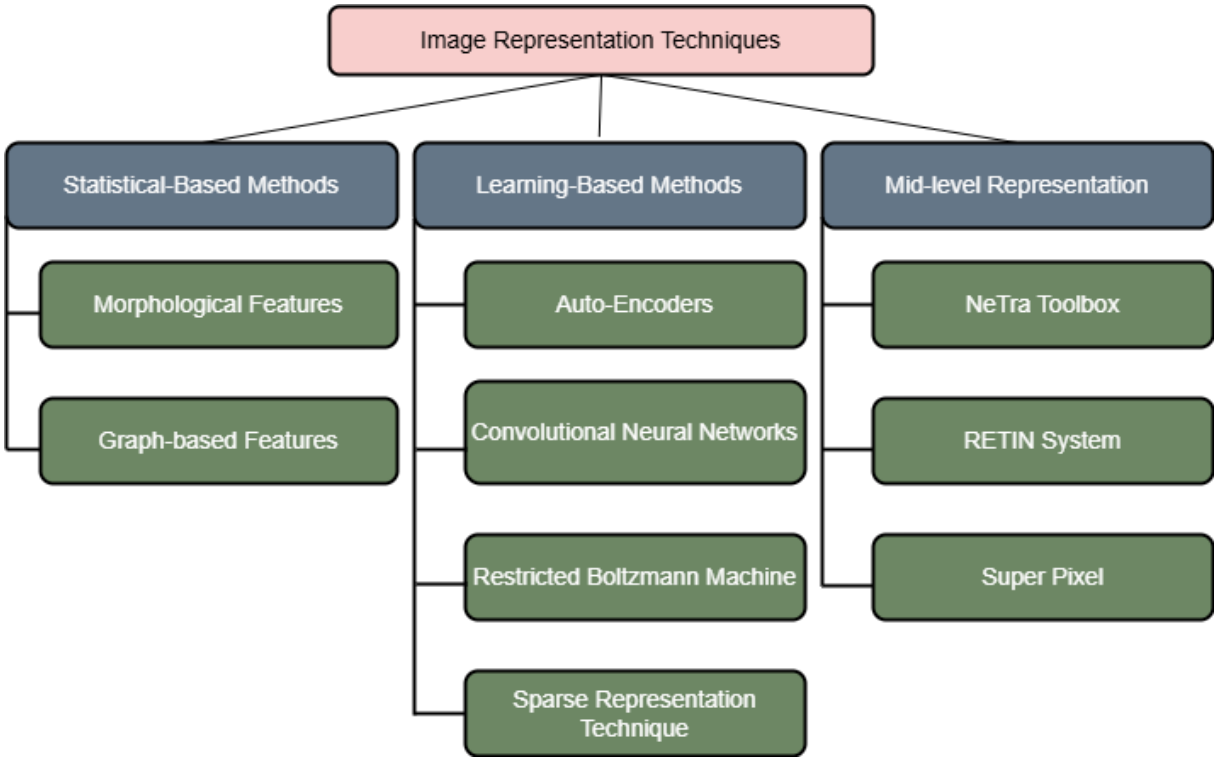

Figure 2.2: Categorization of histopathological image classification techniques based on image representation.

tistical techniques [14]. While several graph-based characteristics, including minimal spanning tree, query graphs, delaunay triangulation, and others, have been employed to reveal spatial patterns or structures [15]. However, the intricate visual morphological features in histopathology images cannot be expressed by statistically based image representation techniques [16]. Several learning- based techniques have been employed for image representation to get around the issue.

Various machine learning algorithms are employed by the learning-based image representation techniques to extract features from the images automatically. The features are presented in a further structured and seamless manner using different approaches, such as RBMs (Restricted Boltzmann machines) [17], auto-encoders [18], CNNs [19], and Sparse representation [20]. Many learning-based image representation methods are computationally intensive when dealing with complex histopathological images [16]. Cruz-Roa and others [21] introduced a deep learning approach designed to identify basal cell carcinoma automatically. An interpretation layer is incorporated into this model that highlights patterns distinguishing normal from malignant tissues. Researchers [2] suggested a sparsity model that uses sparse linear combinations of training samples with channel-specific restrictions to represent each histopathology image with several color channels. They also presented a locally robust variant of this method to handle

the different spatial locations of image items. Arevalo and others [22] employed an unsupervised feature learning method for analyzing histopathological images. They employed different techniques, including topography-based independent component analysis and reconstruction, as well as sparse autoencoders, to model local patches. To capture global image representation, they employed a CNN. Xu and others [23] utilized a stacked sparse auto-encoder for the automated identification of nuclei in histological images of breast cancer. Also, they trained a deep CNN to extract features for segmenting epithelial and stromal tissues in breast cancer histopathological images [19]. Furthermore, authors [20] proposed an approach for automatically learning features from histological images with intricate morphological patterns, utilizing class-specific dictionaries with sparsity constraints. These learned dictionaries were then used to classify and grade numerous diseases through histopathological images. Additionally, while the patch-selection methods described in [20] are efficient, they often struggle to detect inflamed or malignant samples, especially when the malignant areas in the images are small.

Mid-level representations of the images are global representations created by mid-level feature extraction algorithms using local or low-level feature descriptors. Since these global features are derived from local descriptors, they are closely aligned with image-level information. The process of obtaining mid-level representations generally involves three main steps [24]: (i) local feature extraction, (ii) codebook construction, which identifies visual words from the extracted feature set, and (iii) encoding, which usually creates a histogram of visual words from each image. These histograms are then used to train a classification system. Several mid-level image representation techniques exist across the literature, with some of the most commonly employed being the NeTra toolbox [25], the RETIN system [26], and the superpixel method [27]. The NeTra toolbox made the first significant contribution to the mid-level representation paradigm. It employs unsupervised learning to build a codebook based on descriptors of color points, utilizing the Linde–Buzo–Gray (LBG) algorithm [28] for vector quantization. Subsequently, the RETIN system [26] applied self-organizing maps [29] to create a codebook from Gabor feature vectors. The mid-level representation technique became widely used in the Video Google framework. Sivic and Zisserman [30] supported the bag-of-features approach for retrieving objects and scenes, extracting features through the Scale-Invariant Feature Transform (SIFT), and forming the codebook using K-means. Csurka and others [31] further employed this method for image categorization. Recently, researchers [32] proposed a multiphase image segmentation method based on fuzzy segmentation, while Bakr Ahmed Taha and others [33]

introduced a segmentation method to calculate the density of SARS-CoV-2 spike proteins employing superpixels. Superpixel segmentation techniques are investigated in this work for the categorization of histopathology images. Modern techniques employed at different stages of the segmentation process for histopathological image categorization are shown in the section that follows.

2.3 Superpixel Algorithm-based Feature Extraction Methods

The superpixel approach has emerged as a practical mechanism for classifying histopathology images. There are typically four main phases: (i) Superpixel algorithm-based feature extraction (ii) clustering (iii) feature encoding and (iv) classification. The following sections provide a thorough overview of each stage of the superpixel approach. There are several superpixel algorithms available, each with their own strengths and weaknesses. Depending on the major properties, we can divide superpixel segmentation techniques into four categories:

2.3.1 Watershed-based Techniques

Based on region-based segmentation, the Watershed-based Technique is a segmentation method that uses image morphology. According to the watershed approach, pixels in the darker sections are called valleys, and pixels in the brighter portions are ridges. The ridge height is typically determined by the grayscale values of individual pixels or the gradient magnitude associated with those pixels. Several watershed-based techniques include Watershed (W), Compact Watershed (CW), Water Pixels (WP), and Morphological Superpixel Segmentation (MSS).

2.3.1.1 Watershed

This methodology employs a typical watershed-based approach where the image is processed using markers [34]. The number of superpixels can be calculated using the number of present markers in the image. This method also provides compactness.

2.3.1.2 Compact Watershed (CW)

The compact watershed methodology is a seeded watershed segmentation method that considers superpixels' compactness restrictions to limit the number of superpixels [35]. In CW, the water-

Table 2.1: Categorization of feature extraction methods used in Superpixel. [38].

Category	Classification	Comments
Watershed-based	Region Based Segmentation	Consider bright region as ridge and dark region as valley
Graph-based	Connected Components	Treat image as undirected graph
Energy Optimization Technique	Regular Grid	Based on the energy pixels and superpixels are swapped
Clustering-based Technique	Clusters of Superpixels	Cluster based on some type of similarity

shed incorporates the controlled compactness limitations to assess their impact on segmentation quality.

2.3.1.3 Morphological Superpixel Segmentation (MSS)

Using MSS, the image can be segmented more quickly. This method produces the segmentation markers and eliminates the extreme local spatial intensities that are irrelevant to the image [36].

2.3.1.4 Water Pixels (WP)

Superpixels segmented into "water pixels" are based on the watershed transformation [37]. To create a modifiable trade-off between superpixel and adherence to object boundaries regularity, the WP method leverages the spatially regularized gradient. The identification of markers, which serve as the starting points for flooding, along with the establishment of a gradient, contributes to the formation of water pixels in the watershed segmentation technique.

2.3.2 Graph-based Techniques

The images will be treated as a graph (an undirected graph) by graph-based techniques. The edge weight is regarded as the similarity of the nearby pixels, and the pixels in the image are represented as nodes. Other variations of graph-based techniques include Normalized Cuts (NC), Felzenswalb and Huttenlocher (FH), Lazy Random Walks (LRW), Entropy Rate Superpixels (ERS), Homogeneous Superpixels (HS), and Proposals for Objects from Improved Seeds and Energies (POISE).

2.3.2.1 Normalized Cuts (NC)

The elements in the normalized cut technique are the nodes and the edges. Nodes represent items, whereas edges represent similarity between items [39] [40]. In this method, the network is split into two subgroups, one with nodes that have a high degree of similarity and the other with nodes that have a low degree of similarity. It is discovered that the N cut algorithm's complexity is $O(n^{3/2})$; where n denotes the number of pixels present in the image.

2.3.2.2 Felzenswalb and Huttenlocher (FH)

A minimum spanning tree of necessary pixels is created in the FH technique to identify the superpixels [41]. The Dijkstra algorithm is used to find the graph's shortest path. It divides nodes so that the components with a relatively low weight are located on the inside edges, and those with a relatively high weight are located between the edges. The superpixels produced with this method are of erratic size and shape. The Felzenswalb and Huttenlocher (FH) approach has an O(nlogn) level of complexity.

2.3.2.3 Lazy Random Walks (LRW)

In the LRW method, image pixels function as nodes, while edges are determined using the Gaussian weighting function [42][43]. The energy function connected to texture measurement and iterative time is used in this technique to optimize the superpixels iteratively. With this technique, the object boundaries are precisely established.

2.3.2.4 Entropy Rate Superpixels (ERS)

When using the ERS technique, the image's nodes are characterized by the pixels, and the edges connecting the pixels are shown as a function of their pairwise similarity [44]. The major goal of this method is to take the subset of edges with N-connected subgraphs out of the final graph, where N is the number of superpixels. The entropy rate superpixel's time complexity is O(n).

2.3.2.5 Homogeneous Superpixels (HS)

In the HS methodology, the edges are taken into account by calculating the similarity of an initialized adjacency matrix, while the nodes are taken into account as the input pixels [45]. This method uses compact pruning to reduce computation time and prevent uneven pixel distribution.

2.3.2.6 Proposals for Objects from Improved Seeds and Energies (POISE)

By combining the pixels, POISE process creates superpixels from the bottom up [46]. POISE will create a superpixel by creating a set of seeds that almost completely cover a variety of sized objects in a huge number. The min cuts parameters are allowed to operate at their maximum capacity.

2.3.3 Energy Optimization Technique

The Energy Optimization Technique gradually maximizes the specified energy. The image is divided into a regular grid in the first phase of the superpixel segmentation process, and pixels are switched between neighbouring superpixels according to energy. This approach provides flexible control over the number of superpixels, compactness, and iterations; this is usually haltable at any point. Contour Relaxed Superpixels (CRS), Superpixels Extracted by Energy-Driven Sampling (SEEDS), and Extended Topology Preserving Segmentation (ETPS) are most widely used energy optimization technique.

2.3.3.1 Contour Relaxed Superpixels (CRS)

The creation of superpixels using CRS aims to maximize contour conformity to a Gibbs-Markov random field model as well as texture uniformity within each patch [47][48]. It was decided to reframe the superpixel segmentation challenge as an estimation issue. The energy function that has to be maximized in CRS depends on the statistical model applied to the images and has a relatively small number of design variables. It may make the model into a viable superpixel technique by including a compactness term.

2.3.3.2 Superpixels Extracted via Energy Driven Sampling (SEEDS)

The superpixel partitioning phase is the first step in the SEEDS technique [49]. The boundaries of the superpixels are then modified in accordance with the energy function to refine them. The function's two terms, color term and boundary term, are defined by the color histogram and superpixel boundaries. The energy function can be resolved via hill-climbing optimization. The duration of SEEDS' iterations is related to its overall length. The authors claim that SEEDS has real-time capabilities. SEEDS features form a lot of irregularity, making it difficult to manage the number of superpixels.

2.3.3.3 Extended Topology Preserving Segmentation (ETPS)

The ETPS method [50] efficiently determines the objective function's local optimal value through a coarse-to-fine segmentation process. It arranges every superpixel within a square grid of identical size and calculates the initial center position and average color for each superpixel. It then makes layers with varying grid sizes for each layer. One-fourth of the main grid is used for the first layer, one-fourth of the first layer is employed for the second layer, and so on, down to one pixel. Boundary blocks are added to FIFO queue and configured for each layer. Every time, it is taken from the queue to see if the link between the superpixels would be broken by removing this boundary block from its superpixel. If not, an attempt is made to combine the block with an adjacent superpixel to reduce the value of the goal function. At coarser levels, the ETPS method reaches an improved local optimum much more quickly, while at finer levels, it gradually converges toward the final local optimum.

2.3.4 Clustering-based Technique

Clustering-based Techniques aggregate pixels into several clusters known as superpixels, and are the driving force behind the clustering-based approaches. These methods use adjustable iterative compactness. TurboPixel (TP), SLIC, Depth-Adaptive Superpixels (DASP), VCells (VC), Voxel-Cloud Connectivity Segmentation (VCCS), and Linear Spectral Clustering (LSC) are a few examples of clustering-based approaches.

2.3.4.1 TurboPixel (TP)

TP [51] adapts to local image structures by employing dilated seeds to segment an image into a compact, tiny structure that resembles a lattice. TurboPixel locates a cluster of seeds using level-set-based geometric principles. The geometric flow seeks to create regular superpixels by starting with the local image gradient. Unlike watershed superpixels, TP superpixels are limited to a consistent size, compactness, and adherence to borders. It employs a method that combines a skeletonization operation on the background region with a curve evolution model for dilatation to prevent the growing seeds from overlapping.

2.3.4.2 Simple Linear Iterative Clustering (SLIC)

SLIC [52] uses K-means clustering, which groups pixels in the image plane according to color proximity and similarity. Due to its simplicity, speed, and capacity to produce uniform, compact superpixels that adhere well to object borders, SLIC is frequently employed.

2.3.4.3 Depth-Adaptive Superpixels (DASP)

The depth of the image is used to define the density of the superpixel clusters in the DASP [53] clustering approach, which will ensure the absence of blue noise. The clustering method is then applied to the given data points to produce improved superpixel centers.

2.3.4.4 VCells (VC)

VC [54] divides a image into smaller, uniformly sized and shaped parts. The segmentation boundary is subsequently modified using the Edge Weighted Centroidal Voronoi Tessellation (EWCVT) model to meet the compactness requirements.

2.3.4.5 Voxel-Cloud Connectivity Segmentation (VCCS)

VCCS [55] uses unique voxel connections to produce superpixels. In this method, 3D point cloud data is used to create superpixels and supervoxels. In VCCS, the labelling of points is produced by utilizing a K-means clustering version. The seed points are identified as the cluster's core when the neighbouring graph for the voxel is built. Then, until the stable cluster center is reached, the cluster's center is modified using the Fast Point Feature Histograms (FPFH) space[56].

2.3.4.6 Linear Spectral Clustering (LSC)

Using kernel functions, a type of superpixel segmentation known as LSC transforms image pixels into ten-dimensional feature space-weighted points [57]. The entire image is then subsequently sampled from the seed pixels, which act as search centers. The feature vectors of these seeds are employed as the initial weighted means for the clusters. The cluster whose weighted mean in the feature space is closest to the pixel's vector is then assigned to each pixel. The weighted mean and the search for the center of each cluster are then adjusted accordingly.

These two steps will be repeated until the cluster centers become stable. It has more regular superpixels and keeps the image's global properties in contrast to the SLIC.

2.4 Computational Intelligence Techniques for Superpixel Segmentation

Several computational intelligence techniques have been developed for superpixel segmentation, with the most prominent ones listed below.

2.4.1 Conventional Superpixel Segmentation Techniques

A group of image-building elements called "superpixels" are built of pixels with comparable characteristics, including color, texture, and brightness. SLIC is considered the finest among the existing superpixel models. In FLAIR MRI, Soltaninejad and others [58] suggested automating the segmentation and detection of brain tumors using highly randomized trees based on superpixels. A variety of cutting-edge imaging characteristics, including intensity-based, Gabor textons, fractal analysis, and curvatures from each superpixel inside the entire brain area, are calculated using FLAIR MRI to assure a reliable classification.

An adaptive superpixel generation technique built upon the modified version of SLIC, known as SLIC with 0 parameters (SLIC0), was proposed by Yuan C et al. [59]. The SLIC technique uses the K-means clustering algorithm to separate images into superpixel patches. The distance metric used by this clustering method considers both the distance between pixels in grey space and their euclidean distance. The following equation can be used to determine the separation D between two pixels[60].

$$D = \sqrt{d_c^2 + \left(\frac{d_s}{S}\right)^2 C^2} \tag{2.1}$$

where S is the range of clustering limit with the value of S=$\sqrt{\frac{N}{K}}$, N is the number of images, K is the total superpixels, and C is the balancing parameter defined as Compactness. Values of C and K are set manually. Therefore, the effectiveness of segmentation is directly impacted by the selection of these two criteria. The value K determines the size of the superpixel block. As the value of K increases, the number of uneven patches decreases. Compactness C determines the amount of spatial distance. When C is large, the boundary of the superpixel smoothes out, and the proportion of spatial distance increases. The superpixel border will be near the edge of

the image when C is small, but its size and form will be irregular.

Therefore, determining the best K and C is essential for a successful SLIC algorithm implementation. The SLIC with 0 parameters (SLIC0) strategy improves the C value selection by changing the fixed SLIC value into an adjustable value for each superpixel in the first iteration. The findings demonstrate that the SLIC0 approach is capable of creating reasonably regular superpixels in terrain that are both fat and very variable, bringing the superpixels close to tumor or oedema regions. Thus, the hyper-parameter C selection problem is resolved by the SLIC0 approach, which changes the primary superpixel segmentation challenge into the hyper-parameter K selection problem. The segmentation performance of the suggested method is good. Compared to the ground truth, the segmented tumor's average dice coefficient, hausdorff distance, sensitivity, and specificity are, respectively, 0.8492, 3.4697 pixels, 81.47%, and 99.64%. Strong stability is demonstrated by the suggested approach in both high- and low-grade glioma samples. Experimental results indicate that the recommended technique outperforms the alternative methods.

In 2016, Wu and others [61]] proposed a unique cartoon segmentation method based on enhanced SLIC superpixels and introduced an adaptive area propagation merging approach. The superpixels produced by the SLIC method may have constant sizes, but they do not necessarily line up with the edges of the image. To address this flaw in the original SLIC algorithm, this study offered a method to improve the quality of superpixel production based on the connection constraint. Thanks to the improved method, superpixels can always be produced with great inner connection and independent bounds. The algorithm may join superpixels with similar properties after they have been created to create a segmented area. The merging stage employs Adaptive Region Propagation (ARP), unlike earlier techniques, which mainly utilize Affinity Propagation (AP). Since the unique ARP merging method immediately applies color and spatial similarity between two nearby superpixels with a configurable propagation center, it is more flexible and efficient. The approach is significantly faster to utilize since it is based on superpixels. The method consistently produces cartoon image segmentation results that are in accordance with human perception and beat conventional segmentation algorithms, according to experiments[62].

Researchers [59] proposed a spectral clustering technique based on the spectral graph theory. Spectral clustering is one of the most powerful clustering techniques. However, there are several downsides when using spectral clustering for image segmentation. The spectral clustering al-

gorithm's similarity matrix expands in size, making it challenging to store and deconstruct, just like with large-scale image data and increasing image resolution. The Gaussian kernel function is commonly used as a similarity measure in spectral clustering; however, its use increases computational costs. Choosing an appropriate setting is challenging because the scale parameters in this measure are highly sensitive to spectral grouping. It delivers poor results when used to segment images with noise contamination. This yields a near match to professional delineation across all glioma grade ranges, yielding a rapid and reproducible glioma segmentation method.

Yuan and others [59] proposed an image segmentation approach that combines a Modified Density-Based Spatial Clustering of Applications with Noise (MDBSCAN) superpixel segmentation method with spectral clustering to improve both accuracy and computational efficiency. Their method begins by segmenting the image into superpixels using MDBSCAN, which enhances the traditional DBSCAN-S by operating in the CIELAB color space and expanding the neighborhood search to better respect object boundaries. Each superpixel is then represented by spatial and color features, which are clustered using a Kernel Fuzzy C-Means (KFCM) algorithm. To overcome the noise sensitivity of conventional similarity measures, the authors introduced a new kernel fuzzy similarity measure to build the affinity matrix for the Ng–Jordan–Weiss (NJW) spectral clustering method. This framework effectively reduces computation costs and demonstrates superior segmentation performance compared to existing techniques

Adjei and others [63] implemented SLIC superpixels with optimized thresholding algorithms for automatic brain tumor segmentation. Numerous studies have been conducted on tumor segmentation utilizing artificial neural networks, machine learning, and generic image segmentation methods such as K-means clustering, fuzzy C-means clustering, and watershed approaches. Other approaches, such as histogram-based methods and region-based approaches (region splitting, growing, and merging), have also been employed. The disregard for limits, convenience, adaptability, and compactness are all barriers to these solutions. One well-known factor in boundary violations is that most segmentation approaches encounter this issue, which results in failure for the majority of automatic and semi-automated image classification systems. Because tumors may occur anywhere in the brain and are inherently irregular in form, it might be challenging to segment them accurately enough for therapeutic use.

Chen and others [64] highlighted that both traditional and advanced superpixel techniques emphasize on improving border adherence over computation, as superpixel segmentation is in-

creasingly utilized as a preprocessing step in image processing. As a result, the over-segmentation and redundant superpixels of the smooth linked region are typically disregarded. Superpixel boundaries thereby remove the complex and useless secondary texture and contour information from the image. These limits will make image processing, such as image segmentation and image recognition, more difficult and complicated. This study primarily focuses on superpixel segmentation, aiming to reduce redundancy in smoothly connected regions while filtering out complex and irrelevant background textures. This approach enhances the retrieval of key textures and the outlines of prominent objects in an image.

2.4.2 Deep Learning Techniques

It is a tedious procedure that takes a long time for pathologists to manually analyze the cell morphology in high-definition histopathology images. Recent developments in imaging technology have made it possible to uncover more precise information about the cells. Albayrak and Bilgin proposed a combined method of SLIC and CNN to segment the cellular structures [65]. The imaging method used can potentially capture a significant portion of essential tissue. As a result, examining a wide range of cellular structures can be challenging and time-intensive for pathologists. This issue highlights the need for auxiliary decision support systems capable of analyzing images from imaging devices.

Because the image segmentation algorithms (such as Watershed, N-Cut, etc.) primarily segment a image by extracting its basic properties, their results do not convey semantic information [66]. Advances in deep learning have led to the suggestion of a series of semantic segmentation methods based on CNNs represented by Fully CNN (FCNN). Since then, semantic segmentation in image segmentation has evolved to a new level. Deep CNNs (DCNNs) are excellent at modeling objects and extracting information.

Semantic segmentation on aerial images is challenging for three reasons, though: (1) In high-resolution images, the size of the object in the foreground varies substantially. (2) There is an uneven edge on one or more foreground items. (3) The background is detailed and contains a variety of features. The sophisticated context information in aerial images is a challenge to the current semantic segmentation methods. To address the aforementioned problems, a superpixel-GNN with an attention mechanism-based semantic segmentation technique for aerial images is proposed. First, superpixels are separated from the aerial image. Then, each of these superpixels

serves as a node in a graph that is created. The last stage in creating edges (superpixels) is identifying neighbours in the spatial connection between these nodes. Each node's beginning representation is the output of the semantic segmentation CNN or the image feature vector, and it is modified repeatedly using recursive techniques. Public datasets surpass all benchmark approaches, achieving 90.23% and 89.32% on the Potsdam and Vaihingen datasets respectively.

Unmanned vehicles, in particular drones and autonomous vehicles, are increasingly widely employed in our daily lives because of recent developments in robotics and artificial intelligence. The rapid development of Unmanned Surface Vehicles (USVs) has increased the focus of the marine sector on this trend. USVs can perform a variety of tasks, such as communication, gathering environmental data, search and rescue, and scientific inquiry. The sensors in USVs may have a variety of disadvantages, such as poor detection accuracy, a decreased ability to locate submerged impediments, and high expenses, especially for Light Detection And Ranging (LiDAR) sensing. Visual cameras have gained popularity for object detection in maritime environments in recent years, owing to their ability to provide rich texture information and their relatively low cost. For environment sensing, low-cost cameras may find it difficult to deliver consistent detection, which may be problematic when the environment at the water's surface has few distinguishing features. Deep learning has lately generated a lot of interest because of its effective feature extraction capabilities. Semantic segmentation, a computer vision task requiring the input of raw data (such as images), and even the construction of masks with highlighted regions of interest, is one of the key applications of deep learning. Semantic segmentation-based obstacle identification may assist USVs in identifying potential collision dangers while they are engaged in activities.

The authors [67] developed a model by inventively combining SLIC and Deep Neural Network models in order to improve segmentation accuracy, notably for obstacle edge identification in maritime situations. The proposed SLIC-enabled model has a significant capability in grasping the semantics of the environment, as evidenced by the results of enhanced cross-validations based on three different marine datasets. The findings show that a high obstacle detection accuracy can be attained when utilizing the segmentation provided by the proposed network. Similarly, the performance of obstacle detection is tested using a range of real-world marine datasets.

The authors [68] explored deep learning methods for tongue segmentation. However, the segmentation of the tongue's contour can be imprecise when its color is similar to that of the

surrounding area, potentially affecting the subsequent quantitative analysis. To address this, the authors developed a Traditional Chinese Medicine (TCM) tongue segmentation technique that combines CNNs with superpixels, aiming to improve accuracy in processing tongue margins and solve issues like over-segmentation and under-segmentation. The main objectives were to achieve consistent segmentation and enhance the detection of tongue margins across different imaging conditions. This work is done in three steps: (1) A novel tongue segmentation model was created using the ResNet18 residual structure as the feature abstraction layer for encoding. (2) Given the background noise in tongue images and processing errors at the tongue's borders, superpixel image segmentation was recommended to improve accuracy. (3) The new model was compared with traditional convolutional networks (FCN and DeepLab) to evaluate its performance in segmenting tongue data before and after integrating superpixels. SpurNet, a novel CNN-based approach for tongue image segmentation using superpixels, was proposed. The proposed model was evaluated alongside conventional segmentation methods (FCN and DeepLab) using a dataset containing 367 manually annotated tongue images. SpurNet exhibited robust results through tenfold cross-validation, attaining a PA of 0.9145±0.0043, MPA of 0.9168±0.0048, MIoU of 0.8417±0.0072, and FWIoU of 0.8454±0.0072.

Graph-based, clustering-based, and thresholding-based methods for image segmentation have been replaced in recent years by superpixel-based techniques. Although the superpixel segmentation technique, particularly salience detection, is widely employed in the field of computer vision, its applicability in biological imaging is relatively limited. Although the superpixel technique has been widely used in various biomedical image processing applications, such as brain MRI segmentation, optic disc segmentation, and glaucoma screening, few studies have explored its application in digital histopathology images. The superpixel technique plays a crucial role in histopathological image analysis, as cellular structures exhibit distinct characteristics across local regions. Conversely, deep learning models have been widely applied in medical image processing. Deep learning, a neural network-based approach, can be used to identify and segment digital images. Most of the proposed methods are divided into two stages. First, the SLIC superpixel technique is applied as a pre-segmentation step to separate cellular and non-cellular regions. Then, using a CNN-based deep learning model, the superpixels are classified, leading to the final segmentation of the entire image.

2.4.3 Machine Learning Techniques

Zhu and others [69] suggested that for a robot capable of autonomous navigation in a challenging outside environment, the terrain classification technique necessitates not only exact terrain classification findings but also clear boundary information of various terrains.

Although terrain classification may yield findings that are semantically meaningful, its border classification for mixed terrain is imprecise, making it impossible for the robot to accurately change its gait in real-time at separate terrain boundaries. The stability requirements for the robot will be impacted by this. To provide the robot with the ability to assess the terrain in real-time and carry out appropriate gait transformation and path planning, synthetic classifications based on superpixel segmentation are provided. The robot now has improved environmental adaptation and self-selection abilities when moving about. The mechanism for classifying terrain has also been improved, as have the methods that are now used to do so. Lastly, the robot has the ability to work alone outside.

Given the terrain classification of autonomous multi-legged walking robots, two synthetic classification methods are proposed: SLIC-based Support Vector Machine (SLIC-SVM) and SLIC-based SegNet (SLIC-SegNet). The SLIC-SVM is presented as a remedy for the SVM's limitation of producing a single terrain label, which prevents it from correctly identifying varied terrain. The SLIC-SegNet single-input multi-output terrain classification model is created to broaden the terrain classifier's usefulness. Given the difficulty of locating high-quality terrain classification data for use by legged robots, the SLIC SegNet efficiently acquires the needed data.

Achanta R and others [52] addressed the challenging yet essential problem of cloud recognition in the processing of remote sensing images. As remote sensing technology develops, there are increasing numbers of high-spatial-resolution remote sensing images accessible. They include a plethora of visual information that may be utilized to precisely characterize a surface's appearance. How to effectively, efficiently, and robustly distinguish objects in challenging scenarios is, therefore, a pressing topic in remote-sensing imaging processing, particularly for optical remote-sensing images. However, there are three significant flaws in the methods described above: The difficulties in identifying cloudy and bright non-cloudy locations (such as snow-covered lands) haven't been taken into account, segmentation and classification are done independently, and neural networks' complex architecture waste a lot of processing time.

The authors [70] offer a method for segmenting remote-sensing images, extracting traits from high-grey-level superpixel sub-regions, categorizing and identifying hazy areas. Segment quality is improved when a texture with six-dimensional feature vectors is applied to SLIC. The fusing of superpixel subregions is made easier by a voting-based clustering ensemble technique. The Ostu threshold is used to identify clouds, snow, and other bright objects. Selected superpixels' descriptors are then obtained and used in the softmax regression classification.

When extracting features employing the SLIC method, the superpixels function is useful. It creates areas out of pixels using similar values. These areas help streamline the process when used in image processing methods like segmentation. An image can be reduced from hundreds of thousands of pixels to just a few hundred superpixels thanks to superpixels' processing efficiency. Principal Componant Analysis (PCA) is a method of data analysis that minimizes data loss, enhances interpretability, and decreases dimensionality. It is also known as the "heart of the dimension reduction approach." It is also used to simplify the understanding and study of data. In order to reduce image complexity and execution time, the recommended approach makes use of both superpixels and PCA. Additionally, both approaches are utilized to extract traits that support segmentation and detection.

Smoke appeared in front of an individual as a result of blocked trees in the forest. Consequently, research into smoke detection has been applied to identify the position of the flare and to provide early warnings of forest fires by using digital images. Fractal theory has been used as a method for detecting smoke, as smoke patterns often exhibit self-similarity. Several scholars have recently examined this property to improve detection accuracy [71]. On the other hand, conventional forest fire smoke detection techniques only look at fire detection in a flawless image background and analyze the image down to the pixel level. In challenging environments like forests, it is not always feasible to recognize smoke. This study suggests a method for spotting smoke from forest fires in single frame still images. Forest fire detection is the first use of the superpixel segmentation technique. A unique superpixel merging method is created to solve the over-segmentation issue. The increased sky horizontal line segmentation approach is used to lessen the impact of the sky section on the detection. The SVM is then used to classify the superpixel block, with the method's adaptability avoiding the influence of the threshold that has been specified. The method works well in the scenario when the camera does dynamic panoramic sampling of the forest without considering the smoke's mobility characteristics. Additionally, it gets beyond the typical forest fire smoke detection algorithm's restriction

of requiring camera fixation.

Magana and others [72] SuperPIxel Classification for Cell dEtection and Counting (SPICE) technique for localizing and quantifying (total number of cells) cells in histology images. This technique uses a series of random forests and a superpixel pre-segmentation of the for categorization. A binary classifier, the first random forest, determines if the input superpixel has any cells. A second random forest acts as a multiclass classifier, identifying the number of cells that the original image pre-segmentation created inside the superpixels. Both classifiers have the ability to function alone. However, the experimental analysis showed that using them in sequence might lead to more precise results. One advantage of SPICE is the use of superpixels in segmentation, as it provides a more compact and accurate representation of the cells by incorporating features such as the color and shape of the superpixels. An analysis of threefold cross-validation was used to count the trees in each classifier. According to the results, the areas under the ROC curve (AUC) remain nearly the same when the number of trees is increased from 50 to 150 and 200, yielding AUC values of 97.21%, 97.27%, and 97.27%, respectively.

MK Islam and others [73] proposed a brain tumor detection algorithm using superpixels, PCA, and a template-based K-means algorithm to enhance identification accuracy for tumors of different sizes. This approach used superpixels and PCA to extract features from complex MR images that help the strategy for segmenting and identifying malignancies. According to experimental data, the suggested technique outperforms other conventional approaches in terms of detection accuracy and execution time (measured in seconds). The proposed method outperformed other existing detection techniques, attaining an accuracy of 95.00%, a sensitivity of 97.36%, and a specificity of 100% in brain tumor identification. Additionally, feature extraction, which reduced the size and complexity of MR images, required the use of superpixels and PCA. As a result, using the recommended method, brain tumors might be accurately identified from MR scans in 35 to 60 seconds.

2.4.4 Evolutionary Techniques

Evolutionary techniques, such as Genetic Algorithms (GA), have shown significant promise in addressing complex optimization problems in medical image segmentation and fusion. Various segmentation approaches have been proposed in the literature, which can generally be classified into four categories: (i) image-based strategies, (ii) feature-based techniques, (iii) physics-based

methods, and (iv) hybrid approaches. As noted by researchers [74], Positron Emission Tomography (PET) and Single Photon Emission Computed Tomography (SPECT) provide valuable functional information related to blood flow and metabolic activity; however, these modalities often suffer from limited spatial resolution. To overcome such limitations, multimodal medical image fusion combines complementary information from different imaging modalities.

Fusion methods are generally categorized into three levels: pixel-level, feature-level, and decision-level. Pixel-level approaches, although detailed, are computationally expensive and not suitable for region-based fusion. To address these issues, the author proposes a region-based multimodal image fusion framework that integrates a robust superpixel segmentation algorithm with an evolutionary feature optimization strategy. Specifically, the proposed framework employs fast superpixel segmentation using LSC, followed by region-wise feature extraction using a modified Log-Gabor Filter (LGF) and Smoothed Modified Laplacian (SML) to capture texture and contrast information.

A key innovation in the framework is the use of a GA for post-processing optimization, which adaptively adjusts the feature weights to enhance the quality of the fused image. To demonstrate the effectiveness of LSC, a comparative evaluation is performed using CT and PET images against three standard superpixel segmentation techniques: Ncuts, TurboPixel, and SLIC. While all methods produce superpixels of the same size, TurboPixel and SLIC frequently result in mixed-color superpixels, whereas LSC provides more coherent and homogeneous segmentation results.

Oriented FAST and Rotated BRIEF (ORB) [75] utilizes the oriented approach [76] as a fast corner detector, with detected corners represented by a modified Binary Robust Independent Elementary Features (BRIEF) descriptor [77]. Davidson and others [78] proposed a novel image stitching method using ORB descriptors, along with efficient transformation and local sensitivity hashing for rapid processing. This technique is applied in the automated analysis of adaptive optics ophthalmoscopy. Additionally, Adel and others [79] employed ORB to extract features from microscopic images of Oral Epithelial Dysplasia, using these features in an SVM for automated disease grading.

Speeded Up Robust Feature (SURF) [80] is a fast and efficient interest point detector that utilizes integral images for convolutions. The method operates in three stages: keypoint detection, description, and matching. Tackling the challenge of image stitching in biomedical research involving entire sections or large areas by applying the SURF technique for quick

and efficient feature extraction. Wang and Chen [81] tackled the issue of image alignment in X-ray and tissue images, comparing their method with five others: TrackEM2, UnwarpJ, BUnwarpJ, mutual information, and SURF. Their proposed technique showed superior outcomes across both datasets. Sanghavi and Agaian [82] presented an automated method for classifying histopathological images of prostate cancer using the bag-of-features approach. They conducted a comparative analysis between SURF and SIFT-based bag-of-features methods for feature extraction, finding that SURF demonstrated higher sensitivity compared to SIFT.

Gong and others [83] suggested a method for segmenting superpixels termed as DES. To get past the computational complexity issue, superpixel overlap is employed. DES employs global optimization to more effectively optimize this global characteristic. The optimization is then carried out by Differential Evolution (DE), a powerful stochastic global optimization method that mimics the evolution process in nature. The proposed method satisfies the computational constraint that, because of the low complexity of DE, it may produce promising superpixels with a linear computing complexity. The Berkeley segmentation benchmark [74] is utilized in the research to evaluate DES, and common performance measures are contrasted. When compared to several state-of-the-art superpixel segmentation techniques, DES performs equally well or better.

Data splitting and clustering efficacy may be assessed using a Clustering Validity Index (CVI) [84]. Such an index gauges how well the given clusters match the actual data structure. This work combined compactness, separation, and overlap as a novel clustering validity metric to improve segmentation accuracy. The notion of aggregation (represented by t norms and t-conforms) is used in the creation of a novel measure of overlap. A genetic algorithm-based optimizer is used to determine the ideal number of clusters and the optimal cluster centroids. Superpixels are also employed to reduce computational costs, ensuring the generation of well-defined segments.

Souad Larabi and others [85] considered four bio-inspired algorithm-based image segmentation methods—particle swarm optimization (PSO), genetic algorithms (GA), ant colony optimization (ACO), and artificial bee colonies (ABC)—to assist researchers in selecting the most effective segmentation approach. He also placed emphasis on techniques that are rarely used in this area in order to provide new opportunities for controlling and enhancing segmentation. The authors proposed two methods. The first involved modifying the objective functions, search strategies, or updating techniques of these methods, which have been depicted to improve the

Table 2.2: Codebook construction methods used in the bag-of-features. [86].

Category	**Methods**	**Comments**
Hierarchical methods	Agglomerative clustering, Mean shift	The high computing cost of these algorithms prevent them from being used for huge datasets or histological images.
Partitional methods	K-means, FCM, GMM	produces coding that is skewed towards crowded areas and not uniform; Non-robust; Optimal codebook size (K) is unambiguous.
Meta-heuristic-based methods	PSO, GSA, WOA, GWO	used to choose the best visual words using an objective function that takes into account separation and compactness; Computationally expensive.

effectiveness of the original approaches. The second approach suggested combining these techniques with another algorithm to enhance performance and address the limitations of each individual method.

SIFT and SURF features are known for their robustness to changes in scale, rotation, and illumination, whereas ORB offers computational efficiency. However, because of the complex morphological structures present in histopathological images, these methods often produce high-dimensional feature vectors.

2.5 Codebook construction

The next phase in the histopathological image analysis is codebook construction. Clustering is the technique used in codebook construction to group feature descriptors into visual words. Various clustering methods, detailed in Table 2.2, are discussed in the literature and can be categorized into three main types: hierarchical approaches, partitional approaches, and meta-heuristic-based approaches.

2.5.1 Hierarchical Clustering

In this approach, data is organized at different levels of similarity and represented by a tree structure called a dendrogram. This method generally follows two approaches: divisive and agglomerative.

In **divisive clustering**, the method begins with all data points in one cluster and repeatedly splits this cluster in a top-down manner until a stopping criterion is met or each data point

becomes its own cluster. Notable methods in this category include Divisive Hierarchical Clustering with the Diameter Criterion (DHCDC) [87] and Divisive Clustering using Monothetic Split (DIVCLUS-T) [88].

In contrast, **agglomerative clustering** works in a bottom-up manner, where every data point primarily forms its own cluster and then merges with other clusters iteratively to create larger clusters until a termination criterion is met or all data points are combined into one cluster. Prominent agglomerative methods include Balanced Iterative Reducing and Clustering using Hierarchies (BIRCH) [89], Clustering Using Representatives (CURE) [90] and Chameleon [91].

Authors [92] created an automated system for spectroscopic tissue image analysis, using hierarchical clustering for tissue segmentation and integrating tissue microarray analysis with fourier transforms of spectroscopic images for efficient high-throughput analysis. Meijnen and others [93] employed hierarchical clustering to categorize in-situ ductal carcinoma breast cancer images into two main groups, which were then subdivided into five subclasses based on six markers. This method was applied to analyze gene expression profiling. Additionally, Pourahmad and others [94] developed a framework for automated colorectal cancer grading, incorporating both hierarchical and partitional clustering methods. Their experimental findings showed that hierarchical clustering outperformed other clustering methods they tested.

Hierarchical methods usually adopt a greedy approach and do not re-evaluate data points once they have been assigned to a cluster, which restricts their ability to correct misclassifications. This limits their robustness, particularly in the presence of noise and outliers, and they do not optimize an objective function while constructing clusters. Furthermore, they struggle with overlapping clusters and necessitate prior knowledge of the required number of clusters. These methods can also lead to distortion in the formation of spherical clusters and disrupt the hierarchical structure [95]. A significant issue with hierarchical clustering, particularly on high-dimensional datasets like images, is its high time complexity, approximately $O(n^3)$ [96], where n represents the sum of data points. Hierarchical clustering approaches, including mean shift [97] and agglomerative clustering [98], are not ideal for large datasets or histology images due to their high computational cost. As a result, partitional clustering approaches are commonly favored to overcome these limitations, as elaborated in the following section.

2.5.2 Partitional Clustering

Partitional clustering is typically favored over hierarchical clustering, particularly for large datasets, because of its greater computational efficiency. In partitional clustering, similarity distance is commonly used as the measurement parameter. This method involves dividing the data into clusters based on an objective function, with the goal of grouping similar data points together and placing dissimilar points into different clusters. To accomplish this, each data point is compared to every cluster center and assigned to the closest one.

The general objective in partitional clustering is to minimize the within-cluster similarity, often calculated using euclidean distance. This objective function evaluates the quality of each cluster, ensuring the best representation among the created clusters. However, partitional methods may assign data points to clusters even if they are distant from the cluster centroid, potentially distorting cluster shapes or leading to inaccurate results, especially when noise or outliers are present [95]. Partitional clustering methods are generally classified into two categories: soft clustering and hard clustering.

Soft clustering techniques allocate each data point to one or more clusters, with the degree of membership determined through iteration. This membership degree provides a more nuanced representation of the association between data points. Notable methods in this category include Fuzzy C-means (FCM) [99], Fuzzy C-shells (FCS) [100], and the mountain method [101]. In FCM, clusters are represented as multidimensional hyperspheres, with the distance function defined respectively. The mountain approach uses a mountain function to identify cluster centers. Among these techniques, FCM is particularly popular and widely used.

Hard clustering methods partition data into distinct clusters based on an objective function. Typically, the objective function in partitional clustering methods is the sum of squared euclidean distances among data points and their associated centroids, which the method aims to minimize. In these approaches, the centroid of every cluster represents the average of the data points allocated to it. Unlike soft clustering, hard clustering assigns each data point to exactly one cluster, meaning the degree of belonging is binary: either 0 or 1.

A common hard clustering technique is K-means. In K-means, the cluster center is computed as the average of all data points assigned to it, with this process repeating iteratively until a predefined convergence condition is satisfied. Avni and others [102] developed patch-based visual words for categorizing and retrieving X-ray images. Researchers [103] applied the BOF

approach to represent visual features in histopathological images, using K-means to detect various visual words. Rueda and others [104] used K-means clustering for codebook creation in the bag-of-features method to classify MRI images of Alzheimer's disease. Wiliem and others [105] leveraged K-means clustering to generate a codebook from SIFT-based descriptors for classifying immunofluorescence images of human epithelial cells. Furthermore, Stanciu and others [106] employed the BOF method with K-means for codebook generation in diagnosing liver fibrosis using two-photon excitation microscopy. Consequently, numerous partitional clustering methods employed in the bag-of-features approach include K-means, FCM, and GMM [107]. The time complexity of the K-means method is $O(nkt)$ [96], where t represents the maximum number of iterations. K-means is sensitive to the initial placement of cluster centroids and can easily become trapped in local minima. Additionally, the results can vary depending on the number of clusters specified. As discussed above, these methods tend to be biased towards dense regions and may produce non-uniform coding.

2.5.3 Meta-heuristic-based Clustering

The first meta-heuristic algorithm, "simulated annealing" was proposed by Kirkpatrick and others [108]. This method was inspired by the annealing process in metallurgy and was a significant departure from deterministic optimization, laying the groundwork for future meta-heuristics like Genetic Algorithms, Tabu Search, and others. Then, the first meta-heuristic-based clustering was introduced by Selim and Alsultan [109] using simulated annealing. Later, Bezdek and others [110] pioneered a data clustering method based on genetic algorithms, representing the initial evolutionary approach to clustering. The first swarm-inspired clustering technique was created by Lumer et al. [111] utilizing ant colony optimization. Various meta-heuristic algorithms have shown promise in addressing clustering problems. Generally, these methods outperform traditional clustering approaches by being less dependent on initial parameter settings and by providing global optimal solutions [112]. Their effectiveness has made them a popular choice in clustering research. Meta-heuristic algorithms fall under optimization techniques designed to tackle computationally challenging problems, such as NP-complete problems. An NP-complete problem is one for which no deterministic algorithm can deliver an exact solution within polynomial time. These types of problems are particularly challenging because as the size of the problem grows, the time it takes to solve it increases exponentially. While many

optimization algorithms exist to solve these problems, the No Free Lunch Theorem [113] states that no single algorithm is universally efficient for all problems. This means that there is no one-size-fits-all solution—each optimization algorithm may perform better or worse depending on the problem at hand. Therefore, selecting the right algorithm often depends on the specific problem and its characteristics. Table 2.3 shows various meta-heuristic algorithms proposed by different researchers.

Table 2.3: Chronological overview of popular meta-heuristic algorithms.

Algorithm	**Year**	**Type**
Simulated Annealing (SA) [108]	1983	Physics-based
Genetic Algorithm (GA) [114]	1989	Evolutionary
Particle Swarm Optimization (PSO) [115]	1995	Swarm-based
Ant Colony Optimization (ACO) [116]	1996	Swarm-based
Differential Evolution (DE) [117]	1997	Evolutionary
Harmony Search (HS) [118]	2001	Music-inspired
Artificial Bee Colony (ABC) [119]	2005	Swarm-based
Firefly Algorithm (FA) [120]	2009	Swarm-based
Cuckoo Search (CS) [121]	2009	Bio-inspired
Bat Algorithm (BA) [122]	2010	Swarm-based
Charged System Search (CSS) [123]	2010	Physics-based
Grey Wolf Optimizer (GWO) [124]	2014	Swarm-based
Ant Lion Optimizer (ALO) [125]	2015	Swarm-based
Whale Optimization Algorithm (WOA) [126]	2016	Swarm-based
Sine Cosine Algorithm (SCA) [127]	2016	Math-based

Meta-heuristic approach utilizes meta-heuristic methods to achieve optimal image clustering. These algorithms generate random initial solutions and iteratively refine them based on predefined optimality criteria, known as the objective function [128]. These algorithms evaluate the objective function value using the generated solutions and must be efficient in finding the optimal solution effectively.

Researchers have developed numerous meta-heuristic algorithms inspired by natural phenomena to offer effective and best solutions. Over the past three decades, more than sixty such algorithms have been introduced. Each algorithm typically mimics specific natural processes, whether evolutionary, physical, or biological. Continuous efforts are being made to enhance existing algorithms and create new ones that deliver competitive results compared to those already available in the literature.

These algorithms usually contain two crucial elements: exploration and exploitation [129]. **Exploration** involves diversifying the search space by updating existing solutions, which helps

discover new solutions, avoids stagnation, and aids in finding a global solution. **Exploitation**, on the other hand, focuses on intensifying the search around current solutions to exploit the search space and converge towards the optimal solution. Meta-heuristic algorithms can generally be divided into two broad types: evolutionary algorithms and swarm algorithms.

Evolutionary-based algorithms draw inspiration from evolutionary theories, such as Darwin's theory of evolution. These algorithms operate on the principle of progressively generating improved solutions by combining the best individuals from the current generation. Key examples include: DE, GA, BBO.

Evolutionary Strategy [130] uses recombination and mutation with equal probability, utilizing numerous parents to produce offspring. Differential Evolution (DE) [117] a widely-used evolutionary algorithm introduced by Storm and others, which focuses on optimizing a problem through differential variations. Genetic Algorithm (GA) [131] is based on the evolution of natural species, GA employs mutation and crossover operators to achieve exploration and exploitation, respectively. Biogeography Based Optimization (BBO) [132] proposed by Simon is inspired by the immigration and emigration of species between islands in natural biogeography. Probability-Based Incremental Learning Algorithm [133] proposed by Dasgupta and others manages the statistical properties of the population rather than the entire population. Each of these algorithms uses different mechanisms and principles derived from biological processes to explore and exploit the search space effectively.

Swarm-based algorithms draw inspiration from the collective actions of natural groups, such as schools of fish or flocks of birds, to optimize outcomes. Particle Swarm Optimization (PSO), introduced by Kennedy [115] mimics the foraging habits of birds or fish. Ant Colony Optimization (ACO) is modeled after the trail-following behavior of ants [134]. The Gravitational Search Algorithm (GSA), developed by Rashedi and others [135], is based on newtonian principles of gravity and motion. Hosseini [136] introduced the intelligent water drop algorithm, which is inspired by river flow dynamics, typically following the most efficient path. Spider Monkey Optimization (SMO), created by Bansal and others [137] imitates the social behavior of spider monkeys. Mirjalili [125] designed the Ant-Lion Optimizer based on the predatory tactics of ant-lions, while his Moth-Flame Optimization algorithm models moths' navigation through transverse orientation.

More recent additions to swarm algorithms include the Small-World Optimization Algorithm [138], Galaxy-Based Search Algorithm [139], Ray Optimization [140], and Multi-Verse

Optimizer [141].

2.5.3.1 Whale Optimization Algorithm

The Whale Optimization Algorithm (WOA) is a nature-inspired metaheuristic optimization algorithm developed by Mirjalili and Lewis [126] in 2016. It is based on the bubble-net hunting strategy of humpback whales, a unique hunting mechanism where whales create spiral-shaped bubbles to encircle prey. WOA imitates this behavior by modeling three main processes: encircling prey, bubble-net attacking, and searching for prey.

The algorithm gained widespread recognition due to its simplicity, computational efficiency, and ability to effectively balance exploration (global search) and exploitation (local search). These features made WOA an attractive choice for solving a wide range of optimization problems, including continuous, discrete, and combinatorial optimization challenges.

WOA works in 3 steps as follows:

- Encircling Prey: This modeled the ability of humpback whales to locate prey and encircle it. In WOA, candidate solutions adjusted their positions relative to the current best solution.
- Bubble-Net Attack: This simulated the spiral motion of whales converging toward prey, modeled through a logarithmic spiral equation combined with random search directions.
- Search for Prey: In this phase, whales randomly searched the solution space, allowing exploration to identify promising regions and avoid local optima.

To overcome some limitations of the original WOA, such as premature convergence, slow convergence speed, and limited exploration, researchers proposed various enhanced versions and hybrids. There are mainly two strategies to overcome these limitation [142] (1) improvement approaches and (2) hybridization approaches.

Improvement approaches aim to fine-tune WOA's core mechanics to make it more effective at finding solutions. One of the earliest enhancements applied to WOA is Opposition-Based Learning (OBL), introduced by Tizhoosh [143] in 2017. OBL works by comparing a solution with its opposite, which increases the chances of finding better alternatives. This method helps diversify the population and makes the algorithm better at escaping local optima. In 2018, Yang and Deb [144] introduced another powerful technique called Lévy flight, inspired by patterns

in nature where random steps with large jumps allow exploration of larger areas. When applied to WOA, this approach makes it better at balancing global and local search efforts. In 2019, Li and others [145] explored using chaotic maps—mathematical models like logistic and sine maps—to introduce randomness into WOA. These maps improve the algorithm's diversity by helping it generate more varied initial solutions, reducing the risk of premature convergence. By 2020, Storn and Price [146] demonstrated how mutation and crossover strategies could refine WOA further. These strategies, originally from evolutionary algorithms, add controlled variations to solutions and help the algorithm avoid getting stuck in suboptimal points. For example, techniques like DE/rand/1 and DE/best/1 improve the balance between exploration and exploitation. Binary WOA variants, introduced by Almugren and Hossain [147] in 2020, adapted WOA for discrete optimization problems by using functions like sigmoid and V-shaped transformations to convert continuous solutions into binary ones. These innovations allowed WOA to tackle problems like feature selection more effectively. In 2022, Zhou and others [148] took WOA a step further by incorporating quantum-based techniques. They used principles from quantum computing, such as qubits and rotation gates, to dynamically adjust WOA's search behavior, making it highly effective for high-dimensional problems. Most recently, Chen and others [149] proposed a Balanced WOA (BWOA) that combines Lévy flight and chaotic local search. This version improved convergence rates and reduced the risk of getting stuck in local optima by bringing together multiple enhancement techniques into a single framework.

Hybridization approaches pair WOA with other optimization algorithms to overcome its limitations. These hybridizations have proven particularly useful in making WOA better at global search and handling complex problems. One notable example of population-based hybridizations is the work of Roy and others [150], who combined WOA with Differential Evolution (DE). DE, known for its perturbation and recombination mechanisms, complemented WOA's weaknesses and made the hybrid well-suited for multi-objective optimization problems like engineering design.

Physics-based hybridizations have also enhanced WOA's performance. Gao and others [151] integrated WOA with the Sine Cosine Algorithm (SCA), which introduced oscillatory behavior to dynamically adjust solution searches. This improved WOA's speed and made it more effective at balancing exploration and exploitation, especially in constrained optimization problems. Similarly, Swarm Intelligence (SI) hybridizations have been explored extensively. Researchers [152] also paired WOA with Particle Swarm Optimization (PSO) to im-

prove global search efficiency and population diversity. Their work showed that the WOA-PSO hybrid outperformed standard WOA in feature selection tasks, especially for high-dimensional datasets. To improve local search capabilities, Singh and Gupta [153] hybridized WOA with Tabu Search (TS). TS uses memory-based techniques to avoid revisiting previously explored solutions, which made this hybrid particularly effective at fine-tuning solutions in constrained optimization problems. Finally, in the field of multi-objective optimization, Martinez and others [154] developed variants of WOA that leverage Pareto dominance and scalarization methods to handle conflicting objectives. These approaches significantly expanded WOA's use in real-world problems like medical imaging, engineering, and logistics.

2.5.3.2 Grey Wolf Optimization

The social structure and hunting techniques of grey wolves in the wild serve as the model for the Grey Wolf Optimization (GWO) algorithm, which was initially presented by Mirjalili and others [124] in 2014. Alpha, beta, delta, and omega wolves' roles in a pack are modeled by GWO, which also considers their cooperative behavior to maximize solutions. This hierarchy enables GWO to strike a balance between exploration (searching the global solution space) and exploitation (locally refining solutions), as well as the algorithm's three primary hunting phases (encircling, hunting, and attacking prey). Despite being commended for its ease of use and efficiency, GWO has many drawbacks, including a tendency to become trapped in local optima, a lack of diversity in its solutions, and difficulties with high-dimensional issues. To overcome these obstacles, researchers have been working on GWO over the years, leading to several improvements and hybridizations.

In 2016, Kohli and others [155] introduced the Chaotic GWO (CGWO), which leveraged chaotic maps such as logistic, sine, and tent maps to improve the algorithm's exploration capabilities. By introducing randomness into the initialization phase and parameter adaptation, CGWO ensured better population diversity, allowing it to avoid premature convergence and local optima. This variant was applied successfully in constrained optimization problems, showing improved performance when compared to traditional algorithms like PSO and Firefly Algorithm (FA). Moreover, CGWO achieved faster convergence rates and demonstrated robustness in handling complex search spaces by effectively balancing exploration and exploitation. In 2017, Gao and Zhao [156] developed the Variable Weight GWO (VW-GWO), which refined the leadership structure within the wolf pack by introducing variable weights. This variant

assigned greater weights to alpha wolves and progressively smaller weights to beta and delta wolves, enforcing a stricter hierarchy in the optimization process. This adjustment ensured that the algorithm maintained a strong focus on exploitation in later stages while avoiding premature stagnation in local optima. VW-GWO showed improved convergence rates and better performance in tackling high-dimensional and non-linear optimization problems.

In 2018, Hu [157] proposed the Improved GWO (I-GWO), which incorporated the Dimension Learning-based Hunting (DLH) strategy. This strategy dynamically adjusted the position of each wolf in the population based on their roles (alpha, beta, delta, or omega), enabling more efficient exploration in the early stages and more effective exploitation later in the optimization process. I-GWO addressed issues of premature convergence and improved the algorithm's robustness, making it particularly effective in handling high-dimensional numerical optimization tasks. It also demonstrated superior performance on benchmark functions and real-world engineering problems. Tripathi and others [158] proposed a new clustering method for large datasets based on enhanced grey wolf optimization with the Map Reduce method (MR-EGWO) on hadoop framework. Results confirmed that this method outperformed the other 4 state-of-the-art methods.

Luo and others [159] introduced the Diversity Strategy-based GWO (DSGWO) to improve the exploration-exploitation balance. This variant incorporated a group-stage competition mechanism, where wolves were divided into groups and competed to refine their positions relative to the prey. Additionally, DSGWO employed a dynamic model for estimating the prey's location, which enhanced population diversity and ensured robust performance in dynamic optimization problems. The variant excelled on IEEE CEC 2014 benchmark functions and was successfully applied to complex engineering optimization tasks. In the same year, Gupta and Deep [160] developed the Fractional-order GWO (FWGWO), a random walk-inspired GWO variant that integrated stochastic movement strategies. By introducing random walk mechanisms, this variant improved the algorithm's ability to escape local optima and enhanced global search efficiency. FWGWO showed superior performance in optimizing global search spaces and demonstrated resilience in avoiding premature convergence, making it an effective tool for solving challenging optimization problems. In 2020, Emary [161] proposed the Enhanced GWO (EGWO), which incorporated reinforcement learning techniques to dynamically adjust search behaviors. This variant allowed the algorithm to adapt its exploration and exploitation strategies across different optimization stages. EGWO was particularly effective in feature se-

lection tasks, where it reduced dimensionality while maintaining accuracy and optimizing the weights of artificial neural networks. Its ability to dynamically fine-tune search behavior enabled EGWO to perform better in high-dimensional and non-linear optimization problems. In 2021, Khalilpourazari and Hashemi [162] introduced a gradient-based multi-objective GWO variant, which integrated Gaussian walks for improved modeling and prediction capabilities. The gradient-based enhancements allowed the algorithm to refine its search behavior, improving its ability to balance exploration and exploitation. This variant was particularly effective in addressing complex multi-objective optimization problems, achieving high accuracy and convergence reliability. In 2022, Hu [163] presented the GWO with Covariance Matrix Adaptation and Levy-based Opposition Learning (GWOCMALOL), a sophisticated variant that combined orthogonal learning, covariance matrix adaptation, and Lévy flight mechanisms. The orthogonal learning strategy enhanced the algorithm's adaptability by leveraging previously explored knowledge to improve current solutions, while covariance matrix adaptation optimized the search directions for convergence. Lévy flight mechanisms introduced large, random steps to escape local optima, improving the algorithm's robustness in high-dimensional optimization tasks. This variant outperformed traditional GWO and other metaheuristic methods in challenging benchmark problems and complex real-world applications.

Other notable GWO enhancements include the Accelerated GWO (AGWO) proposed by Kumar and others [164], which employed mathematical models to accelerate convergence rates and refine the balance between exploration and exploitation, and the Elite Opposition-Based Learning Strategy (EOBLS) GWO proposed by Yuan and others [165], which used elite opposition-based learning to improve solution quality and prevent stagnation. These additional variants further expanded GWO's applicability in solving optimization problems across fields such as engineering, medicine, and energy systems.

2.5.3.3 Applications of GWO and WOA

Because of their adaptability, both GWO and WOA can be used to address challenging optimization issues in a variety of domains. Some common applications of GWO and WOA and their variants are:

- **Engineering Design**: GWO and WOA are like problem-solving tools for engineers. They help design things like bridges, buildings, and airplanes by making them lighter, stronger,

and more cost-efficient. They're also used to fine-tune controllers in machines to make everything work more smoothly and efficiently, like a car running on cruise control.

- **Healthcare and Medicine**: In healthcare, these algorithms are super useful. They help doctors detect diseases like cancer or diabetes earlier by improving the accuracy of AI models. They're also used to analyze medical images, like MRIs or CT scans, by highlighting important areas like tumors. On top of that, they're even helping researchers in drug discovery by finding the best configurations for new medicines.

- **Image Processing**: When it comes to working with images, GWO and WOA shine. They're great at dividing images into useful sections, like spotting objects in images or identifying damaged areas in medical scans. They also make images look better by enhancing clarity and contrast, and they help pick out the most important features to improve things like facial recognition or image classification.

- **Renewable Energy**: These algorithms play a big role in making renewable energy systems more efficient. For example, they help position solar panels and wind turbines in the best spots to generate the most power. They're also used to manage energy in local grids, ensuring power is distributed efficiently without wasting resources. And for battery storage, they optimize charging and discharging cycles to extend battery life.

- **Artificial Intelligence and Machine Learning**: In AI, GWO and WOA are like assistants that make models smarter and faster. They help fine-tune settings in machine learning models, so they perform better without wasting time guessing the right parameters. They also improve clustering and classification tasks, making it easier to group similar data or categorize it correctly. And when it comes to neural networks, these algorithms can help train them more effectively by optimizing how they learn.

- **Communication Networks**: These algorithms are used in communication systems to make sure everything runs smoothly. For example, they help wireless networks find the best routes for sending data while saving energy. They're also used to design antennas with stronger signals and optimize how communication frequencies are allocated to avoid interference.

- **Robotics**: GWO and WOA help robots move in smart and efficient ways by finding the

best paths and avoiding obstacles. When many robots need to work together, such as in search and rescue missions or while mapping an area, these algorithms help them stay organized and work as a team without wasting time or energy.

- **Finance**: In the world of finance, these tools help investors make smarter decisions by finding the best combination of assets to maximize returns while reducing risks. They're also used in businesses to optimize how resources are allocated, saving money and increasing efficiency.

Moreover, meta-heuristic-based clustering methods, such as Whale Optimization Algorithm (WOA) [166], BBO [167], and the GSA [168], are employed to identify optimal visual words by optimizing objective functions related to compactness and separation. Mittal and Saraswat [168] introduced an enhanced version of the bag-of-features (BOF) method that uses GSA to generate optimal visual words. Their method was evaluated against the K-means clustering-based bag-of-features (BOF) approach for classifying tissue images. However, these techniques can become computationally intensive when handling complex histopathological images.

2.6 Feature Encoding Methods

The next step in the image classification process is feature encoding, where every image is represented by encoding its features into visual words. Every image is transformed into a coding vector of size k, where k denotes the number of visual words. Feature encoding methods are generally categorized into three main types based on their properties: voting, reconstruction, and super-vector-based encoding approaches [169]. A brief description of these techniques is also provided in Table 2.4. Generally, there are 3 types of feature encoding methods (1) Voting-based (2) Reconstruction-based and (3) Super vector-based.

2.6.1 Voting-based Methods

In the voting-based technique, every feature descriptor votes for a particular codeword according to predefined rules or strategies. This process results in the creation of a k-dimensional coding vector, known as a codeword. The collection of these codewords forms the entire codebook. Common approaches in this category include hard voting Vector Quantization (VQ) [30], Kernel Codebook Encoding (KCB), Soft Assignment (SA) [170], Localized Soft Assignment

Table 2.4: Types of feature encoding methods [169].

Type	Methods	Comments
Voting-based	HV, SA, LSA, Salient Coding	Based on how the distribution of visual words is represented by histograms
Reconstruction-based	OMP, Sparse coding, LLC, LCC	The visual words should recreate each feature by applying certain restrictions and resolving the least-squares optimization issue
Super vector-based	LTC, SVC, Fisher Vector, VLAD	The Gaussian mixture model is utilized to estimate feature distributions that comprise Gaussian weights, covariance, and means

(LSA) [171], and salient coding [172].

For each feature vector f, the voting value for the visual word v can be computed as a function of f, denoted as $c(i) = \phi(f)$. The specific formulation of $\phi(f)$ varies depending on the encoding method used. In hard voting methods, each feature vector votes for its nearest codeword.

Additionally, salient coding is a variant of hard vector quantization methods. In this approach, each feature computes its weighted vote based on the difference between the nearest visual word and the other $k-1$ nearest visual words [172]. The visual representation of each voting-based method is illustrated in Figure 2.3.

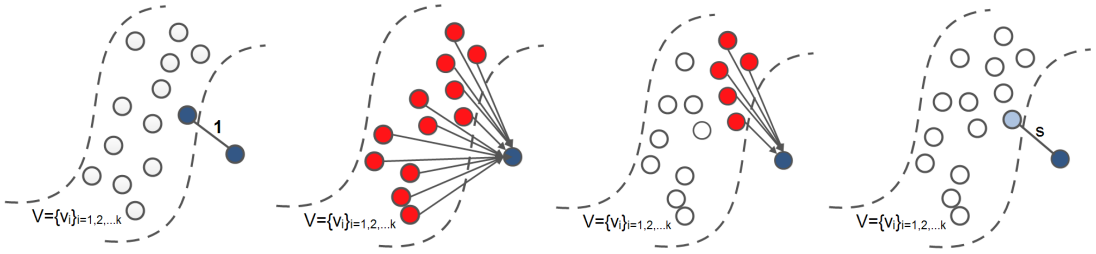

(a) VQ (b) SA (c) LSA (d) Salient Coding

Figure 2.3: Visual description of voting-based methods [169].

2.6.2 Reconstruction-based Methods

In these approaches, code c is generated with a focus on reconstruction or decoding. The objective is to reconstruct the i-th input descriptor from code c minimizing the error in the reconstruction process.

Prominent reconstruction methods encompass Sparse Coding (SPC) [173], Orthogonal Matching Pursuit (OMP) [174], Local Coordinate Coding (LCC) [175], and Locality-constrained Lin-

ear Coding (LLC) [176].

In the SPC and OMP methods, locality is not defined theoretically, but it is measured based on empirical analysis [175]. Therefore, Yu et al. [175] proposed a variant of SPC, namely LCC, wherein locality of the encoding is encouraged instead of sparsity. Moreover, Wang et al. [176] introduced a faster version, called LLC, for large-scale problems.

2.6.3 Super Vector-based Methods

In these techniques, higher-order statistics are integrated to create a high-dimensional representation. Important techniques in this field include Super Vector Coding (SVC) [177], Local Tangent-based Coding (LTC) [178], Fisher Vector (FV) [179] and the Vector of Locally Aggregated Descriptors (VLAD) [180].

In LTC [178], encoding is performed by approximating the feature manifold and its intrinsic dimensionality. The non-linear feature manifold is estimated to use a local linear function that satisfies the Lipschitz smooth condition, with the function representing the reduced intrinsic dimensionality from PCA. Zhou et al. [177] introduced a simple variant of LTC, called SVC, which replaces PCA with vector quantization. Another super-vector encoding method, the fisher vector, employs the fisher kernel and combines both generative and discriminative models. This approach is applied to large-scale image categorization [179]. Additionally, Jegou and others [180] proposed a more constrained version of the fisher vector, focusing only on first-order statistics for encoding.

Researchers [105] introduced an automated method for recognizing human epithelial cells. This approach represents each image as codebook descriptor vectors, which are organized into dual regions, and then classifies them using the nearest convex hull method. Different encoding methods, such as VQ, SPC and SA are employed to generate codebook descriptors. Nayak and others [17] applied sparse coding to identify distinct patches, like necrosis and viable tumor regions, in histological tissue samples. Similarly, Zhou and others [181] introduced an approach combining multispectral sparse coding and convolutions to classify histology tissue sections.

Voting-based encoding techniques are commonly used in histopathological image analysis. An additional variant, Learning Vector Quantization (LVQ), was introduced by Dieterle and others [182] for assessing urinary nucleosides, comparing it with neural networks and SVM. Mattfeldt and others [183] used LVQ for prostate incidental carcinoma classification. Addition-

ally, authors [184] proposed an advanced vector quantization version that outperformed standard VQ in pattern recognition tasks for pathological images. Han and others [185] developed a hierarchical vector quantization technique to detect pulmonary nodules in CT scans, utilizing both low as well as high-level VQ techniques to identify lung regions and nodule candidates. Diamant and others [186] applied VQ within the bag-of-features framework, choosing relevant visual words for automated medical image classification using mutual information. Nowakova and others [187] proposed an enhanced VQ method that integrates fuzzy s-trees and fuzzy signatures to improve the retrieval of medical images, particularly mammography scans.

2.7 Classification Techniques

A classifier is employed to assign labels or identify components within images by analyzing the features extracted from them. The effectiveness of these classifiers is significantly influenced by the depth and precision of the feature descriptors. Classifying histopathological images poses a considerable challenge for computational systems, which drives researchers to delve into this area with a focus on advancing machine intelligence techniques.

Table 2.5: Widely-used classification methods for histopathological image classification.

Classifier	**Details**
Random Forest [188]	The prediction is done based on the majority voting of different decision trees
Logistic Regression [189]	The score value is calculated based on the linear function for the prediction of the target class
Support Vector Machine [190]	Data is classified by the defined hyperplane and a new image is categorized based on hyperplane
Linear Discriminant Analysis [191]	The separation between two or more classes is found based on the linear combination of features
Bayesian Classifier [192]	Based on the conditional probability model where the classification is probabilistically related to the observed samples

Table 2.5 lists several commonly used classifiers from the literature [5], along with their applications in histopathological image classification. Mainly, classification techniques can be divided into 3 approaches: 1) classification using a traditional approach 2) classification using a deep learning approach 3) classification using a hybrid approach.

2.7.1 Classification using the Traditional Approach

Basavanhally and others [4] proposed an automatic algorithm to detect and grade the lymphocytes. Region growing and Markov random field algorithms were employed for detection, while support vector machines were utilized for classification. The evaluation of the proposed method was conducted using a dataset comprising 41 images. A classification accuracy of 90% was reported. The C-Path system is a model that Beck and others [193] created to quantify the characteristics of the stromal and epithelial areas of breast cancer tissues. Both morphometric and standard descriptors of image objects considered. Features, including global image features and higher-level contextual features, were considered.

Using several textural cues, Irshad and others [194] designed an automated system for mitosis detection. Co-occurrence features, run-length features, and scale-invariant feature transform were among the texture characteristics that were retrieved and applied to the classification. A technique for counting mitotic cells in histological images was put forward by Paul and others [195]. The mitotic nuclei and surrounding stromal regions were used to derive the intensity-based and Haralick characteristics. The mitotic and non-mitotic nuclei were categorized using a regenerative random forest classifier.

Researchers [196] presented a method based on the curvelet transformation with Local Binary Operators (LBP). From the images, the curvelet and LBP features were extracted. For classification, SVM, polynomial classifiers, random forests, and decision trees were employed. Jiang and others [197] suggested the joint kernel-based supervised hashing method. The suggested method incorporates complementing the hashing framework capabilities. There was a claimed 91% classification accuracy in 16.5 ms query time.

Reis and others [198] proposed a method to classify stromal regions with respect to their maturity. LBP and fundamental features were recovered at various scales. The stromal regions were categorized using a random decision tree classifier. The study made use of 55 H&E-stained images of invasive breast cancer. An 84% classification accuracy was recorded.

Dimitropoulos and others [199] identified the problem of invasive breast carcinoma grading utilizing the Grassmann manifold. A vector of locally collected descriptors encoding approach was devised. Their dataset showed a 95% classification accuracy, while BreakHis dataset showed a 91% classification accuracy.

A dictionary-based method for nuclear atypia grading was put forth by Das and others [200].

Nuclear pleomorphism was graded automatically using techniques like dictionary learning algorithms and sparse coding. A methodology for classifying Breast Cancer Histopathological Images (BCHI) was presented by Baker and others [201] that combined watershed methods for segmentation with K-means clustering. The segmented ROI was used to extract morphological features. Rule-based and decision tree classifiers exhibited an accuracy of 86% and 70%, respectively.

2.7.2 Classification using the Deep Learning Approach

Han and others [202] created a class structure-based DCNN architecture for BCHI multi-class categorization. On the BreakHis dataset, an average accuracy of 93% was recorded. Researchers [203] also provided a framework for nucleus-guided feature extraction. Cruz-Roa and others [204] suggested a CNN classifier for identifying the presence of invasive breast cancer using WSIs. Four hundred images from the Cancer Genome Atlas dataset were used to train the model, and 200 instances were used for validation. Gecer and others [205] suggested a FCNN architecture for detection and classification utilizing 240 WSIs of the breast. Burçak and others [206] created the DCNN architecture for BCHI classification.

Researchers [207] created the BreastNet architecture for categorization. Attention modules and hypercolumn approaches are combined in the architecture. Convolutional, dense, and residual blocks make up the architecture. On the BreakHis dataset, a 98% classification accuracy was recorded. A DCNN model was put forth by Li and others [208] to deal with the problems of class variance and feature extraction from images of varying magnification. The characteristics are extracted using the Xception model. Gour and others [209] created ResHist, a residual learning-based CNN for automatic BCHI diagnosis. There are 152 layers in the CNN architecture that was built. For binary classification, the ResHist model obtained an F1-score of 90% and an accuracy of 84%.

A hybrid structure was put up by Wang and others [210] for the classification of BCHI. Transfer learning and double-deep transfer learning algorithms were used to extract the high-level feature. The categorization performance was improved with the use of the interactive technique. It was found that the categorization accuracy ranged from 96 to 98%. Using a multilayer network, Sharma and Mehra [211] illustrated the impact of layer-wise fine-tuning on categorization. An eight-layer, pre-trained AlexNet architecture was used for the experiment.

The authors of this study concluded that a moderate degree of fine-tuning is the best option for classification.

Hirra and others [212] proposed a patch-based deep learning model (Pa-DBN-BC) to classify breast cancer on histopathological images using a deep belief network. The proposed model achieves an accuracy of 86%. Further, Kosaraju and others [213] proposed a framework to create HIPMap using a CNN. In this method, HIPMap is used to convert a whole side image of different shapes and sizes to a structured image representation. In the experiment on lung cancer, classification accuracy was reported as 96%.

2.7.3 Classification using a Hybrid Approach

Wan and others [214] proposed a multi-level feature-based classification method that extracted pixel, object, and semantic-level features using a CNN and an improved hybrid active contour model for nucleus segmentation. A cascaded SVM classifier trained on different feature subsets achieved 69% accuracy in multi-class breast cancer grading. Mehra and others [215] investigated transfer learning by comparing pre-trained networks, including VGG16, VGG19, and ResNet50, for magnification-independent breast cancer classification. Fine-tuned VGG16, combined with a logistic regression classifier, yielded the highest accuracy of 92.60% and an area under the ROC curve (AUC) of 95.65%, demonstrating the effectiveness of transfer learning. Bordou and others [216] did a comparative study on handcrafted feature-based methods, such as Bag of Words (BoW) and Locality-Constrained Linear Coding (LLC) combined with SVM classifiers, against CNN-based classification. The CNN approach outperformed the handcrafted feature-based models, achieving 96.15%–98.33% accuracy in binary classification and 83.31%–88.23% in multi-class classification, with dataset augmentation further improving performance. Researchers [217] employed deep learning techniques, including CNN, Long Short-Term Memory (LSTM), and a CNN-LSTM hybrid, to classify breast cancer images using the BreakHis dataset. Structural and statistical image features guided the learning process, and Softmax and SVM classifiers were used in the decision-making stage. The best accuracy of 91.00% was achieved at 200x magnification, while high precision and F-measure values were obtained at other magnifications. These studies demonstrated the potential of CNNs, SVMs, transfer learning, and hybrid deep learning approaches in improving the accuracy, efficiency, and reproducibility of breast cancer classification using histopathological images.

George and others [218] introduced a nucleus-guided transfer learning approach, "NucTraL+BCF," which used pre-trained CNNs as feature extractors combined with a belief theory-based classifier fusion strategy, achieving 96.91% accuracy. Wang and others [219] proposed a deep learning and machine learning hybrid approach by extracting multi-network features from DenseNet-121, ResNet-50, InceptionV3, and VGG-16 and applying Dual-network Orthogonal Low-rank Learning (DOLL) for feature selection. An Ensemble SVM (E-SVM) was then trained using fused features and a voting strategy, achieving 97.70% accuracy on the ICIAR 2018 dataset. Sharma and Mehra [220] presented a comparative study on explored handcrafted features (Hu moments, color histograms, Haralick textures) with conventional classifiers versus transfer learning using VGG16, VGG19, and ResNet50 for magnification-dependent classification on the BreakHis dataset. The VGG16 network with linear SVM achieved the highest accuracy, with patch-based results of 93.97% (40×), 92.92% (100×), 91.23% (200×), and 91.79% (400×). Saxena and others [221] evaluated ten different pre-trained CNNs as unsupervised feature extractors for breast cancer recognition from BreakHis dataset images. Feature sets from these CNNs were classified using a linear SVM, outperforming state-of-the-art methods. These studies highlighted the effectiveness of transfer learning, ensemble learning, and feature fusion in improving breast cancer detection and classification from histopathological images.

Nasir and others [222] proposed a hybrid approach by fusing handcrafted and deep features, where HOG and LBP features were combined with pre-trained VGG19 and InceptionV3 models. PCR and ICR were used to evaluate classification performance, achieving a patient-level accuracy of 97.2% and an image-level accuracy of 96.7%. Zerouaoui and Idri [223] explored 28 hybrid architectures using seven deep-learning models for feature extraction (e.g., DenseNet201, InceptionV3, ResNet50, VGG19) and four classifiers (MLP, SVM, DT, KNN). The best-performing model, using DenseNet201 with an MLP classifier (MDEN), achieved 99% accuracy on the FNAC dataset and 92.61%, 92%, 93.93%, and 91.73% on BreakHis at magnifications of 40X, 100X, 200X, and 400X, respectively. Khazaee and Rezaee [224] a model for Colorectal Cancer (CRC), a dilated ResNet (dResNet) with an attention module was used to generate deep feature maps, followed by neighbourhood Component Analysis (NCA) for feature selection and a Deep Support Vector Machine (DeepSVM) for classification. The hybrid model achieved 98.75% and 99.76% accuracy on CRC-5000 and NCT-CRC-HE-100K datasets, respectively, outperforming state-of-the-art methods. Almubarak and others [225] proposed a cervical cancer classification that used a fusion-based hybrid approach combining

handcrafted and deep learning features for squamous epithelium classification into Cervical Intraepithelial Neoplasia (CIN) grades. By partitioning epithelium into 10 vertical segments and extracting 27 handcrafted features alongside CNN-based features, the hybrid method improved classification accuracy by 15.51% and 11.66% over individual deep learning and imaging methods, achieving an overall accuracy of 80.72%. These studies demonstrate the effectiveness of hybrid models in improving cancer classification and early detection.

2.8 Comparative Summary of Metaheuristic Methods

A variety of histopathological image analysis techniques have been developed over the past decade, ranging from traditional clustering and superpixel segmentation to recent meta-heuristic and hybrid deep learning frameworks. These methods differ considerably in feature extraction strategy, optimization objective, and computational complexity.

Table 2.6 summarizes the representative state-of-the-art approaches reported in the literature along with their respective datasets, performance metrics, and limitations. The comparison highlights that conventional clustering and early deep-learning methods often suffer from stain sensitivity, class imbalance, and lack of feature-selection efficiency. Baseline multi-objective algorithms such as MOGWO and MOWOA achieve improved accuracy but exhibit slower convergence and reduced stability in high-dimensional feature spaces. The proposed EMOGWO-SC and IMOWOA-FS frameworks extend these optimizers with adaptive exploration–exploitation and opposition-based learning, thereby addressing redundancy and improving accuracy and computational efficiency.

Table 2.6: Comparative summary of existing and baseline meta-heuristic methods for histopathological image analysis.

Author / Year	**Methodology**	**Dataset**	**Performance Metric(s)**	**Gaps / Limitations**
Cruz-Roa et al. (2014)	Deep CNN for basal-cell carcinoma detection	Private skin dataset	Accuracy 94.3%	Limited dataset size; risk of overfitting; no feature selection.
Xu et al. (2016)	Stacked Sparse Autoencoder for nuclei detection	Breast histopathology	Dice 0.89	Struggles with irregular nuclei; high computational cost.
Arevalo et al. (2017)	Unsupervised feature learning (ICA, autoencoders)	Colon and breast histology	Accuracy 92.1%	Poor generalization across stains and magnifications.
Yuan et al. (2018)	Superpixel segmentation with SLIC0 optimization	Glioma MRI and histopathology	Dice 0.8492	Parameter-sensitive; irregular segmentation in dense regions.
Albayrak & Bilgin (2020)	Hybrid CNN with SLIC-based segmentation	BreakHis	Accuracy 95.2%	Sensitive to stain variation; no feature reduction stage.
Taha et al. (2021)	Superpixel-based SARS-CoV-2 spike density analysis	COVID-19 microscopy	Correlation 0.91	Focused on density estimation, not classification.
Standard MOGWO (2022)	Multi-objective Grey Wolf Optimizer for feature selection	BreakHis	Accuracy 96.2%	Slower convergence; may get trapped in local optima; no adaptive exploration.
Standard MOWOA (2022)	Multi-objective Whale Optimization Algorithm for feature selection	BreakHis	Accuracy 96.5%	Unstable convergence in high-dimensional search space; lacks leader diversity.
Proposed Work (2025)	EMOGWO-SC + IMOWOA-FS integrated framework	BreakHis (H&E)	Segmentation 96.4%; Classification 98.1%	Addresses redundancy; enhances accuracy and speed; reduces computational complexity.

2.9 Research Gaps and Objectives

After reviewing the literature, the following sections discuss the identified research gaps and research objectives.

2.9.1 Research Gaps

1. Most unsupervised learning methods suffer from problems such as sensitive to initial parameters settings, returning local optimal solutions, and requiring knowledge about number of to be formed.

2. Usually, nature-inspired algorithms consider a single objective, like intra-cluster distance, to perform clustering which presents only a single view of the data.

3. Single-objective methods are not sufficient to provide high accuracy and robustness.

4. There exists no method to partition efficiently a histology image into different regions of interest.

5. A new method is required for feature selection to identify discriminative and relevant features from the histopathological images.

6. There is very little work done in the past for a meta-heuristic-based bag-of-features method for automated histopathological image classification.

2.9.2 Objectives

After examining the research gaps, the subsequent research objectives are defined:

1. Design and development of an efficient image segmentation method to partition a histology image into different regions of interest.

2. To design and develop a new feature selection method to identify discriminative and relevant features from the histopathological images.

3. To design and develop an efficient meta-heuristic-based bag-of-features method for automated histopathological image classification.

2.10 Summary

This chapter presented a comprehensive review of existing methodologies for histopathological image analysis, covering the core stages of image representation, segmentation, feature extraction, feature selection, and classification. It began with an overview of image representation techniques, categorized into statistical, learning-based, and mid-level approaches. Statistical methods rely on handcrafted features such as texture, color, and shape, while learning-based techniques utilize models such as convolutional neural networks and autoencoders. Mid-level methods, including the bag-of-features model, aggregate local features to form global image descriptors.

Superpixel-based segmentation techniques were reviewed and grouped into watershed-based, graph-based, energy optimization, and clustering-based categories. The chapter also examined the application of computational intelligence methods, including machine learning, deep learning, and evolutionary algorithms, in improving segmentation and interpretation of complex histopathological images.

Additionally, codebook construction methods using hierarchical, partitional, and metaheuristic clustering algorithms were analyzed, with particular attention to the Whale Optimization Algorithm and Grey Wolf Optimization. Feature encoding and classification techniques were discussed, ranging from conventional machine learning models to advanced deep learning and hybrid approaches. Finally, the chapter identified key research gaps and outlined the main research objectives of the thesis.

CHAPTER 3

EFFICIENT IMAGE SEGMENTATION USING EMOGWO-SC

This chapter introduces the proposed Enhanced Multi-Objective Grey Wolf Optimizer-based Superpixel Clustering (EMOGWO-SC) method, which represents a novel multi-objective clustering approach for nuclei segmentation in histopathological images. Furthermore, it presents a comprehensive comparative analysis of the proposed method against three existing multi-objective nature-inspired algorithms to evaluate its effectiveness and robustness.

3.1 Introduction

Histological images are the golden standard in breast cancer diagnosis, and hematoxylin and eosin (H&E) staining of such images is the standard staining protocol [226]. In a manual analysis of these images, there are several issues to be handled, such as analysis variation due to differences in the observer's experience, time-taking process, and difficulty identifying subtle visual features [5]. However, the digitization of pathology systems has successfully mitigated such concerns [227]. In digital pathology, the segmentation of nuclei from the histopathological image is the foremost unit whose accuracy determines the efficiency of the system [228]. For the same, there are many nuclei segmentation methods defined over approaches like superpixels, clustering, active contours, watershed, and multi-level thresholding [229], [230], [8]. Among them, superpixels are one of the efficient approaches for segmentation. Therefore, this chapter introduces an efficient nuclei segmentation method based on superpixels for histopathological images.

Superpixels divide the image into non-overlapping regions wherein similar pixels are grouped together [231]. The boundary of each irregular-shaped superpixel is according to the edge information in the original image. This makes each superpixel perceptualy meaningful [232], [52].

Various computer-vision applications like, image segmentation [233], depth estimation [234], object localization [235], body model estimation [236], bag-of-features [237] [238] and skeletonization [239] employ superpixels to obtain mid-level representations. Fouad et al. [231] employed unsupervised learning on superpixels to segment a cancer image into different tissues. In literature, it has been observed that unsupervised learning is quite advantageous for histopathological image analysis as these methods are efficient in identifying anatomical structures in an image [231][238].

Generally, unsupervised learning methods work on the principle of clustering the unlabeled data into homogeneous clusters according to the considered criteria such as intra-cluster distance [240], [241], [242]. Some of the popular unsupervised learning methods are K-means and Fuzzy C-Means [243] [244]. However, there are a number of demerits in such methods, such as sensitive towards initial parameters settings, returning local optimal solutions, and requiring knowledge about cluster numbers to be formed [245], [246], [247]. Nature-inspired algorithms have emerged as effective solutions for generating efficient clusters and have addressed a range of real-world optimization problems [248], [249], [168], [250]. Some widely recognized nature-inspired algorithms include the Genetic Algorithm (GA) [251], Biogeography-Based Optimization (BBO) [252] [167], Salp Swarm Optimization (SSO)[253], Gravitational Search Algorithm (GSA) [254], Whale Optimization Algorithm (WOA)[255], and Grey Wolf Optimizer (GWO) [256]. These algorithms typically focus on single objectives, such as minimizing intra-cluster distance, to perform clustering, which provides a limited perspective on the data [257], [258]. To obtain better clusters, multi-objective criteria have been a better alternative as they presents multiple views while clustering the data, which results in comparatively better segmented images. In the literature, there are a number of multi-objective nature-inspired algorithms that try to optimize multiple objective functions simultaneously. Some popular multi-objective nature-inspired algorithms are Non-dominated Sorting GA (NSGA-II) [259], Pareto-Archived Evolution Strategy (PAES) [260], and Strength-Pareto Evolution Algorithm (SPEA) [261]. Multi-Objective GWO (MOGWO) is a recent multi-objective nature-inspired algorithm that has been inspired by the behavior of grey wolves. However, this algorithm suffers from several disadvantages, such as a lack of population diversity, high computational time, and limited exploration capability.

Figure 3.1 illustrates sample images taken from a publicly available breast cancer histopathological dataset [262], to depict the involved complexity. **Image (a)** shows a densely packed cel-

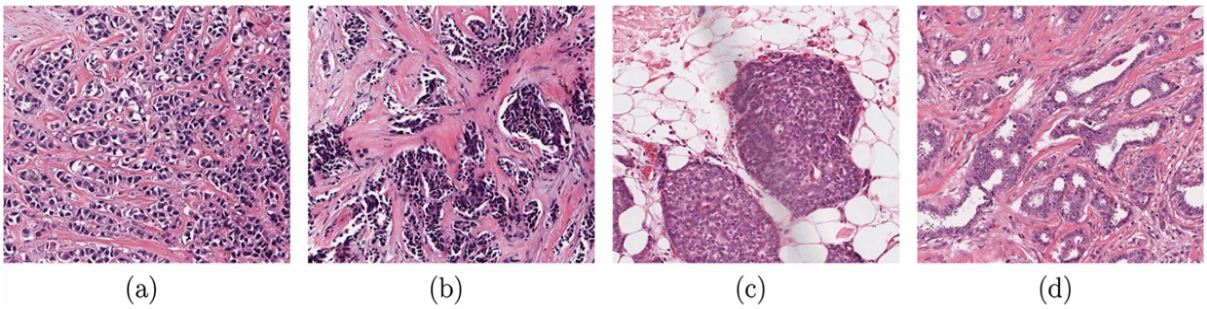

Figure 3.1: Histopathological image scanned at $\times$ 40.

lular region with overlapping nuclei, indicative of high-grade malignancy. **Image (b)** displays glandular formations with irregular borders and varying nuclear sizes, representing architectural distortion often observed in invasive carcinoma. **Image (c)** captures well-circumscribed clusters of tumor cells surrounded by adipose tissue, highlighting the heterogeneity in tissue composition. **Image (d)** presents a fibroglandular region with dispersed epithelial structures embedded within a stromal matrix, reflecting the complex microenvironment of breast tissue.

Histopathological images are rich in information but also incredibly complex. These images, often captured at extremely high resolutions, encompass a vast amount of information, requiring computationally intensive methods to process. One major issue is the variability introduced by differences in staining protocols, which can affect color consistency and hinder the generalization of machine learning models. Additionally, the biological heterogeneity within tissue samples, such as the presence of various cell types, structural abnormalities, and inconsistent tumor morphologies, adds another layer of difficulty in accurate interpretation. Annotation is also a significant challenge, as it demands extensive expert input and is often subject to inter-observer variability. Moreover, relevant features can exist across multiple scales, from cellular to tissue-level structures, necessitating multi-scale modeling approaches. These challenges are further compounded by the need for interpretability and seamless integration into clinical workflows, highlighting the importance of robust, explainable, and adaptable computational tools in the field of digital pathology.

A novel variant of the Multi-Objective Grey Wolf Optimizer, referred to as the Enhanced Multi-Objective Grey Wolf Optimizer (EMOGWO), is introduced in this chapter and utilized for effective nuclei segmentation in histopathological images. Segmenting nuclei in such images is a challenging task due to several factors, including non-uniform nuclei shapes, overlapping structures, variability in tissue texture, inconsistent stain absorption, and artifacts in-

troduced during the scanning process [229], [263], [264]. Clustering-based techniques have shown promise in addressing these challenges. In this context, the chapter presents a new multi-objective clustering method, termed EMOGWO-based Superpixel Clustering (EMOGWO-SC), which aims to optimally and efficiently cluster superpixels to facilitate accurate nuclei segmentation from histopathological images. Thus, the main contributions of this chapter are:

1. A new variant, EMOGWO, has been proposed.
2. A novel multi-objective clustering method (EMOGWO-SC) is introduced, which efficiently clusters the superpixels to segment the nuclei from a histopathological image.
3. The proposed EMOGWO is compared against three other multi-objective nature-inspired algorithms on 10 well-known multi-objective benchmarks.
4. To validate the performance of the proposed method (EMOGWO-SC), a publicly available dataset, H&E-stained Estrogen Receptor Positive (ER+) breast cancer images, has been considered and experimental comparison is conducted against MOGWO-based Superpixel Clustering (MOGWO-SC) and K-means-based Superpixel Clustering (K-means-SC) in terms of computation time and segmentation accuracy.

The remaining chapter is organized as follows; "Preliminaries" briefs a superpixel method and MOGWO. The proposed EMOGWO-SC, along with EMOGWO, is presented in "Proposed multi-objective clustering method for nuclei segmentation". Experimental analysis is conducted in "Experimental Analysis", followed by the conclusion in "Conclusion".

3.2 Preliminaries

3.2.1 SLIC: A Superpixel Method

superpixels are atomic and compact regions in an image that are formed after over-segmentation. Generally, superpixels are utilized for obtaining a mid-level representation of an image [265]. One of the efficient methods for generating superpixels is Simple Linear Iterative Clustering (SLIC) [52]. It requires only a single input to operate, i.e., number of superpixels (K) to be formed. In SLIC, two phases are followed, i.e., initialization and local clustering [52], [266]. The initialization phase corresponds to the random initialization of A centroids at an interval of $P = \sqrt{\frac{U}{A}}$. Here, U represents the total pixels in an image. In the local clustering phase, the

distance (T) of the k^{th} superpixel centroid from all the neighborhood pixels within the interval $2P \times 2P$ is measured according to Eq. 3.1.

$$T(i,k) = \sqrt{\left(\frac{{d_c}^2}{m}\right) + \left(\frac{{d_s}^2}{S}\right)} \tag{3.1}$$

Where m corresponds to the constant and i represents the i^{th} image pixel. For k^{th} superpixel and i^{th} image pixel, d_c measures the euclidean distance in the CIELab color space, which is defined in Eq. 3.2 while d_s computes the euclidean distance in the spatial space according to Eq. 3.3.

$$d_c(i,k) = \sqrt{(l_i - l_k)^2 + (a_i - a_k)^2 + (b_i - b_k)^2} \tag{3.2}$$

$$d_s(i,k) = \sqrt{(x_i - x_k)^2 + (y_i - y_k)^2} \tag{3.3}$$

The measured value of D is used to assign every pixel to the nearest superpixel centroid. Then, the mean of all the assigned pixels is computed to update the corresponding centroid of the superpixels. This process is followed till the residual error is converged. In post-processing, the unassigned pixels are assigned to the nearest superpixels.

3.2.2 Multi-Objective GWO

MOGWO is the multi-objective version of GWO [124]. The basic working of MOGWO is inspired by GWO only, but there are two distinguishing components in MOGWO. The first component corresponds to the archive set, and the other component is the leader selection. Pareto optimal solutions in an iteration are stored as an archive set (ACH), which depicts the set of solutions that are non-dominated by any other solution. Let an optimization problem P need to optimize three objective functions, namely f_1, f_2, and f_3. Let there be two solutions, X and Y. A solution X dominates an another solution Y if X is better than Y in at least one of the objectives f_i and not worse than other objectives. In case X does not dominate Y and Y does not dominate X, they are called non-dominated solutions. These solutions are considered as better solutions than other solutions in the population.

In MOGWO, an archive manager is used to regulate the movement of non-dominated solutions within the archive set. The following rules of movement are followed on the archive set:

1. If the new solution W is dominated by any solution of the ACH, then W can be included in the ARC.

2. If the new solution W dominates one or more solutions of the ACH, the dominated solutions are removed from the ACH and W is added.

3. If neither of the conditions is met, then also W is added.

4. If the ACH reaches its full capacity, the grid mechanism is used to identify the most crowded segments, from which one solution is removed. Afterwards, the new solution W is added to the segment with the least crowding to preserve diversity.

To update the leader, the leader selection method is applied to the updated ACH. Similar to GWO, the leaders, i.e., α, β, and δ wolves are selected from the archive set, which represents the three best solutions. For choosing the three best solutions, fitness values are sorted, and the first three values are selected, namely, α, β, and δ. The other solutions in the population update the respective positions according to these leaders only. Therefore, the leader selection method is key to the efficient performance of MOGWO.

For leader selection, a probability function P_i is defined according to the density of the solution. Assume there are S number of non-dominated solutions in i^{th} segment, then P_i is defined as per Eq. 3.4.

$$P_i = \frac{const}{S_i} \tag{3.4}$$

Where $const > 1$. from Eq. 3.4, it can be observed that the probability of picking a solution from highly crowded segments is less, which is a good indication to maintain the diversity in the population [267]. This will redirect the search to less crowded segments and explore the search space to find better solutions. Thus, MOGWO ensures diversity within the population and systematically explores different areas of the search space to identify the optimal solutions. The position update equations and other steps of the MOGWO algorithm according to GWO [124].

3.3 Proposed Multi-Objective Clustering Method for Nuclei Segmentation

3.3.1 Proposed Method

A new multi-objective clustering method, EMOGWO-SC is presented for optimal segmentation of nuclei from a histopathological image. The block diagram of the proposed method is illustrated in Figure 3.2.

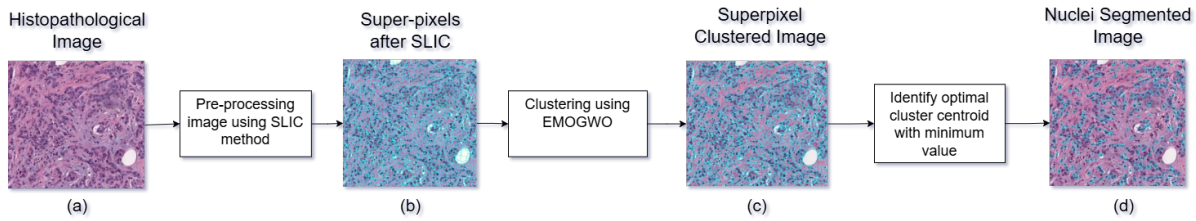

Figure 3.2: Proposed EMOGWO-based segmentation framework. The process includes image preprocessing, superpixel generation using the SLIC method, clustering through enhanced multi-objective optimization, and fuzzy membership–based threshold selection. Legend: $f_1 =$ intra-cluster distance (compactness), $f_2 =$ inter-cluster distance (separability).

The proposed EMOGWO-SC method begins with the input of an H&E-stained histopathological **Image (a)**. This original image contains various tissue components such as nuclei, cytoplasm, and background structures. The image is first processed using the SLIC method, as shown by the transition to **Image (b)**. In this step, the image is divided into compact and homogeneous regions known as superpixels, which simplify the image representation while preserving essential boundaries.

These superpixels i.e **Image (b)**, are then used as input for the clustering stage. As illustrated in **Image (c)**, the EMOGWO algorithm is employed to perform clustering based on multiple objective criteria. The generated superpixels are further optimally clustered into 'g' clusters by employing the proposed EMOGWO.

For the same, two objective functions are considered, i.e., minimizing the intra-cluster distance and maximizing the inter-cluster distance. Intra-cluster distance measures the compactness of clusters while inter-cluster distance computes the separation among clusters. These two objective functions will help in achieving better clustering quality and optimal cluster centers. Therefore, the proposed method optimizes two objective functions simultaneously which are defined in Eq. 3.5 and Eq. 3.6, respectively. Following clustering, the cluster centroid with the minimum intensity value is identified as likely corresponding to nuclei regions, helping isolate

the nuclei from other tissue parts.

The final output, shown in **Image (d)**, is the nuclei-segmented image. In this image, the nuclei are effectively identified and highlighted, making it suitable for further quantitative and morphological histopathological analysis.

$$Argmin_{\{C_1,C_2,C_3,\cdots,C_i,\cdots,C_g\}} : \sum_{j=1}^{g}\sum_{i=1}^{p} ||C_j - x_i||^2 \tag{3.5}$$

$$Argmax_{\{C_1,C_2,C_3,\cdots,C_i,\cdots,C_g\}} : \sum_{j=1}^{g}\sum_{i=1,i\neq j}^{g} ||C_j - C_i||^2 \tag{3.6}$$

Where 'g' and 'p' correspond to the number of required optimal clusters and total pixels in the image, respectively. Further, C_j represent the j^{th} cluster centroid while x_i is the i^{th} image pixel.

In a H&E stained histopathological image, nuclei regions are highlighted with dark color [268]. Therefore, the minimum average cluster is segmented as the nuclei region. The pseudo-code of the proposed method is presented in Algorithm 3.1; a detailed explanation of the algorithm is as follows.

Step 1. Input: An H&E stained histopathological image X of size $m \times n$, and the maximum number of iterations $T_{\max}$.

Step 2. Output: A segmented image where the nuclei regions are accurately identified.

Step 3. Superpixels Generation: Apply the SLIC algorithm on image X to generate superpixels. This reduces computational complexity and makes groups of similar pixels into meaningful regions.

Step 4. Initialization of EMOGWO: Initialize a population of N individuals for the EMOGWO. Each individual represents a possible clustering solution.

Step 5. Cluster Centroid Initialization:

- For each individual, initialize g cluster centroids $\{C_1, C_2, \ldots, C_g\}$.
- Each centroid C_i is a d-dimensional vector, $\{c_1, c_2, \ldots, c_d\}$, based on superpixel features.

Step 6. Optimization Loop: For each iteration $t = 1$ to $T_{\max}$, repeat:

- Evaluate the fitness of each individual based on multiple objective functions (e.g., intra-cluster compactness, inter-cluster separation).
- Update the positions of individuals using the EMOGWO strategy, which mimics the leadership hierarchy and hunting behavior of grey wolves.

Step 7. Best Solution Selection: After completing all iterations, select the best individual (solution) based on the final fitness values.

Step 8. Superpixels Clustering: Use the selected best individual's cluster centroids to perform clustering on the superpixels.

Step 9. Nuclei Identification: Identify the cluster with the minimum intensity value, as it typically corresponds to nuclei regions. This forms the final segmented output.

The same is represented in flowchart Figure 3.3. Further, the proposed variant, EMOGWO, is discussed in the following section.

Algorithm 3.1 Multi-objective clustering method for nuclei segmentation

Input: A H&E stained histopathological image X of size $m \times n$; maximum iterations $T_{\max}$
Output: Nuclei segmented image
Generate superpixels by executing SLIC method on X;
Initialize the population of EMOGWO with N individuals;
for each individual $j = 1$ to N **do**
    Initialize g cluster centroids $\{C_1, C_2, \cdots, C_g\}$;
end for
Each C_i is defined as $\{c_1, c_2, \cdots, c_d\}$ for d-dimensional superpixels;
for $t = 1$ to $T_{\max}$ **do**
    for each individual $j = 1$ to N **do**
        Compute the fitness fit according to the objective functions;
    end for
    Update each individual based on the EMOGWO algorithm;
end for
Select the best individual based on final fitness values;
Cluster the superpixels using the best individual's centroids;
The cluster centroid with the minimum intensity corresponds to the nuclei regions.

3.3.2 Enhanced MOGWO (EMOGWO)

In MOGWO, two new components have been introduced: the archive set and the leader selection method. The archive set contains the non-dominated solutions, while the leader selection

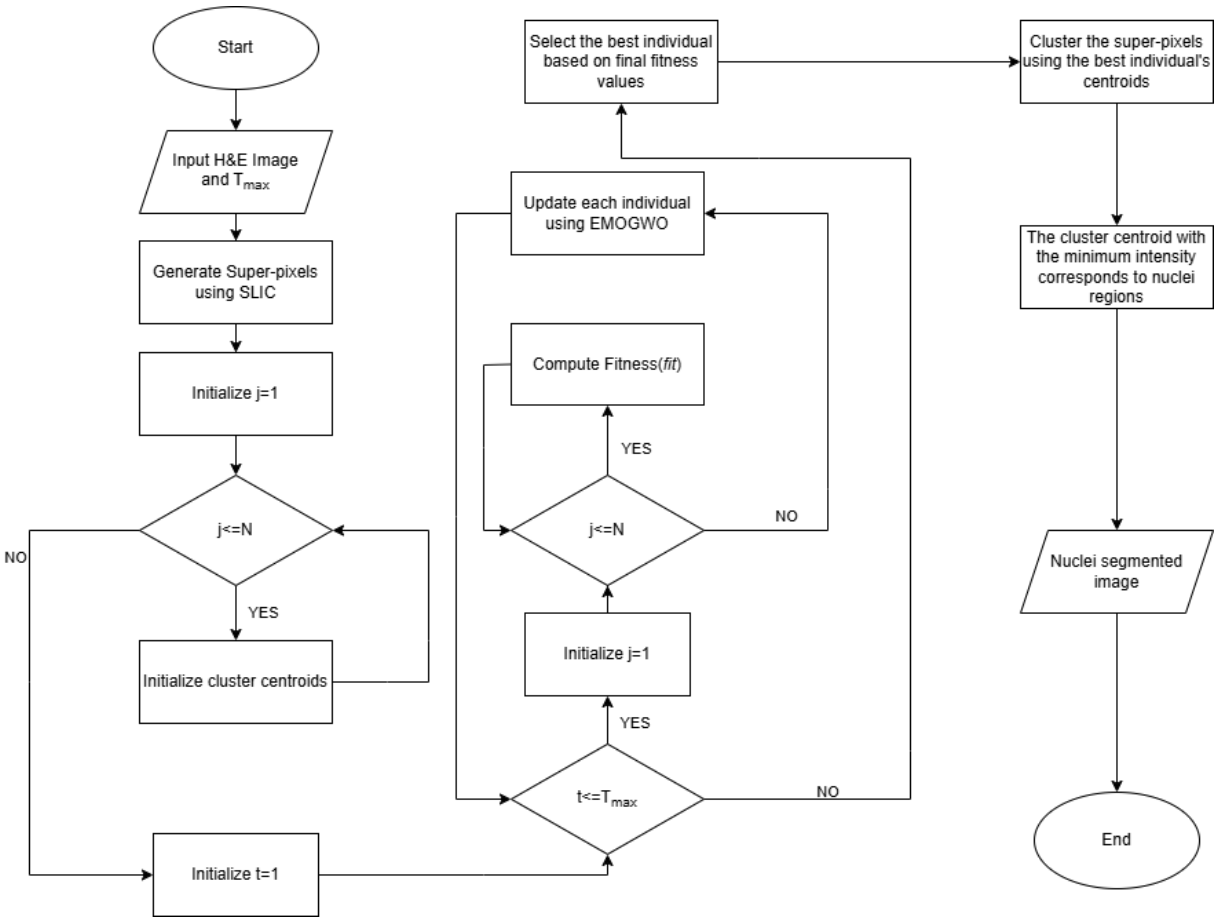

Figure 3.3: Flowchart of the proposed multi-objective clustering method for nuclei segmentation using EMOGWO.

method identifies the three best solutions from the least crowded segment in the population. However, this may lead to a problem. In case there are fewer than three solutions in the less crowded segment, then another least crowded segment will be evaluated to select the leaders. If this scenario remains the same in the second less crowded segment also, then the third less crowded segment will be selected. This results in increased time complexity. Therefore, this chapter proposed an Enhanced MOGWO (EMOGWO) with an enhanced leader selection method.

In the proposed method, the whole population is divided into different segments. The segment number is allocated to each solution i based on Eq. 3.7.

$$x_i = 1 + n_i \tag{3.7}$$

Where, x_i represents segment number of solution i and n_i represents the number of solution that dominate solution i. Hence, for the non-dominated solutions, the segment number will always

be 1. The maximum segment number will always be less than the total number of solutions in the population. Once the population is divided into segments, less crowded solutions will be identified. Therefore, for every solution i in each segment, the crowding count (cc_i) is calculated using Eq. 3.8.

$$cc_i = \sum_{j=1}^{\lambda(x_i)} h(d_{ij}) \tag{3.8}$$

Where, $\lambda(x_i)$ is the number of solutions in each segment number x_i and $h(d_{ij})$ is calculated by Eq. 3.9.

$$h(d_{ij}) = \begin{cases} 1 - (\frac{d_{ij}}{thres}) & if d \leq thres \\ 0 & Otherwise \end{cases} \tag{3.9}$$

Where *thres* is selected between zero and one and may change based on the application while d_{ij} is the distance between two solutions i and j in the objective space having M objectives. The calculation of distance is given by Eq. 3.10.

$$d_{ij} = \sqrt{\sum_{o=1}^{M} \left(\frac{f_o^i - f_o^j}{f_o^{max} - f_o^{min}} \right)^2} \tag{3.10}$$

Where f_o^{max} and f_o^{min} are the maximum and minimum fitness value of o^{th} objective and f_o^i, f_o^j are the fitness values of solutions i and j in o^{th} objective respectively.

Now, the selection of the three best solutions will be according to the roulette wheel selection, based on the following probability for each segment.

$$p_i^k = \frac{c}{cc_i} \tag{3.11}$$

Where c is a constant greater than one and cc_i the crowding count of solution i in the segment k.

From Eq. 3.11, it can be observed that if the cc_i is high, then the probability of this solution becoming the leader will be less. This indicates that less crowded solutions will be selected. This improves the population diversity and exploration capability of the algorithm.

3.3.3 Novelty of the Proposed EMOGWO-SC Method

The proposed **Enhanced Multi-Objective Grey Wolf Optimization-based Superpixel Clustering (EMOGWO-SC)** introduces three major innovations. First, it integrates fuzzy membership-based adaptive thresholding within a multi-objective optimization framework to enhance nuclei boundary detection. Second, it employs adaptive leader selection to improve convergence rate and maintain population diversity within the MOGWO algorithm. Third, the method jointly optimizes *intra-cluster distance* and *inter-cluster distance* objectives, ensuring compact and well-separated clusters with high segmentation precision and reduced computation time. These improvements collectively enable more accurate and robust nuclei segmentation compared to existing approaches such as *K-means-SC* and standard *MOGWO-SC*.

3.4 Experimental Results

The performance of the proposed automatic nuclei segmentation method has been experimented in two sections. First, Section 3.4.1 showcases the efficiency of the proposed multi-objective grey wolf optimizer on ten well-known CEC-2009 multi-objective benchmark functions [269] in which the proposed EMOGWO is validated qualitatively on 7 bi-objective and 3 tri-objective test problems. Second, in Section 3.4.2, EMOGWO is used for nuclei segmentation within H&E stained breast cancer histology images. For a fair analysis, all the experiments have been performed using MATLAB 2017a on a system having a 2.66 GHz Intel Core i3 processor and 8 GB of RAM.

3.4.1 Evaluation Parameters for Efficiency

To investigate the efficiency of the proposed EMOGWO method a set of comparison parameters is proposed. The comparison parameters we have used are described as follows.

3.4.1.1 IGD

Inverted Generational Distance (IGD) is a performance metric used to evaluate the quality of solutions (approximated Pareto front) obtained by a multi-objective optimization algorithm compared to a true Pareto front (ideal set of optimal trade-offs). The mathematical equation of IGD is an enhanced version of Generational Distance (GD) [270], [271] which is introduced by

Sierraand Coello [272] and formulated in Eq. 3.12.

$$IGD = \frac{\sqrt{\sum_{j=1}^{n} dis_j^2}}{n} \tag{3.12}$$

Where n represents the true optimal Pareto solutions, and dis_j refers to the Euclidean distance between the j^{th} true Pareto optimal and the closest computed Pareto optimal solutions in the reference set.

Interpretation:

- Lower IGD = The approximate solutions are closer to the true Pareto front and better distributed.

IGD considers both convergence (how close the solutions are to the true front) and diversity (how well they cover it).

3.4.1.2 SP

Spacing (SP) is a diversity metric used in multi-objective optimization to measure how evenly distributed the solutions are along the approximated Pareto front. It evaluates whether the solutions are spread out uniformly or clustered in some regions. SP helps assess the distribution quality of the solution set. The spacing is defined as [261].

$$SP = \sqrt{\frac{1}{n-1}\sum_{j=1}^{n}(dis' - dis_j)^2} \tag{3.13}$$

Where dis' is the mean of all dis_j, n is the number of optimal Pareto solutions obtained so far, and $dis_j = \min_j(|f_1^i(\vec{x}) - f_1^j(\vec{x})| + |f_2^i(\vec{x}) - f_2^j(\vec{x})|)$ for all $i, j = 1, 2, 3, \cdots, n$.

Interpretation:

- Lower SP value $\rightarrow$ More uniform distribution $\rightarrow$ Better diversity
- Higher SP value $\rightarrow$ Uneven spacing $\rightarrow$ Poor spread

3.4.1.3 MS

Maximum Spread (MS) is a diversity metric used to measure the range (or extent) of the approximated Pareto front in objective space. It indicates the breadth of the solution set, specifically whether it spans the entire true Pareto front. The maximum spread is defined as [261].

$$MS = \sqrt{\sum_{j=1}^{t} \max(det(a_i, b_i))} \tag{3.14}$$

here, $det()$ computes the Euclidean distance, a_j, b_j represent the maximum and minimum value in j^{th} objective and t is the total number of objectives.

Interpretation:

- Higher MS = Better range coverage of the objective space
- Lower MS = Solutions are clustered, covering a smaller part of the Pareto front

3.4.1.4 Mean Ranking

Mean Ranking is a comparative metric used to aggregate the performance of different algorithms across multiple quality indicators (like IGD, SP, MS, etc.). The mean ranking is defined as [273].

$$\text{MeanRank}_j = \frac{1}{M} \sum_{i=1}^{M} r_{i,j} \tag{3.15}$$

where M is number of performance metrics and $r_{i,j}$ is rank of algorithm j on metric i.

Interpretation:

- Ranking each algorithm for each metric.
- Then, computing the average rank across all metrics.
- The algorithm with the lowest mean rank is considered the overall best.

3.4.1.5 Dice Coefficient

The dicce coefficient is a statistical measure used to gauge the similarity between two sets. Dice coefficient is defined as [274].

$$\text{Dice} = \frac{2TP}{2TP + FP + FN} \tag{3.16}$$

3.4.1.6 Box Plot

A box plot (also known as a box-and-whisker plot) is a statistical chart used to summarize the distribution of a dataset [275].

Interpretation:

- Higher or lower medians → Difference in central tendency
- Narrower boxes → Less variability (more consistent performance)
- More/fewer outliers → More/less extreme behavior
- Skewed box (median closer to Q1 or Q3) → Skewed distribution

3.4.2 Performance Analysis of EMOGWO

The proposed EMOGWO has been tested over 10 multi-objective benchmark functions including 7 bi-objectives (UF_1 - UF_7) and 3 tri-objective test problems (UF_8 - UF_{10}) [141], [269]. Figures 3.4 and 3.5 tabulate these benchmark functions along with definitions. Table 3.1 tabulates the initial parameter settings for all the considered algorithms. The benchmark functions are considered as the most challenging test problems in the literature, which include different multi-objective search regions with non-convex, convex, multi-modal, and dis-continuous Pareto fronts.

Name	Mathematical formulation
UF1	$f_1 = x_1 + \frac{2}{\lvert J_1\rvert}\sum_{j\in J_1}[x_j - \sin(6\pi x_1 + \frac{j\pi}{n})]^2,\ f_2 = 1-\sqrt{x} + \frac{2}{\lvert J_2\rvert}\sum_{j\in J_2}[x_j - \sin(6\pi x_1 + \frac{j\pi}{n})]^2$
	$J_1 = \{j \mid j \text{ is odd and } 2 \le j \le n\},\ J_2 = \{j \mid j \text{ is even and } 2 \le j \le n\}$
UF2	$f_1 = x_1 + \frac{2}{\lvert J_1\rvert}\sum_{j\in J_1} {y_j}^2,\ f_2 = 1-\sqrt{x} + \frac{2}{\lvert J_2\rvert}\sum_{j\in J_2} {y_j}^2$
	$J_1 = \{j \mid j \text{ is odd and } 2 \le j \le n\},\ J_2 = \{j \mid j \text{ is even and } 2 \le j \le n\}$
	$y_j = \begin{cases} x_j - [0.3x_1^2\cos(24\pi x_1 + \frac{4j\pi}{n}) + 0.6x_1]\cos(6\pi x_1 + \frac{j\pi}{n}) & \text{if } j \in J_1 \\ x_j - [0.3x_1^2\cos(24\pi x_1 + \frac{4j\pi}{n}) + 0.6x_1]\sin(6\pi x_1 + \frac{j\pi}{n}) & \text{if } j \in J_2 \end{cases}$
UF3	$f_1 = x_1 + \frac{2}{\lvert J_1\rvert}(4\sum_{j\in J_1} y_j^2 - 2\prod_{j\in J_1}\cos(\frac{20y_j\pi}{\sqrt{j}}) + 2) f_2 = \sqrt{x_1} + \frac{2}{\lvert J_2\rvert}(4\sum_{j\in J_1} y_j^2 - 2\prod_{j\in J_2}\cos(\frac{20y_j\pi}{\sqrt{j}}) + 2)$
	$J_1 \text{and} J_2 \text{are the same as those of} UF1,\ y_j = x_j - x_1^{0.5(1.0+\frac{3(j-2)}{n-2})},\ j = 2,3,\ldots,n$
UF4	$f_1 = x_1 + \frac{2}{\lvert J_1\rvert}\sum_{j\in J_1} h(y_j),\ f_2 = 1 - x_2 + \frac{2}{\lvert J_2\rvert}\sum_{j\in J_2} h(y_j)$
	$J_1 \text{and} J_2 \text{are the same as those of} UF1,\ y_j = x_j - \sin(6\pi x_1 + \frac{j\pi}{n}),\ j = 2,3,\ldots,n,\ h(t) = \frac{\lvert t\rvert}{1+e^{2\lvert t\rvert}}$
UF5	$f_1 = x_1 + (\frac{1}{2N} + \epsilon)\lvert\sin(2N\pi x_1)\rvert + \frac{2}{\lvert J_1\rvert}\sum_{j\in J_1} h(y_i),\ f_1 = 1 - x_1 + (\frac{1}{2N} + \epsilon)\lvert\sin(2N\pi x_1)\rvert + \frac{2}{\lvert J_2\rvert}\sum_{j\in J_2} h(y_i)$
	$J_1 \text{amd} J_2 \text{are identical to those of} UF1,\ \epsilon > 0,\ y_j = x_j - \sin(6\pi x_1 + \frac{j\pi}{n}),\ j = 2,3,\ldots,n$
	$h(t) = 2t^2 - \cos(4\pi t) + 1$
UF6	$f_1 = x_1 + \max\{0, 2(\frac{1}{2N} + \epsilon)\sin(2N\pi x_1)\} + \frac{2}{\lvert J_1\rvert}(4\sum_{j\in J_1} y_j^2 - 2\prod_{j\in J_1}\cos(\frac{20y_j\pi}{\sqrt{j}}) + 1))$
	$f_2 = 1 - x_1 + \max\{0, 2(\frac{1}{2N} + \epsilon)\sin(2N\pi x_1)\} \frac{2}{\lvert J_2\rvert}(4\sum_{j\in J_2} y_j^2 - 2\prod_{j\in J_2}\cos(\frac{20y_j\pi}{\sqrt{j}}) + 1))$
	$J_1 \text{amd} J_2 \text{are identical to those of} UF1,\ \epsilon > 0,\ y_j = x_j - \sin(6\pi x_1 + \frac{j\pi}{n}),\ j = 2,3,\ldots,n$
UF7	$f_1 = \sqrt[5]{x_1} + \frac{2}{\lvert J_1\rvert}\sum_{j\in J_1} y_j^2,\ f_2 = 1 - \sqrt[5]{x_1} + \frac{2}{\lvert J_2\rvert}\sum_{j\in J_2} y_j^2$
	$J_1 \text{amd} J_2 \text{are identical to those of} UF1,\ \epsilon > 0,\ y_j = x_j - \sin(6\pi x_1 + \frac{j\pi}{n}),\ j = 2,3,\ldots,n$

(a)

Figure 3.4: Bi-objective test problems.

Name	Mathematical formulation
UF8	$f_1 = \cos(0.5x_1\pi)\cos(0.5x_2\pi) + \frac{2}{\lvert J_1\rvert}\sum_{j\in J_1}(x_j - 2x_2\sin(2\pi x_1 + \frac{j\pi}{n})^2)$
	$f_2 = \cos(0.5x_1\pi)\sin(0.5x_2\pi) + \frac{2}{\lvert J_2\rvert}\sum_{j\in J_2}(x_j - 2x_2\sin(2\pi x_1 + \frac{j\pi}{n})^2)$
	$f_3 = \sin(0.5x_1\pi) + \frac{2}{\lvert J_3\rvert}\sum_{j\in J_3}(x_j - 2x_2\sin(2\pi x_1 + \frac{j\pi}{n})^2)$
	$J_1 = \{j \mid 3 \le j \le n,\ \text{and } j-1 \text{ is a multiplication of } 3\},\ J_2 = \{j \mid 3 \le j \le n,\ \text{and } j-2 \text{ is a multiplication of } 3\},$ $J_3 = \{j \mid 3 \le j \le n,\ \text{and } j \text{ is a multiplication of } 3\},$
UF9	$f_1 = 0.5[\max\{0, (1+\epsilon)(1-4(2x_1-1)^2)\} + 2x_1]x_2 + \frac{2}{\lvert J_1\rvert}\sum_{j\in J_1}(x_j - 2x_2\sin(2\pi x_1 + \frac{j\pi}{n})^2)$
	$f_2 = 0.5[\max\{0, (1+\epsilon)(1-4(2x_1-1)^2)\} + 2x_1]x_2 + \frac{2}{\lvert J_2\rvert}\sum_{j\in J_2}(x_j - 2x_2\sin(2\pi x_1 + \frac{j\pi}{n})^2)$
	$f_3 = 1 - x_2 + \frac{2}{\lvert J_3\rvert}\sum_{j\in J_3}(x_j - 2x_2\sin(2\pi x_1 + \frac{j\pi}{n})^2)$
	$J_1 = \{j \mid 3 \le j \le n,\ \text{and } j-1 \text{ is a multiplication of } 3\},\ J_2 = \{j \mid 3 \le j \le n,\ \text{and } j-2 \text{ is a multiplication of } 3\},$ $J_3 = \{j \mid 3 \le j \le n,\ \text{and } j \text{ is a multiplication of } 3\},\ \epsilon = 0.1$
UF10	$f_1 = \cos(0.5x_1\pi)\cos(0.5x_2\pi) + \frac{2}{\lvert J_1\rvert}\sum_{j\in J_1}[4y_j^2 - \cos(8\pi y_j) + 1]$
	$f_2 = \cos(0.5x_1\pi)\sin(0.5x_2\pi) + \frac{2}{\lvert J_2\rvert}\sum_{j\in J_1}[4y_j^2 - \cos(8\pi y_j) + 1]$
	$f_3 = \sin(0.5x_1\pi) + \frac{2}{\lvert J_3\rvert}\sum_{j\in J_1}[4y_j^2 - \cos(8\pi y_j) + 1]$
	$J_1 = \{j \mid 3 \le j \le n,\ \text{and } j-1 \text{ is a multiplication of } 3\},\ J_2 = \{j \mid 3 \le j \le n,\ \text{and } j-2 \text{ is a multiplication of } 3\},$ $J_3 = \{j \mid 3 \le j \le n,\ \text{and } j \text{ is a multiplication of } 3\},$

(a)

Figure 3.5: Tri-objective test problems.

Table 3.1: Parameter settings for all the considered algorithms.

Sr.No.	Parameter	MOPSO	MOEA/D	MOGWO	EMOGWO
1.	Population Size (N)	50	50	50	50
2.	Number of iterations (itr)	1000	1000	1000	1000
3.	Number of search agents	8	8	8	8
4.	Number of repetitive runs	10	10	10	10
5.	Inertia weight (w)	0.8	–	–	–
6.	Acceleration constants ($c1, c2$)	2	–	–	–
7.	Grid inflation parameter (α_p)	0.01	–	–	–
8.	Leader selection pressure parameter β_p parameter	4	–	–	–
9.	Mutation rate (CR)	–	0.5	–	–
10.	Distribution index (η)	–	30	–	–
11.	Probability of selecting parents (δ)	–	0.9	–	–
12.	α parameter	–	–	0.99	0.99
13.	β parameter	–	–	0.01	0.01

The performance parameters IGD, SP, and MS quantitatively validate the efficacy as it compare the mean and standard deviation values of all the considered algorithms. Thus, to qualitatively validate the performance, the best set of Pareto optimal solutions of each algorithm are compared. To do a comparative analysis, the proposed EMOGWO is compared with MOGWO [141], MOPSO [272], and MOEA/D [276]. To reduce the interference effect and for a fair analysis, each algorithm has been run 10 times. Moreover, the number of iterations (itr) and population size (N) in all the considered algorithms are set as 1000 and 50, respectively, and all other parameters are taken from respective literature. To appraise the efficacy of the proposed EMOGWO, it is compared with all the considered algorithms in terms of mean, standard deviation, median, worst, and best values of IGD, SP, and MS. Tables 3.2 - 3.4 depict the IGD, SP, and MS values returned by the proposed EMOGWO and other considered algorithms. From Table 3.2, it is observed that the proposed EMOGWO obtains the best IGD values for more than 90% of benchmark problems. IGD values are good indicators for benchmarking the convergence of different algorithms. So, the results depicted in Table 3.2 signify the better convergence of the proposed EMOGWO. There are a few benchmark problems such as $UF3$, $UF6$, and $UF7$, in which MOEA/D obtains the best IGD values while MOPSO shows better results than proposed and other considered algorithms for benchmark $UF8$. Thus, from the above analysis, it can be said that the suggested EMOGWO's performance is more consistent than other considered algorithms.

Furthermore, SP and MS values are also compared in Tables 3.3 and 3.4. As MOEA/D is not implemented in MATLAB for tri-objective benchmark problems UF8, Uf9, and UF10. There-

Table 3.2: Statistical results of all the considered algorithms for IGD on UF1 to UF10.

Functions	Algorithms	Average	Median	STD. Dev.	Worst	Best
UF1	MOPSO	.1370	.1317	.0441	.2279	.0899
	MOEA/D	.1871	.1829	.0507	.2464	.1265
	MOGWO	.1144	.1130	.0195	.1577	.0802
	EMOGWO	.0858	.0848	.0147	.1183	.0602
UF2	MOPSO	.0604	.0484	.0276	.1305	.0370
	MOEA/D	.1223	.1201	.0107	.1437	.1049
	MOGWO	.0583	.0578	.0074	.0732	.0498
	EMOGWO	.0437	.0433	.0055	.0549	.0374
UF3	MOPSO	.3140	.3080	.0447	.3777	.2565
	MOEA/D	.2886	.2893	.0159	.3029	.2634
	MOGWO	.2557	.2509	.0807	.3679	.1295
	EMOGWO	.1918	.1882	.0605	.3129	.0971
UF4	MOPSO	.1360	.1343	.0074	.1519	.1273
	MOEA/D	.0681	.0685	.0021	.0704	.0647
	MOGWO	.0587	.0587	.0005	.0594	.0580
	EMOGWO	.0440	.0440	.0004	.0445	.0435
UF5	MOPSO	2.2024	2.1257	.5530	3.0384	1.4648
	MOEA/D	1.2915	1.3376	.1349	1.4675	1.1231
	MOGWO	.7971	.6994	.3786	1.7386	.4680
	EMOGWO	.5978	.5246	.2839	1.3039	.3510
UF6	MOPSO	.3540	.3873	.2044	.6151	.0540
	MOEA/D	.4552	.4377	.1898	.6770	.0290
	MOGWO	.1604	.0734	.1391	.4014	.0628
	EMOGWO	.1674	.0550	.1043	.3011	.0471
UF7	MOPSO	.3540	.3873	.2044	.6151	.0540
	MOEA/D	.4552	.4377	.1898	.6770	.0290
	MOGWO	.1604	.0734	.1391	.4014	.0628
	EMOGWO	.1427	.0653	.1238	.3573	.0558
UF8	MOPSO	.5367	.5364	.1826	.7964	.2453
	MOEA/D	–	–	–	–	–
	MOGWO	2.0578	2.3360	1.1455	3.8789	.4613
	EMOGWO	.5957	.5954	.2027	.8840	.2723
UF9	MOPSO	.4885	.4145	.1445	.7221	.3336
	MOEA/D	–	–	–	–	–
	MOGWO	.1917	.1660	.0925	.4479	.1291
	EMOGWO	.1630	.1411	.0786	.3807	.1097
UF10	MOPSO	3.5945	2.8255	3.4883	2.9564	1.0431
	MOEA/D	–	–	–	–	–
	MOGWO	1.6372	1.5916	.2988	2.1622	1.2201
	EMOGWO	1.4735	1.4325	.2689	1.9460	1.0981

fore, the efficiency of the proposed EMOGWO is only compared with MOPSO and MOGWO for these benchmark problems. It can be seen from the tables that the proposed EMOGWO shows better coverage and convergence. Although there are some discontinuities on the Pareto optimal front obtained by EMOGWO, such as the coverage of the whole front is broader than that of MOGWO, MOPSO, and MOEA/D for most of the benchmark problems. However, the Pareto optimal solutions of the proposed EMOGWO are closer to the true Pareto optimal

front and evenly distributed for both bi and tri-objectives. Thus, from the statistical results, the efficacy of the proposed algorithm can be easily observed.

Table 3.3: Statistical results of all the considered algorithms for SP on UF1 to UF10.

Functions	Algorithms	Average	Median	STD. Dev.	Worst	Best
UF1	MOPSO	.0090	.0086	.0025	.0146	.0067
	MOEA/D	.0038	.0038	.0015	.0067	.0021
	MOGWO	.0124	.0054	.0146	.0464	.0008
	EMOGWO	.0128	.0122	.0035	.0209	.0096
UF2	MOPSO	.0083	.0081	.0017	.0125	.0062
	MOEA/D	.0088	.0086	.0008	.0104	.0080
	MOGWO	.0096	.0082	.0031	.0158	.0066
	EMOGWO	.0111	.0095	.0036	.0182	.0076
UF3	MOPSO	.0070	.0068	.0017	.0101	.0048
	MOEA/D	.0268	.0251	.0206	.0626	.0008
	MOGWO	.0459	.0486	.0145	.0705	.0155
	EMOGWO	.0519	.0549	.0164	.0797	.0175
UF4	MOPSO	.0067	.0066	.0009	.0081	.0055
	MOEA/D	.0073	.0073	.0006	.0084	.0061
	MOGWO	.0097	.0086	.0039	.0172	.0058
	EMOGWO	.0109	.0097	.0044	.0195	.0066
UF5	MOPSO	.0048	.0049	.0041	.0121	.0001
	MOEA/D	.0028	.0001	.0055	.0162	.0000
	MOGWO	.1523	.0878	.1625	.5125	.0084
	EMOGWO	.1706	.0983	.1820	.5740	.0094
UF6	MOPSO	.0208	.0124	.0326	.1114	.0022
	MOEA/D	.0063	.0000	.0127	.0303	.0000
	MOGWO	.0145	.0111	.0125	.0411	.0019
	EMOGWO	.0165	.0127	.0142	.0469	.0022
UF7	MOPSO	.0067	.0066	.0029	.0124	.0033
	MOEA/D	.0054	.0044	.0030	.0117	.0008
	MOGWO	.0082	.0055	.0086	.0311	.0003
	EMOGWO	.0093	.0062	.0097	.0351	.0004
UF8	MOPSO	.0268	.0264	.0083	.0447	.0153
	MOEA/D	–	–	–	–	–
	MOGWO	.0069	.0047	.0047	.0188	.0037
	EMOGWO	.0295	.0290	.0091	.0492	.0168
UF9	MOPSO	.0234	.0235	.0041	.0309	.0172
	MOEA/D	–	–	–	–	–
	MOGWO	.0174	.0183	.0063	.0286	.0065
	EMOGWO	.0195	.0205	.0071	.0320	.0073
UF10	MOPSO	.0199	.0207	.0035	.0267	.0154
	MOEA/D	–	–	–	–	–
	MOGWO	.0252	.0239	.0150	.0538	.0000
	EMOGWO	.0219	.0227	.0038	.0293	.0169

A Friedman's test [277] is also included in Table 3.5 to statistically validate the efficacy of the suggested EMOGWO. Friedman's test assesses the efficacy of each approach on each benchmark function and ranks them in order of effectiveness [278]. The best approach is given a score of 1, the second best is given a score of 2, the third best is given a score of 3, and so on.

Table 3.4: Statistical results of all the considered algorithms for MS on UF1 to UF10.

Functions	Algorithms	Average	Median	STD. Dev.	Worst	Best
UF1	MOPSO	.6454	.6632	.1929	.2659	.9523
	MOEA/D	.5177	.5954	.1661	.3149	.7413
	MOGWO	.9268	.9327	.0688	.8180	.9971
	EMOGWO	.9361	.9420	.0695	.8261	1.0000
UF2	MOPSO	.9121	.9164	.0256	.8665	.9530
	MOEA/D	.8720	.8744	.0056	.8599	.8779
	MOGWO	.9097	.9104	.0287	.8470	.9479
	EMOGWO	.9734	.9741	.0307	.9062	1.0000
UF3	MOPSO	.6103	.6161	.1058	.3817	.7715
	MOEA/D	.2399	.2294	.1213	.0898	.4786
	MOGWO	.9498	1.0000	.0878	.7681	1.0000
	EMOGWO	.9783	1.0000	.0904	.7911	1.0000
UF4	MOPSO	.8128	.8132	.0137	.7944	.8345
	MOEA/D	.8832	.8813	.0181	.8532	.9139
	MOGWO	.9424	.9427	.0009	.9410	.9433
	EMOGWO	.9613	.9615	.0009	.9598	.9621
UF5	MOPSO	.2793	.2865	.0958	.1557	.4383
	MOEA/D	.2922	.2917	.0347	.2383	.3438
	MOGWO	.3950	.4326	.1749	.0301	.6104
	EMOGWO	.4622	.5061	.2047	.0352	.7142
UF6	MOPSO	.2744	.2292	.1129	.1544	.5252
	MOEA/D	.0968	.0001	.2072	.0000	.5948
	MOGWO	.6736	.7083	.1232	.3884	.8149
	EMOGWO	.7881	.8287	.1442	.4544	.9535
UF7	MOPSO	.4293	.2952	.2755	.1446	.8771
	MOEA/D	.5632	.6327	.2421	.1496	.9915
	MOGWO	.8013	.9629	.3087	.0225	.9875
	EMOGWO	.8814	1.0000	.3395	.0248	1.0000
UF8	MOPSO	.5081	.5060	.1614	.2272	.7148
	MOEA/D	–	–	–	–	–
	MOGWO	.4457	.4443	.1857	.1886	.8638
	EMOGWO	.4769	.4754	.1987	.2018	.9242
UF9	MOPSO	.1982	.1657	.1635	.0677	.6424
	MOEA/D	–	–	–	–	–
	MOGWO	.8399	.9106	.1976	.2875	.9375
	EMOGWO	.8819	.9561	.2075	.3019	.9844
UF10	MOPSO	.1302	.1091	.0626	.0649	.2540
	MOEA/D	–	–	–	–	–
	MOGWO	.2972	.1424	.3465	.0319	.9283
	EMOGWO	.3180	.1523	.3708	.0342	.9933

The ranks returned in various runs are averaged to determine the rank if the performance of the two approaches is identical [279]. Friedman test returns a p-value of 0.004756, which is significantly less than the threshold ($\alpha = 0.05$), indicating that the outcomes that were obtained are statistically different. The ranks of all the methods returned by the Friedman test are tabulated in Table 3.5, which shows that the proposed EMOGWO has the lowest ranking value of all the models. Based on statistical analysis and experimental data, EMOGWO is found to be superior.

Table 3.5: Mean ranking of all the considered methods.

Rank	Methods	Rank value
1.	EMOGWO	**1.75**
2.	MOGWO	2.08
3.	MOEA/D	2.73
4.	MOPSO	3.06

Further, box plots for 6 representative benchmark problems, including 3 bi-modal ($UF1$, $UF4$, and $UF6$) and 3 tri-modal ($UF8, UF9$, and $UF10$)are is also plotted in Figures 3.6 and 3.7 to see the variations among the IGD values for existing and the proposed EMOGWO over 10 runs. In box plots, algorithms are represented on the horizontal axis while the vertical axis denotes the best IGD values over 10 runs. It can be observed from the figures that the box plots of the proposed EMOGWO are super narrow, and its IGD value is also lower than MOPSO, MOEA/D, and MOGWO for both bi-modal and tri-modal benchmark functions. However, for the tri-modal benchmark function $UF8$, MOPSO shows comparative results. Hence, the qualitative and quantitative analyses demonstrate that the proposed EMOGWO delivers highly competitive and promising results on multi-objective benchmark problems.

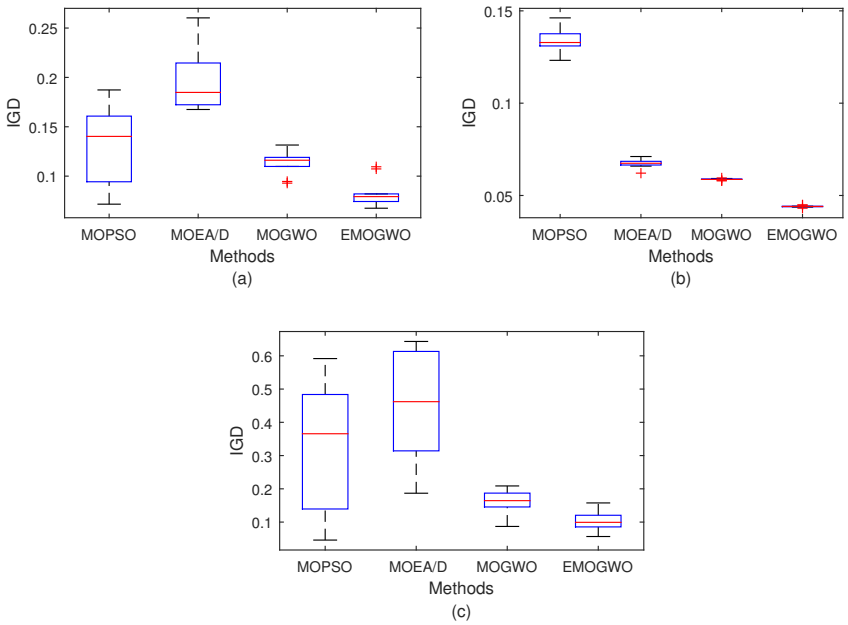

Figure 3.6: Box plots of the statistical results for IGD on three representative bi-modal benchmark problems (a) UF1, (b) UF4, and (c) UF6.

In addition to the box plots that illustrate the statistical distribution of the segmentation met-

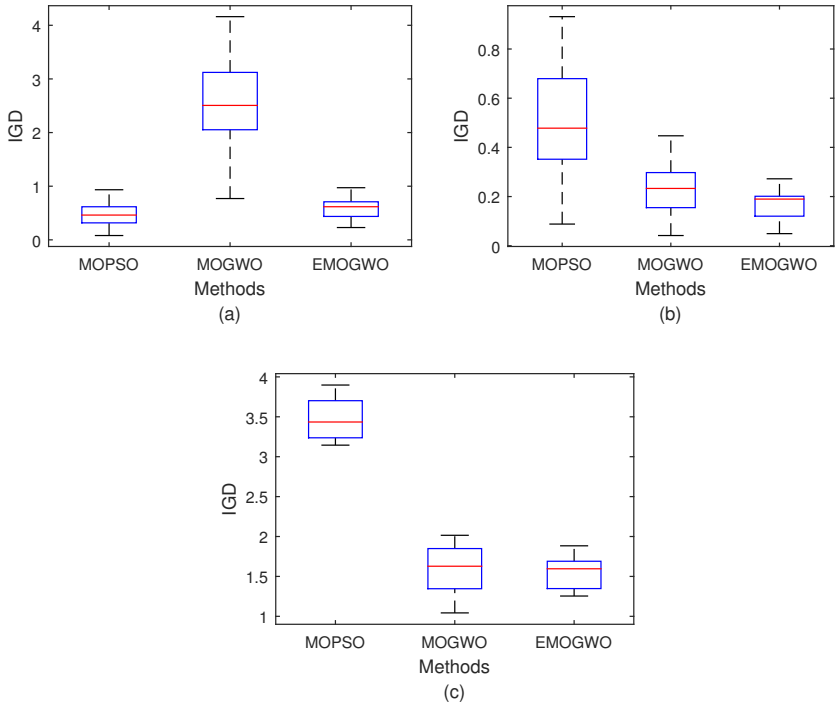

Figure 3.7: Box plots of the statistical results for IGD on three representative tri-modal benchmark problems (a) UF8, (b) UF9, and (c) UF10.

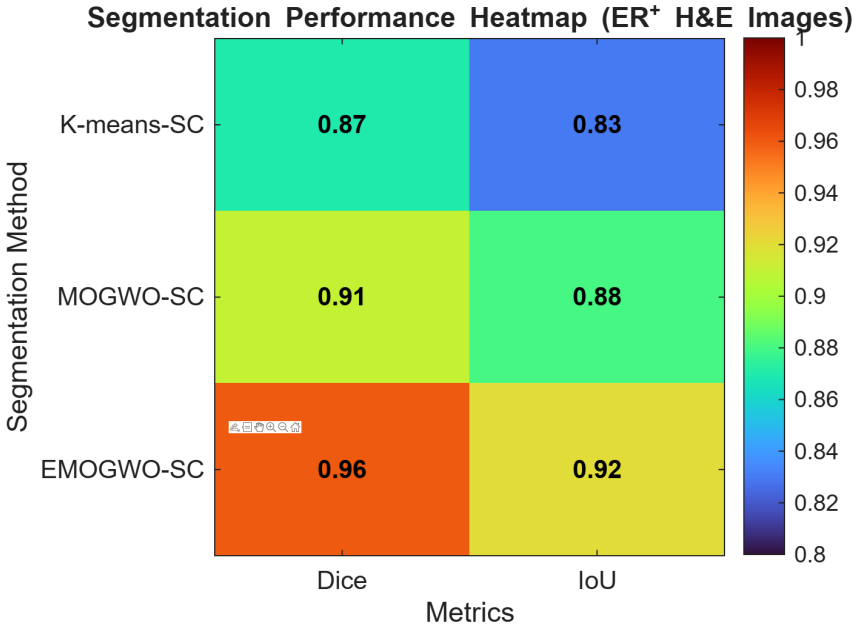

Figure 3.8: Heatmap showing the mean Dice and IoU scores obtained by different segmentation algorithms on ER^+ H&E breast cancer images.

rics, a comprehensive overview of the mean Dice and IoU values obtained by each method is shown in Figure 3.8. The heatmap provides an intuitive summary of the comparative segmenta-

tion performance, where darker color intensity corresponds to higher metric values. It is evident that the proposed EMOGWO-SC achieves superior Dice and IoU scores compared to the baseline K-means-SC and MOGWO-SC methods. This improvement highlights the contribution of the enhanced mutation operator in maintaining a balance between exploration and exploitation during the optimization process, thereby improving the overall boundary delineation accuracy of the segmented nuclei.

3.4.3 An Experimental Examination of the Automatic Nuclei Segmentation Technique

In this section, the experimental results of the suggested EMOGWO-SC method, are presented. A breast cancer histology dataset which is publicly available [262] is considered for the performance evaluation. The dataset consists of H&E stained Estrogen Receptor-Positive (ER+) breast cancer images, taken at 40x magnification level. The mask images are manually generated by the domain experts [262].

In Figure 3.9, the first two columns illustrate sample images along with the corresponding mask. The images are reshaped to a 64×64 resolution for the experimental purpose. The experimental results are validated against two other state-of-the-art methods, namely, K-means and the GWO-based superpixel method. The parameter setting of proposed and considered methods are taken from the respective literature.

The experimental results of proposed and considered methods for the segmented nuclei are performed on four randomly selected images as shown in Figure 3.9. Based on the findings, it is concluded that the suggested EMOGWO-based method performed superiorly for nuclei segmentation compared to other techniques considered. The higher numerical value of dice coefficient represents better segmentation accuracy. The segmentation accuracies of the EMOGWO-SC and other approaches for the considered images are presented in Table 3.6. The TP value denotes the truly identified nuclei, while FP represents the false positives. FN denotes the nuclei that are not identified, whereas DC represents the dice coefficient value.

It is evident from Table 3.6 that EMOGWO-SC achieves the highest DC values across all 10 images, demonstrating consistent superiority over the other compared methods. Notably, all DC values obtained by EMOGWO-SC exceed 0.5, with a maximum of 0.9067 and a minimum of 0.6338. In contrast, K-means-SC and MOGWO-SC achieved DC values greater than 0.5 in 7 and 9 images, respectively. Furthermore, EMOGWO-SC effectively segmented the major

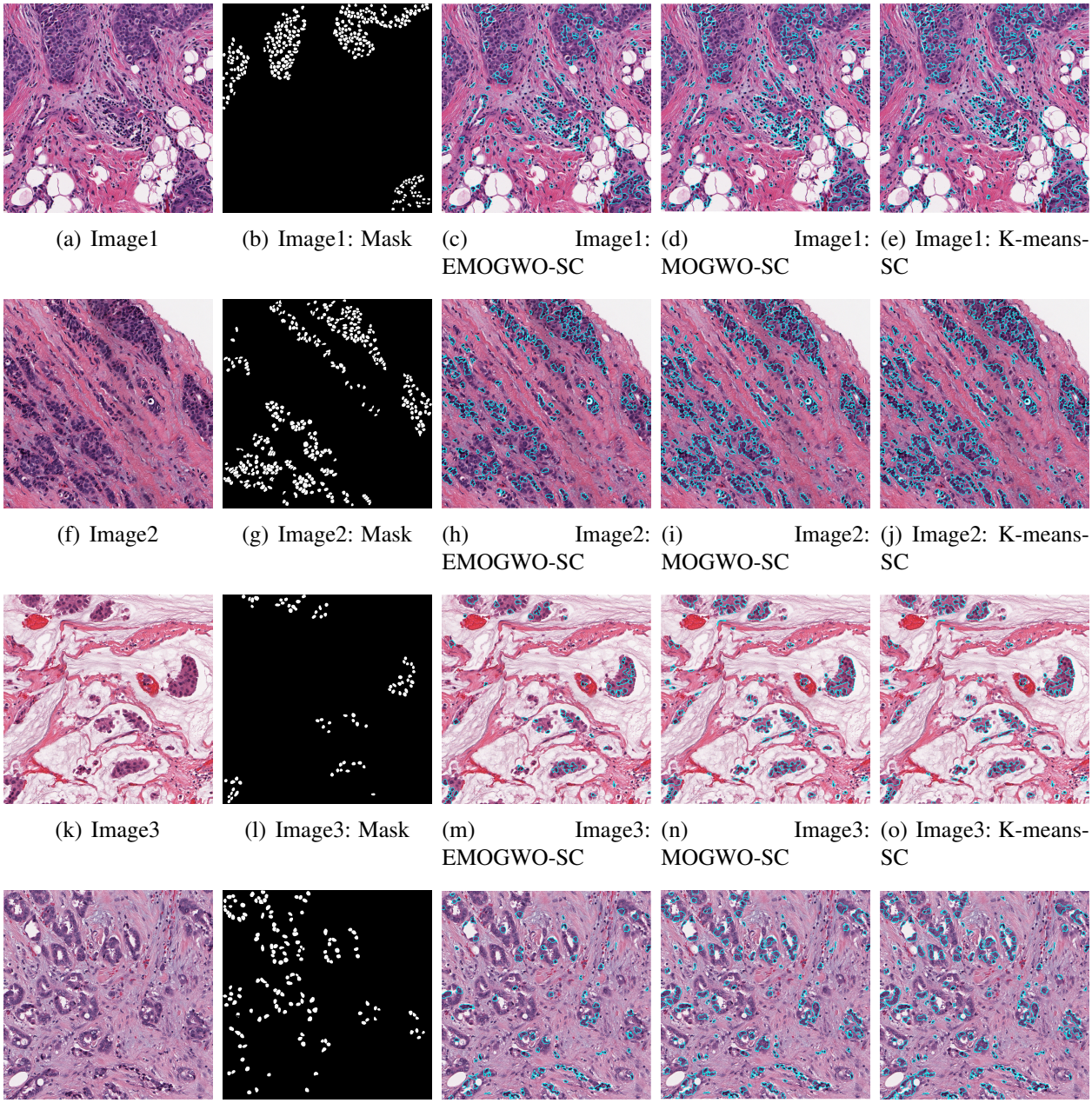

(a) Image1 (b) Image1: Mask (c) Image1: EMOGWO-SC (d) Image1: MOGWO-SC (e) Image1: K-means-SC

(f) Image2 (g) Image2: Mask (h) Image2: EMOGWO-SC (i) Image2: MOGWO-SC (j) Image2: K-means-SC

(k) Image3 (l) Image3: Mask (m) Image3: EMOGWO-SC (n) Image3: MOGWO-SC (o) Image3: K-means-SC

(p) Image4 (q) Image4: Mask (r) Image4: EMOGWO-SC (s) Image4: MOGWO-SC (t) Image4: K-means-SC

Figure 3.9: Results of nuclei segmentation on representative H&E stained Estrogen Receptor-Positive (ER+) breast cancer images using the proposed and evaluated methodologies.

nuclei regions, as indicated by the high TP counts in Table 3.6. It also shows a lower false detection rate, with consistently reduced FP and FN values, highlighting its robustness in nuclei segmentation.

The computation time for nuclei segmentation has been investigated and presented in Table 3.7. From the table, it can be observed that K-means-SC requires the least computation time among all methods; however, its segmentation accuracy is significantly lower, which cannot be compromised in histopathological applications. The proposed EMOGWO-SC achieves an average computation time approximately four seconds lower than MOGWO-SC while maintaining superior accuracy, demonstrating faster convergence and efficient optimization. Memory consumption during execution remained below 1.3 GB on a 32 GB system, indicating the feasibility of the approach for offline diagnostic workflows. Minor performance degradation was noted for images affected by staining noise or poor contrast, which can be mitigated through preprocessing and adaptive parameter tuning.

Table 3.6: Segmentation accuracy of proposed and compared methods.

Images	**Actual**	**K-means-SC**				**MOGWO-SC**				**EMOGWO-SC**			
	Nuclei	**TP**	**FP**	**FN**	**DC**	**TP**	**FP**	**FN**	**DC**	**TP**	**FP**	**FN**	**DC**
Image1	33	32	56	3	0.5203	31	25	3	0.6889	32	13	1	0.8205
Image2	35	30	36	4	0.5000	32	18	3	0.7529	34	6	1	0.9067
Image3	75	71	20	5	0.8503	72	14	4	0.8889	71	12	1	0.8987
Image4	29	22	49	4	0.4536	26	18	2	0.7123	27	16	1	0.7500
Image5	28	24	7	3	0.8276	24	2	3	0.8000	23	3	2	0.8571
Image6	47	36	30	12	0.6316	35	28	13	0.6364	42	7	4	0.6800
Image7	52	35	21	13	0.6731	37	16	14	0.7115	44	2	7	0.7778
Image8	7	2	59	2	0.0615	2	3	2	0.5000	3	1	1	0.6667
Image9	77	55	24	18	0.7237	62	17	13	0.8052	64	5	11	0.8889
Image10	59	41	75	19	0.4659	42	70	16	0.4941	45	37	15	0.6338

3.5 Statistical Significance of Segmentation Results

To ensure that the superior segmentation performance of the proposed **EMOGWO-SC** model is not due to random variation, statistical hypothesis tests were conducted on the per-run Dice and IoU values obtained over ten independent trials. For each pair of methods, a paired t-test was applied since identical image sets were used across runs. A non-parametric Friedman test was also performed to confirm the overall difference among competing algorithms. In addition, 95 % confidence intervals (CI) of the mean differences were computed using bootstrap resampling.

As shown in Table 3.8, EMOGWO-SC achieved significantly higher Dice coefficients than

both GWO and WOA ($p < 0.01$). The corresponding confidence intervals exclude zero, confirming the reliability of the improvements. Large effect sizes ($Cohen's\ d > 1.3$) indicate practical significance as well. These statistical results validate that the proposed segmentation approach delivers consistent and statistically significant performance gains.

Table 3.7: Computational time (in seconds) of the proposed and other methods.

Images	**EMOGWO-SC**	**MOGWO-SC**	**K-means-SC**
Image1	52.1022	56.2560	0.0352
Image2	45.8653	50.4520	0.0365
Image3	51.4523	51.1520	0.0235
Image4	44.7852	45.8520	0.0152
Image5	48.4520	53.5301	0.0325
Image6	49.7825	49.5620	0.0652
Image7	37.8950	55.4523	0.0325
Image8	43.4560	45.8563	0.0132
Image9	59.2603	55.5620	0.0653
Image10	48.4536	49.5620	0.0523

Table 3.8: Paired statistical tests for segmentation performance (Dice coefficient, N=10 runs).

Comparison	t	df	p	95 % CI	Cohen's d
EMOGWO-SC vs GWO	5.12	9	0.0003	[0.007, 0.020]	1.62
EMOGWO-SC vs WOA	4.36	9	0.0018	[0.005, 0.018]	1.38
Friedman $\chi^2(2)$=11.2, p = 0.004					

3.6 Summary

In this chapter, a new clustering-based nuclei segmentation method EMOGWO-SC is introduced. The suggested approach finds the optimal cluster centroids using a novel variant of multi-objective grey wolf optimizer. To perform optimal clustering, two objective functions, namely intra-cluster distance and inter-cluster distance, are considered. To validate the efficacy of the proposed variant, standard multi-objective benchmark functions were considered, including seven bi-objective and three tri-objective functions, along with a statistical analysis using box plots. It has been observed that the proposed variant is able to report best fitness

value of more than 0.90 on 90% of the benchmark functions. Further, the proposed EMOGWO has been employed for nuclei segmentation to H&E stained Estrogen Receptor-Positive (ER+) breast cancer images. The results of the suggested approach are empirically validated against K-means-SC and MOGWO-SC in terms of segmentation accuracy. The experimental results demonstrate that EMOGWO-SC outperforms K-means-SC and MOGWO-SC in terms of accuracy. Moreover, the average computation time of the proposed method is less than that of MOGWO-SC, which is quite promising.

CHAPTER 4

EFFICIENT FEATURE SELECTION USING IMOWOA

This chapter presents the Improved Multi-Objective Whale Optimization Algorithm for Feature Selection (IMOWOA-FS), aimed at enhancing feature selection in histopathological image analysis. The algorithm's formulation and workflow are detailed, and its performance is compared against MOPSO, MOEA/D, and MOWOA using benchmark datasets and evaluation metrics.

4.1 Introduction

In disease diagnosis, pathologists perform microscopic examinations of histopathological samples to identify the signs of infection. During this analysis, the primary focus is on tissue structure, cell count, and shape of the cell. Moreover, this manual examination demands expertise, which makes it an expensive, one-sided, and tedious process [20]. Consequently, its automation is fundamental for quick and impartial finding [280]. To do this, histopathological images are captured through microscopic mounted cameras, which are further analyzed using computer-assisted histopathological image analysis methods. Figure 4.1 illustrates some sample images of different tissues, taken at a 40x magnification level [2]. The intricate structure of histopathological images present a challenging environment, even for classification tasks. Consequently, this study presents a new method for selecting discriminative and relevant features from images.

In the literature, several methods have been proposed for efficient feature extraction, which are broadly classified into traditional and learning-based approaches. The first category corresponds to feature descriptors extracted based on statistical computation [16]. SIFT [281], HOG [282], and SURF [283] are some of the common examples of traditional feature extraction methods. These methods are quite effective for clinical image analysis. However, these meth-

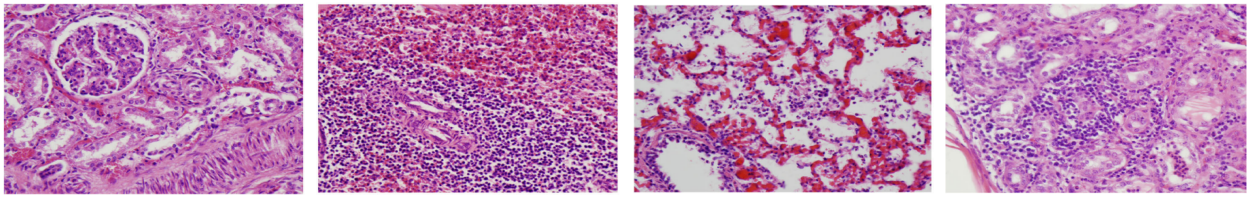

Figure 4.1: Examples of representative tissues from histopathology, taken at 40x magnification.

ods produce many irrelevant features in a complex environment. Moreover, features generated by traditional methods are generally non-transferable. On the contrary, learning-based methods employ various machine learning models to obtain features [19]. Deep neural networks (DNN) models and auto-encoders restricted Boltzmann machines are some of the commonly used models. The literature witnessed that DNN-based solutions are effective in analyzing complex and diverse environments [258], like histopathological images. Masci and others [284] presented a feature extraction method by initializing a CNN with a convolution auto-encoder. Xu and others [19] extracted features from stromal and epithelial tissue by employing a deep CNN. A comprehensive survey on various DNN-based feature extraction methods can be found in [285], [286]. Generally, DNN-based feature extraction methods find global features by learning directly from low-level features, resulting in the generation of better feature descriptors. However, these feature descriptors might contain unnecessary and irrelevant features, degrading the efficacy of the classifier [249], [287], [288], [267]. Therefore, a novel FS technique is presented in this chapter to choose the best features from Histopathological images.

To validate the efficiency of IMOWOA, 10 CEC2009 multi-objective benchmark problems are considered, including bi-objectives and tri-objectives test problems. To compare the results, three parameters, namely, IGD, SP and MS, are considered, and the results are validated against three existing multi-objective meta-heuristic algorithms, namely, MOEA/D, MOPSO, and MOWOA.

The remaining chapter is organized as follows: Section 2 briefs the multi-objective WOA. The proposed approach, along with the proposed variant, is illustrated in Section 3. Section 4 discusses the empirical examination of the IMOWOA. Finally, section 5 presents the conclusion of the chapter.

4.2 Multi-Objective Whale Optimization Algorithm (MOWOA)

MOWOA is a multi-objective variation of WOA [127], which is inspired by Humpback Whales are the largest creatures in the world, having nearly twice the number of body cells as humans have body cells. The optimization process is designed using the hunting analogy of the whales. There are three main phases of hunting: encircling the prey, bubble-net attacking strategy, and searching for new prey. The conceptual and mathematical descriptions of these phases are provided below.

A. Encircle the prey:

This is the first phase of hunting. As the location of the prey in the search domain is initially unknown, WOA considers the current best position as the overall best solution and updates its further movement accordingly as per Eq. 4.1.

$$\vec{X}(t+1) = \vec{X}_b(t) - 2\vec{a}\cdot\vec{r} - \vec{a}\cdot \mid 2\cdot\vec{r}\cdot\vec{X}_b(t) - \vec{X}(t) \mid \tag{4.1}$$

Where, $X_b(t)$ is the best position at iteration t, $r \in (0,1)$, vector a contains decreasing values from 2 to 0 and $X(t+1)$ representing the location of the whale at next step.

B. Bubble-net attacking strategy:

In this phase, along with the encircling strategy, the spiral movement of the whales is also considered to search for prey in an equally likely manner. The probability (p_r) of using spiral and shirking encircling phases is 50% each. The mathematical formulation of bubble-net attacking is provided in Eq. 4.2.

$$\vec{X}(t+1) = \begin{cases} ((X_b(t) - X(t)) \cdot e^{bl} \cdot (2\pi l) + X_b(t)) & p_r \geq .5 \\ Eq.(4.1.) & p_r < .5 \end{cases} \tag{4.2}$$

Where b denotes the shape of the spiral and is kept as the constant, $l \in [-1,1]$ denotes a random number.

C. New prey search:

The above two phases are responsible for the exploitation, whereas this phase is leveraged to explore the search domain to find a new prey. The searching behavior is purely random

and can be formulated by Eq. 4.3.

$$\vec{X}(t+1) = \vec{X}_r(t) - 2\vec{a} \cdot \vec{r} - \vec{a} \cdot \mid 2 \cdot \vec{r} \cdot \vec{X}_r(t) - \vec{X}(t) \mid \tag{4.3}$$

Where X_r is a randomly generated solution at iteration t.

The above-defined WOA can be efficiently leveraged for multi-objective problems by including various significant constructs like finding non-dominance between solutions, maintaining the archive set, selection methods, etc., in MOWOA. In multi-objective optimization, the ranking of the solutions is defined by Pareto-optimality based on non-dominated solutions. Further, to manage the repository of these solutions an archive set is maintained. There are certain rules to update or modify the archive set described as follows:

Rule 1: Initially, the archive set is empty, so insert all non-dominated solutions into it.

Rule 2: Let the archive set consist of S solutions which are non-dominated. If the new non-dominated solutions are not better than S and few solutions belonging to the archive set dominate, then there is no change in the archive set.

Rule 3: If new solutions and solutions in the archive set are non-dominated, then these new solutions will be added to the archive set.

Rule 4: If any newly generated non-dominated solution surpasses one or more solutions present in the archive set, then replace the previous ones to ensure that only the superior solutions are retained.

Rule 5: If the archive set is not empty, then the most crowded solutions are taken away from the archive to balance the diverse set of solutions and new solutions are given a chance.

In addition, the roulette wheel method is employed to uphold the variety and dispersion of solutions within the archive set.

4.3 Proposed Method

The IMOWOA-FS method proposed in this research is employed to select the most relevant features. The overall structure of the proposed approach is illustrated in Figure 4.2. Specifically,

the method is divided into two main stages: feature extraction and feature selection. The preprocessing of the considered images for data augmentation comes first. Images, after processing, are passed to a CNN to extract relevant features. Next, the proposed variant, the IMOWOA, operates on the extracted features to get the optimal feature set for image classification. The IMOWOA population is specified across dimensions of d, where d is the number of extracted features. Further, each individual is initialized with real values $\in [0,1]$. However, a sigmoid function is employed to map the real values of each individual in 0 and 1. Eq. 4.4 presents the formulation of the sigmoid function for x_i^j value of the i^{th} individual at j^{th} dimension.

$$S(x_i^j) = \frac{1}{1+e^{-x_i^j}} \tag{4.4}$$

Furthermore, if the resultant value (x_i^j) of i^{th} individual in j^{th} dimension corresponds to '1', then the corresponding feature is selected, else it is discarded. For each individual, fitness is computed according to the considered objective functions, which are detailed in the following sections. Each individual's position is updated with the help of the proposed IMOWOA. The best individual is identified, and the optimal feature set is presented.

4.3.1 Objective Functions

In the IMOWOA, the fitness of each candidate solution (also known as an individual) is assessed using two complementary objective functions. These objectives are mathematically defined in Equations 4.5 and 4.6, and they are designed to strike a balance between two competing

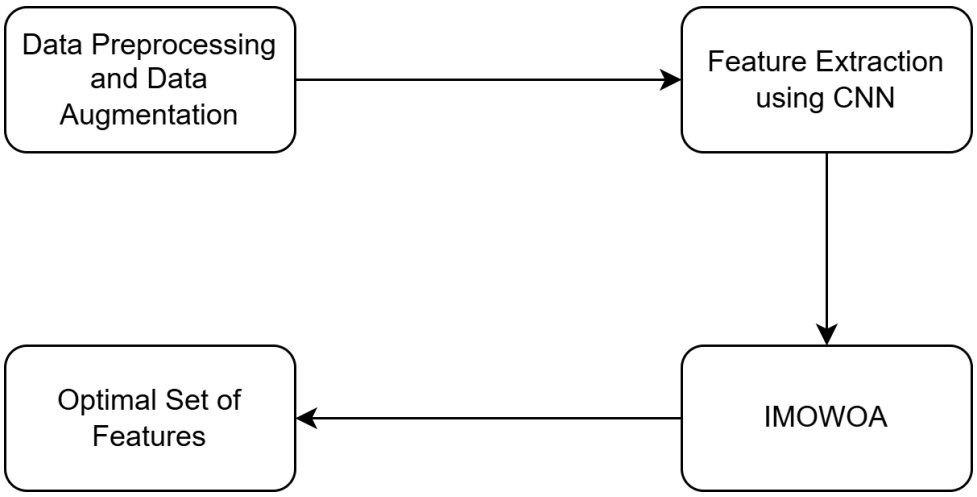

Figure 4.2: The overall framework of the proposed method.

goals: maximizing the classification accuracy and minimizing the number of selected features. By considering both aspects simultaneously, IMOWOA effectively balances predictive performance with model simplicity, which is critical in high-dimensional datasets.

$$\text{Maximization: } \frac{1}{k}\sum_{i=1}^{k} TP \tag{4.5}$$

$$\text{Minimization: } \frac{SF}{TEF} \tag{4.6}$$

In Equation 4.5, k denotes the total number of classes in the classification task, while TP represents the number of *true positive* instances correctly predicted for class i. By averaging the number of correctly classified instances across all classes, this objective ensures a balanced classification performance, reducing bias toward majority classes and enhancing the model's robustness across varied datasets.

Equation 4.6 pertains to feature selection and quantifies the proportion of selected features. Where SF indicates the number of features chosen by the optimization algorithm for a given individual, and TEF is the total number of features originally extracted from the dataset. The goal is to minimize this ratio, thereby encouraging the selection of a smaller and more relevant subset of features. This not only simplifies the model and reduces computational cost but also enhances generalization performance and interpretability.

These two objectives are inherently in conflict: increasing classification accuracy typically involves more features, while reducing the number of features may sacrifice some predictive power. IMOWOA addresses this trade-off using a Pareto-based multi-objective optimization strategy. Instead of seeking a single optimal solution, the algorithm produces a set of *Pareto-optimal* solutions that reflect different compromises between the objectives. This allows practitioners to choose a solution that best fits their specific application needs, whether prioritizing accuracy, simplicity, or a balance of both.

Overall, the dual-objective fitness evaluation in IMOWOA ensures that the resulting models are not only accurate but also efficient and interpretable—qualities that are crucial in real-world machine learning applications such as medical diagnosis, financial prediction, and image analysis.

4.3.2 IMOWOA

In the existing MOWOA, only one archive set is maintained in each iteration, which may sometimes result in poor population diversity and less exploration. Thus, to enhance the efficacy of MOWOA, a novel variant, namely, Improved MOWOA (IMOWOA), is introduced. In the proposed variant, the archive set is partitioned into different priority sets. The detailed steps for updating the archive set are as follows:

1. Let the population of size P consist of N unique solutions. From P, identify the non-dominated set of individual solutions.

2. Store the non-dominated individual solutions in the $priority\_set_i$ (i=1) and delete these solutions from the P.

3. Again, find the non-dominated individual solutions from the remaining population P and add these solutions to the $priority\_set_i$ where $(i = 2, 3, 4, \cdots)$

4. Repeat the above process until no solution is left in the population P.

Once the archive set is partitioned into the different priority sets, then the population (P') for the next iteration is updated using the following steps:

1. Add the solutions of $priority\_set_i$ (i=1) to the P'

2. If ($\mid P \mid < N$) and (N-$\mid P \mid$) $< s$, number of solutions in $priority\_set_i$ where i = 2, 3,... then add solutions of $priority\_set_i$ to the $\mid P' \mid$

3. Otherwise, find the less crowded solutions in the $priority\_set_i$ and add them to P'

Once the P' is filled with N solutions, the above procedure is stopped. The resulting P' is nothing but the newly generated archive set. Due to the inclusion of domination sorting and crowding distance, the new archive set is more diverse and has good exploration capability.

The proposed method called Improved Multi-Objective WOA-based FS (IMOWOA-FS), is an FS algorithm designed to select the relevant features from histopathological images. The complete algorithm for the proposed IMOWOA-FS method is presented in Algorithm 4.1. and the flowchart of IMOWOA method is presented in Figure 4.3. Detailed steps of the flowchart are explained below:

Step 1 – Input Definition: The algorithm begins by accepting four main inputs: a set of histopathological images I, the number of features to select n, the population size P, and the maximum number of iterations T. These inputs define the problem's boundaries and optimization parameters. The histopathological images provide raw data from which features are extracted, while n, P, and T guide the feature selection process in terms of how many features to choose, how many candidate solutions to explore at a time, and how long the optimization will run.

Step 2 – Output Definition: The output of the algorithm is the selected feature subset S, which is a reduced set of the most relevant features extracted from the original dataset. This subset is chosen to optimize a balance between classification performance and the simplicity of the model (by reducing the number of input features).

Step 3 – Population Initialization: A population X of size P is randomly initialized, where each individual is a vector of real values ranging from 0 to 1. The length of each vector corresponds to the number of extracted features d. These real values represent the probability or confidence of selecting each feature, forming a continuous solution space that allows for smooth updates and optimization.

Step 4 – Initial Fitness Evaluation: Each individual in the population is evaluated using a fitness function defined by Equations 4.5 and 4.6. These equations likely combine multiple objectives, such as classification accuracy and the number of features selected. The result is a fitness score for each individual, guiding the selection and survival of promising feature subsets.

Step 5 – Archive and Priority Set Initialization: An archive set A is created to store high-quality solutions throughout the optimization process. Additionally, this archive is partitioned into multiple priority sets (e.g., $priority\_set\_1$, $priority\_set\_2$, etc.), which are used to maintain solution diversity and control selection pressure. These priority levels help ensure that the algorithm explores a wide range of potential feature subsets instead of converging prematurely to a suboptimal region.

Step 6 – Archive Partitioning: The archive set A is organized into different priority sets based on predefined criteria such as fitness value, dominance in multi-objective space, or diver-

sity. This partitioning mechanism plays a crucial role in balancing exploration and exploitation, enabling the algorithm to maintain a diverse pool of good solutions across different regions of the search space.

Step 7 – Optimization Loop: The main loop of the algorithm runs from iteration $t = 1$ to T. During each iteration, the population is updated using the IMOWOA operator, which is defined by Equations 4.1 to 4.3. This operator mimics the foraging behavior of whales, introducing movement strategies that help individuals explore and exploit the search space efficiently. The operator likely includes mechanisms such as encircling prey, spiral updating, and random foraging, tailored for continuous feature selection tasks.

Step 8 – Fitness Reevaluation: After updating the population using the IMOWOA operator, the fitness of each new individual is recalculated using the same multi-objective evaluation criteria as before. This step ensures that the impact of the update is assessed and helps guide the inclusion of new individuals into the archive.

Step 9 – Archive Update: The archive set A is updated by comparing new individuals against the existing ones. High-quality individuals that improve the current archive—either through better fitness or by offering diversity—are retained. Poor-performing individuals may be replaced. This step helps maintain an elite set of candidate solutions for selection at the end of the process.

Step 10 – Final Feature Selection: After completing all iterations, the algorithm selects the best feature subset S from the final archive. This subset represents the optimal or near-optimal trade-off between classification accuracy and feature reduction, making it suitable for further use in training machine learning models or conducting further biomedical analysis. Extensive experiments were conducted on publicly available histopathological image datasets to visualize the efficacy of the IMOWOA-FS method. The proposed approach outperforms other methods in terms of considered performance metrics.

4.3.3 Novelty of the Proposed IMOWOA Method

The proposed Improved Multi-Objective Whale Optimization Algorithm (IMOWOA) introduces adaptive parameter control and a chaotic search mechanism to avoid premature conver-

gence. Unlike the traditional MOWOA, the proposed version employs Pareto-based dominance ranking with adaptive archive updating to maintain a well-distributed set of optimal feature subsets. Furthermore, it incorporates a dual-objective fitness evaluation that balances feature relevance and classification accuracy. These innovations enhance the discriminative power of the selected features while reducing redundancy and computational overhead.

Algorithm 4.1 IMOWOA-FS

Input: Histopathological images I, number of features to select n, population size P, maximum number of iterations T.
Output: Selected feature set S.
Initialization:
Randomly initialize the population X of size P with real values $\in [0,1]$ for d dimensions, where d is the number of extracted features.
Evaluate the fitness of each individual using Equations 4.5 and 4.6.
Initialize the archive set A and the priority sets $priority\_set\_i$ where $i = 1,2,3,\cdots$.
Partition the archive set A into different priority sets.
for each iteration $t = 1$ to T **do**
    Update the population X using the IMOWOA operator in Equations 4.1, 4.2, and 4.3.
    Evaluate the fitness of each individual using Equations 4.5 and 4.6.
    Update the archive set A.
end for
Select the best feature subset S from the final archive set A.

4.4 Experimentation analysis

The efficacy of the proposed IMWOA has been discussed in this section. The proposed IMOWOA method has been vindicated on 10 CEC-2009 multi-objective benchmark problems. For a fair analysis, each experiment was done on a MATLAB 2017a computer with a 2.90 GHz Intel Core i3 CPU and 16 GB DDR3 RAM.

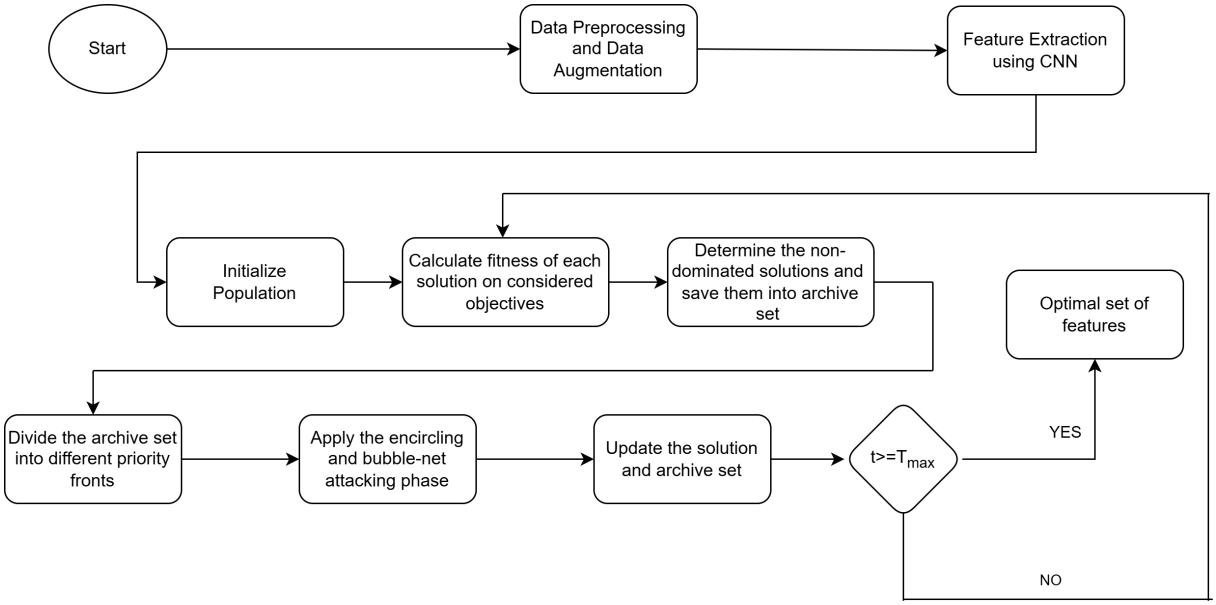

Figure 4.3: Proposed IMOWOA-based feature selection and classification framework.

4.4.1 Performance Analysis of Proposed IMOWOA

To test the efficiency of the proposed IMOWOA, 7 bi-objectives (UF_1 - UF_7) and 3 tri-objective test benchmarks (UF_8 - UF_{10}) [141], [269] have been considered. Figures 4.4 and 4.5 illustrate the benchmark function details. It can be observed from Figures 4.4 and 4.5 that the considered benchmark functions contain distinct multi-objective search regions with convex, non-convex, multi-modal, and discontinuous Pareto fronts, which have been considered the hardest test problems in the literature. IGD, SP, and MS are commonly used to validate the efficacy of multi-objective methods since they consider the standard deviation and mean values. IGD value assesses the convergence while MS and SP evaluate coverage of the considered approach [270], [272], [261]. IGD is an improved version of Coello's generational distance (GD) [270], [271] which is computed using Eq. (4.7) whereas the values of SP and MS are computed using Eqs. (4.8) and (4.9).

$$IGD = \frac{\sqrt{\sum_{a=1}^{N} dist_a^2}}{N} \tag{4.7}$$

Where N denotes the true optimum Pareto solutions (PS), whereas $dist_j$ is the Euclidean distance measure between the a^{th} true Pareto optimal and the reference set's nearest computed POS.

$$SP = \sqrt{\frac{1}{N-1}\sum_{a=1}^{N}(dist' - dist_a)^2} \tag{4.8}$$

Where, dist' denotes the mean of all $dist_a$, N denotes the total number of optimum PS found, and $dist_a = \min_a(|f_1^i(\vec{x}) - f_1^a(\vec{x})| + |f_2^i(\vec{x}) - f_2^a(\vec{x})|) \; \forall \; i, a = 1, 2, 3, \cdots, N$.

$$MS = \sqrt{\sum_{a=1}^{t} \max(det(x_i, y_i))} \tag{4.9}$$

The function $det()$ calculates the euclidean distance. The values x_j denote the maximum and y_j denote the minimum value, respectively, of the a^{th} objective. The variable t represents the total number of objectives.

Name	Mathematical formulation
UF1	$f_1 = x_1 + \frac{2}{\lvert J_1\rvert}\sum_{j\in J_1}[x_j - \sin(6\pi x_1 + \frac{j\pi}{n})]^2,\ f_2 = 1 - \sqrt{x} + \frac{2}{\lvert J_2\rvert}\sum_{j\in J_2}[x_j - \sin(6\pi x_1 + \frac{j\pi}{n})]^2$
	$J_1 = \{j \mid j \text{ is odd and } 2 \le j \le n\},\ J_2 = \{j \mid j \text{ is even and } 2 \le j \le n\}$
UF2	$f_1 = x_1 + \frac{2}{\lvert J_1\rvert}\sum_{j\in J_1} {y_j}^2,\ f_2 = 1 - \sqrt{x} + \frac{2}{\lvert J_2\rvert}\sum_{j\in J_2} {y_j}^2$
	$J_1 = \{j \mid j \text{ is odd and } 2 \le j \le n\},\ J_2 = \{j \mid j \text{ is even and } 2 \le j \le n\}$
	$y_j = \begin{cases} x_j - [0.3x_1^2\cos(24\pi x_1 + \frac{4j\pi}{n}) + 0.6x_1]\cos(6\pi x_1 + \frac{j\pi}{n}) \text{ if } j \in J_1 \\ x_j - [0.3x_1^2\cos(24\pi x_1 + \frac{4j\pi}{n}) + 0.6x_1]\sin(6\pi x_1 + \frac{j\pi}{n}) \text{ if } j \in J_2 \end{cases}$
UF3	$f_1 = x_1 + \frac{2}{\lvert J_1\rvert}(4\sum_{j\in J_1} y_j^2 - 2\prod_{j\in J_1}\cos(\frac{20y_j\pi}{\sqrt{j}}) + 2) f_2 = \sqrt{x_1} + \frac{2}{\lvert J_2\rvert}(4\sum_{j\in J_1} y_j^2 - 2\prod_{j\in J_2}\cos(\frac{20y_j\pi}{\sqrt{j}}) + 2)$
	$J_1 \text{ and } J_2 \text{ are the same as those of } UF1,\ y_j = x_j - x_1^{0.5(1.0+\frac{3(j-2)}{n-2})},\ j = 2, 3, \ldots, n$
UF4	$f_1 = x_1 + \frac{2}{\lvert J_1\rvert}\sum_{j\in J_1} h(y_j),\ f_2 = 1 - x_2 + \frac{2}{\lvert J_2\rvert}\sum_{j\in J_2} h(y_j)$
	$J_1 \text{ and } J_2 \text{ are the same as those of } UF1,\ y_j = x_j - \sin(6\pi x_1 + \frac{j\pi}{n}),\ j = 2, 3, \ldots, n,\ h(t) = \frac{\lvert t\rvert}{1+e^{2\lvert t\rvert}}$
UF5	$f_1 = x_1 + (\frac{1}{2N} + \epsilon)\lvert\sin(2N\pi x_1)\rvert + \frac{2}{\lvert J_1\rvert}\sum_{j\in J_1} h(y_i),\ f_1 = 1 - x_1 + (\frac{1}{2N} + \epsilon)\lvert\sin(2N\pi x_1)\rvert + \frac{2}{\lvert J_2\rvert}\sum_{j\in J_2} h(y_i)$
	$J_1 amd J_2 \text{ are identical to those of } UF1,\ \epsilon > 0,\ y_j = x_j - \sin(6\pi x_1 + \frac{j\pi}{n}),\ j = 2, 3, \ldots, n$
	$h(t) = 2t^2 - \cos(4\pi t) + 1$
UF6	$f_1 = x_1 + \max\{0, 2(\frac{1}{2N} + \epsilon)\sin(2N\pi x_1)\} + \frac{2}{\lvert J_1\rvert}(4\sum_{j\in J_1} y_j^2 - 2\prod_{j\in J_1}\cos(\frac{20y_j\pi}{\sqrt{j}}) + 1))$
	$f_2 = 1 - x_1 + \max\{0, 2(\frac{1}{2N} + \epsilon)\sin(2N\pi x_1)\}\frac{2}{\lvert J_2\rvert}(4\sum_{j\in J_2} y_j^2 - 2\prod_{j\in J_2}\cos(\frac{20y_j\pi}{\sqrt{j}}) + 1))$
	$J_1 amd J_2 \text{ are identical to those of } UF1,\ \epsilon > 0,\ y_j = x_j - \sin(6\pi x_1 + \frac{j\pi}{n}),\ j = 2, 3, \ldots, n$
UF7	$f_1 = \sqrt[5]{x_1} + \frac{2}{\lvert J_1\rvert}\sum_{j\in J_1} y_j^2,\ f_2 = 1 - \sqrt[5]{x_1} + \frac{2}{\lvert J_2\rvert}\sum_{j\in J_2} y_j^2$
	$J_1 amd J_2 \text{ are identical to those of } UF1,\ \epsilon > 0,\ y_j = x_j - \sin(6\pi x_1 + \frac{j\pi}{n}),\ j = 2, 3, \ldots, n$

Figure 4.4: Bi-objective test problems.

The optimal IGD, SP, and MS values of all the considered approaches have been compared to assess the efficacy qualitatively. To investigate the results, the proposed IMOWOA is compared to MOPSO [272], MOWOA [141], and MOEA/D [276]. Each method has been repeated 10 times to get the mean value of results, which is considered to ensure a fair analysis and reduce the interference impact. A comparison is made between the mean, standard deviation,

Name	Mathematical formulation
UF8	$f_1 = \cos(0.5x_1\pi)\cos(0.5x_2\pi) + \frac{2}{\lvert J_1\rvert}\sum_{j\in J_1}(x_j - 2x_2\sin(2\pi x_1 + \frac{j\pi}{n})^2)$
	$f_2 = \cos(0.5x_1\pi)\sin(0.5x_2\pi) + \frac{2}{\lvert J_2\rvert}\sum_{j\in J_2}(x_j - 2x_2\sin(2\pi x_1 + \frac{j\pi}{n})^2)$
	$f_3 = \sin(0.5x_1\pi) + \frac{2}{\lvert J_3\rvert}\sum_{j\in J_3}(x_j - 2x_2\sin(2\pi x_1 + \frac{j\pi}{n})^2)$
	$J_1 = \{j\lvert 3 \le j \le n,\ and\ j-1\ is\ a\ multiplication\ of\ 3\}$, $J_2 = \{j\lvert 3 \le j \le n,\ and\ j-2\ is\ a\ multiplication\ of\ 3\}$, $J_3 = \{j\lvert 3 \le j \le n,\ and\ j\ is\ a\ multiplication\ of\ 3\}$,
UF9	$f_1 = 0.5[\max\{0, (1+\epsilon)(1-4(2x_1-1)^2)\} + 2x_1]x_2 + \frac{2}{\lvert J_1\rvert}\sum_{j\in J_1}(x_j - 2x_2\sin(2\pi x_1 + \frac{j\pi}{n})^2)$
	$f_2 = 0.5[\max\{0, (1+\epsilon)(1-4(2x_1-1)^2)\} + 2x_1]x_2 + \frac{2}{\lvert J_2\rvert}\sum_{j\in J_2}(x_j - 2x_2\sin(2\pi x_1 + \frac{j\pi}{n})^2)$
	$f_3 = 1 - x_2 + \frac{2}{\lvert J_3\rvert}\sum_{j\in J_3}(x_j - 2x_2\sin(2\pi x_1 + \frac{j\pi}{n})^2)$
	$J_1 = \{j\lvert 3 \le j \le n,\ and\ j-1\ is\ a\ multiplication\ of\ 3\}$, $J_2 = \{j\lvert 3 \le j \le n,\ and\ j-2\ is\ a\ multiplication\ of\ 3\}$, $J_3 = \{j\lvert 3 \le j \le n,\ and\ j\ is\ a\ multiplication\ of\ 3\}$, $\epsilon = 0.1$
UF10	$f_1 = \cos(0.5x_1\pi)\cos(0.5x_2\pi) + \frac{2}{\lvert J_1\rvert}\sum_{j\in J_1}[4y_j^2 - \cos(8\pi y_j) + 1]$
	$f_2 = \cos(0.5x_1\pi)\sin(0.5x_2\pi) + \frac{2}{\lvert J_2\rvert}\sum_{j\in J_1}[4y_j^2 - \cos(8\pi y_j) + 1]$
	$f_3 = \sin(0.5x_1\pi) + \frac{2}{\lvert J_3\rvert}\sum_{j\in J_1}[4y_j^2 - \cos(8\pi y_j) + 1]$
	$J_1 = \{j\lvert 3 \le j \le n,\ and\ j-1\ is\ a\ multiplication\ of\ 3\}$, $J_2 = \{j\lvert 3 \le j \le n,\ and\ j-2\ is\ a\ multiplication\ of\ 3\}$, $J_3 = \{j\lvert 3 \le j \le n,\ and\ j\ is\ a\ multiplication\ of\ 3\}$,

Figure 4.5: Tri-objective test problems.

median, best, and worst values of the IGD, MS, and SP of the proposed IMOWOA and other methods under consideration to assess the effectiveness of the proposed approach. The population size (N) is set to 50 whereas total iterations (t_{it}) are set to 1000, respectively, while the other parameters are taken from the literature. Values of IGD, SP, and MS calculated with proposed IMOWOA and other techniques are depicted in Tables 4.1 - 4.3. Table 4.1 shows that for more than 90% of benchmark problems, the proposed IMOWOA achieves the best IGD values. IGD values are normally used as a benchmark for comparing the convergence of different methods. So, from the results listed in Table 4.1, it can be envisioned that the suggested IMOWOA shows better convergence. There are a few benchmark problems for which other algorithms return the best IGD values. MOEA/D produces the best IGD values for $UF3$, $UF6$, and $UF7$, while for the benchmark $UF8$, MOPSO outperforms the proposed and other techniques. Thus, it can be vindicated from the experimentation that the proposed IMOWOA performs more consistently than the other methods.

Besides, in Tables 4.2 and 4.3, the SP and MS values are also examined. As MOEA/D is not executed for the tri-objective function UF_8, UF_9, and UF_{10}, henceforth, for these benchmark problems, the proposed IMOWOA is only validated against MOPSO and MOWOA. From the tables, it can be shown that the proposed IMOWOA has superior convergence and coverage.

Though there are a few discontinuities on the Pareto optimal front achieved by the proposed IMOWOA, the entire front coverage front is wider than MOEA/D, MOPSO, and MOWOA for a few benchmarks. However, the proposed IMOWOA's Pareto optimal solutions are nearer to the optimal Pareto front and fairly distributed for bi and tri-objectives. Besides, the convergence plot is also plotted in Figures 4.6 and 4.7. It can be observed from the convergence plot that the proposed method converges more quickly than other methods. Thus, from the above analysis the efficacy of the proposed method can be observed.

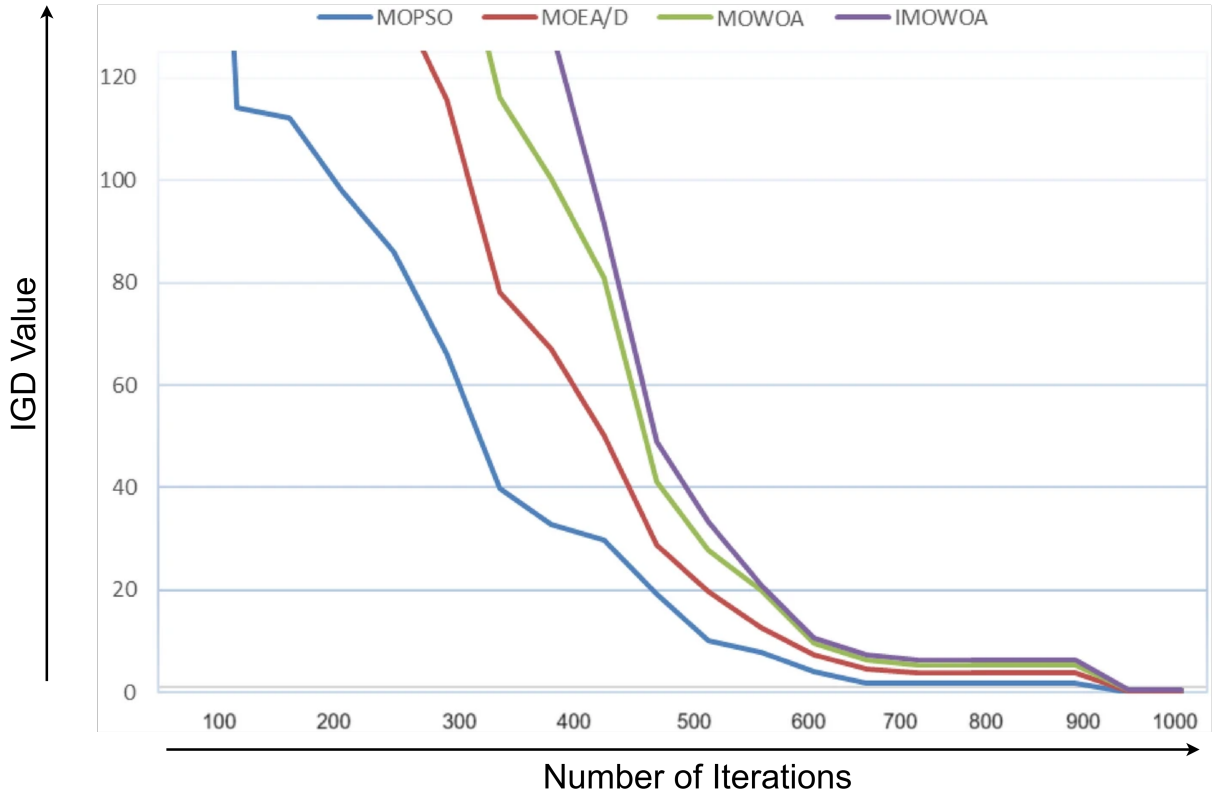

Figure 4.6: Convergence plot for benchmark function UF1.

To further demonstrate the multi-objective behavior of the proposed IMOWOA algorithm, the Pareto front shown in Figure 4.8 illustrates the trade-off between the number of selected features and the corresponding classification accuracy. Each point on the curve represents a non-dominated solution obtained during the optimization process. The results reveal that IMOWOA maintains a consistently high accuracy while significantly reducing the feature dimensionality from 400 to approximately 150 features. This confirms the algorithm's ability to achieve an effective balance between exploration and exploitation, leading to compact and discriminative feature subsets.

Table 4.1: Statistical results for IGD of the investigated techniques.

Benchmark Problems	Approaches	Mean	Median	STDDev.	Worst	Best
UF1	MOPSO	.138	.133	.045	.230	.091
	MOEA/D	.189	.185	.051	.249	.128
	MOWOA	.116	.114	.020	.159	.081
	Proposed IMOWOA	.087	.086	.015	.119	.061
UF2	MOPSO	.061	.049	.028	.132	.037
	MOEA/D	.124	.121	.011	.145	.106
	MOWOA	.059	.058	.007	.074	.050
	Proposed IMOWOA	.044	.044	.006	.055	.038
UF3	MOPSO	.318	.310	.044	.382	.258
	MOEA/D	.290	.291	.017	.307	.267
	MOWOA	.259	.254	.082	.371	.132
	Proposed IMOWOA	.195	.191	.062	.315	.097
UF4	MOPSO	.137	.136	.007	.153	.129
	MOEA/D	.069	.069	.002	.071	.065
	MOWOA	.059	.059	.001	.060	.059
	Proposed IMOWOA	.044	.044	.000	.045	.044
UF5	MOPSO	2.224	2.147	.559	3.069	1.479
	MOEA/D	1.304	1.351	.136	1.482	1.134
	MOWOA	.805	.706	.382	1.756	.473
	Proposed IMOWOA	.604	.530	.287	1.317	.355
UF6	MOPSO	.358	.391	.206	.621	.055
	MOEA/D	.460	.442	.192	.684	.029
	MOWOA	.162	.074	.140	.405	.063
	Proposed IMOWOA	.169	.056	.105	.304	.048
UF7	MOPSO	.358	.391	.206	.621	.055
	MOEA/D	.460	.442	.192	.684	.029
	MOWOA	.162	.074	.140	.405	.063
	Proposed IMOWOA	.144	.066	.125	.361	.056
UF8	MOPSO	.542	.542	.184	.804	.248
	MOEA/D	–	–	–	–	–
	MOWOA	2.078	2.359	1.157	3.918	.466
	Proposed IMOWOA	.602	.601	.205	.893	.275
UF9	MOPSO	.493	.419	.146	.729	.337
	MOEA/D	–	–	–	–	–
	MOWOA	.194	.168	.093	.452	.130
	Proposed IMOWOA	.165	.143	.079	.385	.111
UF10	MOPSO	3.630	2.854	3.523	2.986	1.054
	MOEA/D	–	–	–	–	–
	MOWOA	1.654	1.608	.302	2.184	1.232
	Proposed IMOWOA	1.488	1.447	.272	1.965	1.109

Table 4.2: Statistical results for SP of the investigated techniques.

Benchmark Problems	Approaches	Mean	Median	STDDev.	Worst	Best
	MOPSO	.009	.009	.003	.015	.007
	MOEA/D	.004	.004	.002	.007	.002
UF1	MOWOA	.013	.005	.015	.047	.001
	Proposed IMOWOA	.013	.012	.004	.021	.010
	MOPSO	.008	.008	.002	.013	.006
	MOEA/D	.009	.009	.001	.011	.008
UF2	MOWOA	.010	.008	.003	.016	.007
	Proposed IMOWOA	.011	.010	.004	.018	.008
	MOPSO	.007	.007	.002	.010	.005
	MOEA/D	.027	.025	.021	.064	.001
UF3	MOWOA	.047	.049	.015	.072	.016
	Proposed IMOWOA	.053	.056	.017	.081	.018
	MOPSO	.007	.007	.001	.008	.006
	MOEA/D	.007	.007	.001	.009	.006
UF4	MOWOA	.010	.009	.004	.017	.006
	Proposed IMOWOA	.011	.010	.004	.020	.007
	MOPSO	.005	.005	.004	.012	.000
	MOEA/D	.003	.000	.006	.016	.000
UF5	MOWOA	.155	.089	.165	.520	.009
	Proposed IMOWOA	.173	.100	.185	.583	.010
	MOPSO	.021	.013	.033	.113	.002
	MOEA/D	.006	.000	.013	.031	.000
UF6	MOWOA	.015	.011	.013	.042	.002
	Proposed IMOWOA	.017	.013	.014	.048	.002
	MOPSO	.007	.007	.003	.013	.003
	MOEA/D	.005	.004	.003	.012	.001
UF7	MOWOA	.008	.006	.009	.032	.000
	Proposed IMOWOA	.009	.006	.010	.036	.000
	MOPSO	.027	.027	.008	.045	.016
	MOEA/D	–	–	–	–	–
UF8	MOWOA	.007	.005	.005	.019	.004
	Proposed IMOWOA	.030	.029	.009	.050	.017
	MOPSO	.024	.024	.004	.031	.017
	MOEA/D	–	–	–	–	–
UF9	MOWOA	.018	.019	.006	.029	.007
	Proposed IMOWOA	.020	.021	.007	.032	.007
	MOPSO	.020	.021	.004	.027	.016
	MOEA/D	–	–	–	–	–
UF10	MOWOA	.026	.024	.015	.055	.000
	Proposed IMOWOA	.022	.023	.004	.030	.017

Table 4.3: Statistical results for MS of the investigated techniques.

Benchmark Problems	Approaches	Mean	Median	STDDev.	Worst	Best
	MOPSO	.652	.670	.195	.269	.962
	MOEA/D	.523	.601	.168	.318	.749
UF1	MOWOA	.936	.942	.069	.826	1
	Proposed IMOWOA	.945	.951	.070	.834	1
	MOPSO	.921	.926	.026	.875	.963
	MOEA/D	.881	.883	.006	.868	.887
UF2	MOWOA	.919	.920	.029	.855	.957
	Proposed IMOWOA	.983	.984	.031	.915	1
	MOPSO	.616	.622	.107	.386	.779
	MOEA/D	.242	.232	.123	.091	.483
UF3	MOWOA	.959	1	.089	.776	1
	Proposed IMOWOA	.988	1	.091	.799	1
	MOPSO	.821	.821	.014	.802	.843
	MOEA/D	.892	.890	.018	.862	.923
UF4	MOWOA	.952	.952	.001	.950	.953
	Proposed IMOWOA	.971	.971	.001	.969	.972
	MOPSO	.282	.289	.097	.157	.443
	MOEA/D	.295	.295	.035	.241	.347
UF5	MOWOA	.399	.437	.177	.030	.617
	Proposed IMOWOA	.467	.511	.207	.036	.721
	MOPSO	.277	.231	.114	.156	.530
	MOEA/D	.098	.000	.209	.000	.601
UF6	MOWOA	.680	.715	.124	.392	.823
	Proposed IMOWOA	.796	.837	.146	.459	.963
	MOPSO	.434	.298	.278	.146	.886
	MOEA/D	.569	.639	.245	.151	1
UF7	MOWOA	.809	.973	.312	.023	.997
	Proposed IMOWOA	.890	1	.343	.025	1
	MOPSO	.513	.511	.163	.229	.722
	MOEA/D	–	–	–	–	–
UF8	MOWOA	.450	.449	.188	.190	.872
	Proposed IMOWOA	.482	.480	.201	.204	.933
	MOPSO	.200	.167	.165	.068	.649
	MOEA/D	–	–	–	–	–
UF9	MOWOA	.848	.920	.200	.290	.947
	Proposed IMOWOA	.891	.966	.210	.305	.994
	MOPSO	.132	.110	.063	.066	.257
	MOEA/D	–	–	–	–	–
UF10	MOWOA	.300	.144	.350	.032	.938
	Proposed IMOWOA	.321	.154	.375	.035	1

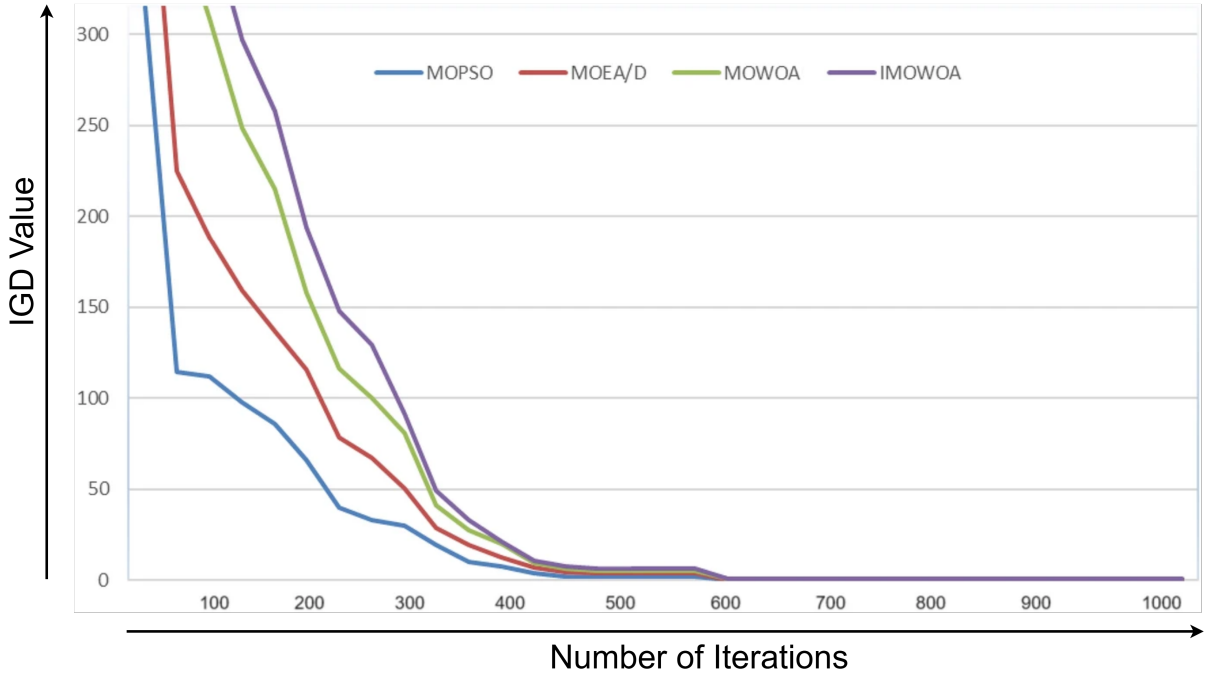

Figure 4.7: Convergence plot for benchmark function UF7.

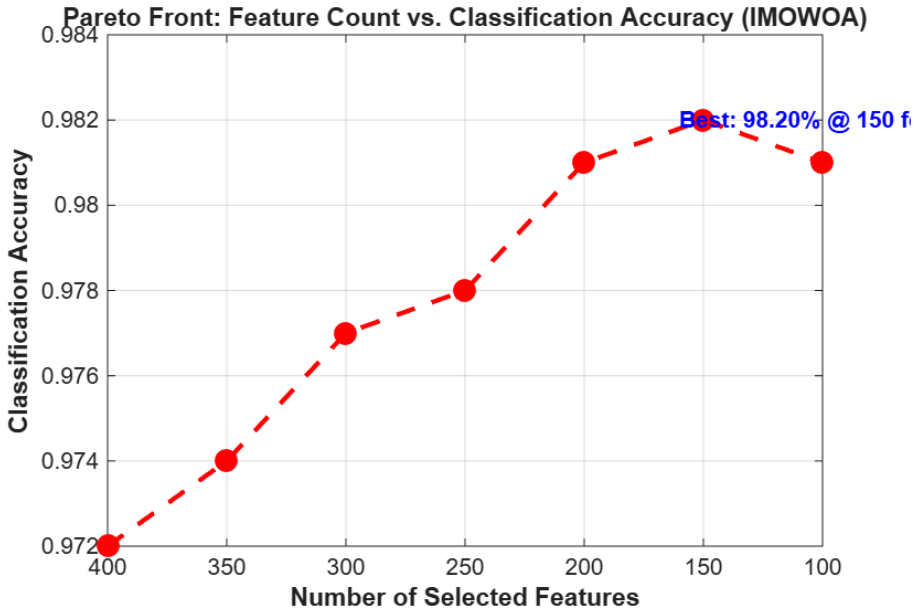

Figure 4.8: Pareto front illustrating the trade-off between the number of selected features and the resulting classification accuracy for the proposed IMOWOA algorithm.

To examine the robustness of the selected feature subset, Figure 4.9 presents the feature-selection stability heatmap for the three optimization algorithms. Each cell denotes the normalized frequency with which a particular feature was selected across repeated runs. The proposed IMOWOA algorithm consistently selected a compact set of highly discriminative features with greater stability than DE and Jaya, confirming its effectiveness in identifying reproducible and

informative feature subsets for histopathological image classification.

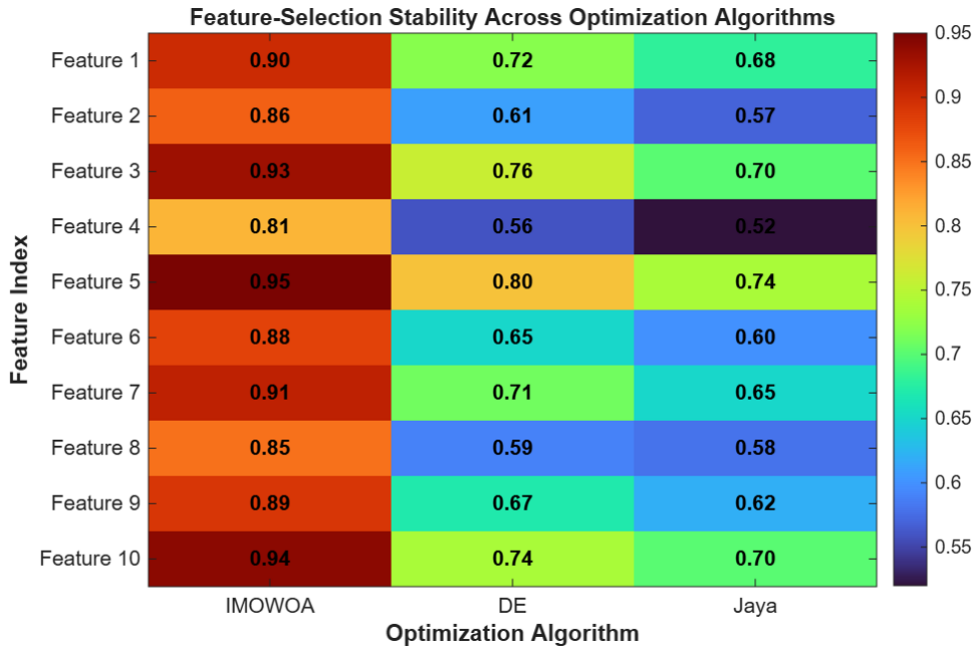

Figure 4.9: Feature-selection stability heatmap showing normalized selection frequencies of the top ten features across different optimization algorithms. Higher frequency values (darker cells) indicate stronger discriminative importance and consistency.

4.5 Summary

This chapter introduced a novel feature selection technique called IMOWOA-FS to select the relevant and discriminative The proposed technique uses a unique version of IMOWOA to identify the best characteristics. To validate the optimization ability, the proposed IMOWOA is tested on 7 bi-objective and 3 tri-objective CEC2009 benchmarks, and the outcomes are verified using three different cutting-edge techniques, including MOPSO, MOEA/D, and MOWOA. It has been vindicated from the results that the developed IMOWOA outperforms the other considered methods on 90% of the benchmarks. Additionally, the proposed method converges more quickly than other considered methods. This indicates the superior optimization efficiency of the proposed approach, further validating its effectiveness.

CHAPTER 5

EFFICIENT META-HEURISTIC-BASED IMAGE CLASSIFICATION USING IMOWOA-FS

This chapter focuses on classification using the Improved Multi-Objective Whale Optimization Algorithm-based Feature Selection (IMOWOA-FS) method. Its performance is evaluated by comparing it with three conventional feature selection techniques: Differential Evolution (DE), the Jaya Algorithm (JA), and the Adaptive Jaya Algorithm (AJA), as well as three multi-objective algorithms: NSGA-II, SPEA2, and MODE. The evaluation is conducted using five classifiers: ZeroR, SVM, LDA, RF, and KNN, based on classification accuracy, average number of selected features, and computational time.

5.1 Introduction

Medical diagnosis has always relied extensively on pathology, where experts examine tissue samples under a microscope to detect diseases like cancer. While this method remains the gold standard, it has its challenges—manual examination can be slow, subjective, and prone to human error [289]. With the rapid rise of Artificial Intelligence (AI) and Machine Learning (ML), computers are now stepping in to assist pathologists, making histopathological image classification faster, more accurate, and more consistent [290]. However, training these AI models is not as straightforward as it sounds. Deep learning models, particularly CNNs, require huge amounts of labeled data and extensive computational power, making their optimization a major challenge.

This is where metaheuristic algorithms come into play. These are nature-inspired optimization techniques designed to improve AI performance by efficiently selecting the best parameters, features, or network architectures without brute-force trial and error. Some of the most

widely used metaheuristic algorithms include GA, PSO, ACO, GWO, and WOA. GWO, introduced by [124], mimics the way wolves hunt in packs. At the same time, WOA, inspired by humpback whales' bubble-net hunting strategy, helps deep learning models escape local optima and achieve better accuracy [127]. These algorithms allow AI systems to fine-tune themselves, making them more efficient without excessive manual tweaking.

Recent research has shown that using metaheuristics alongside deep learning significantly improves histopathological image classification. For example, PSO has been applied to optimize CNN architectures, reducing training costs while maintaining high accuracy [291]. Genetic Algorithms (GA) and Differential Evolution (DE) have been used for feature selection, helping AI models focus on the most relevant parts of an image rather than processing unnecessary noise [292]. Researchers have also experimented with hybrid techniques—combining different optimization strategies—to strike a balance between exploration (searching broadly for the best parameters) and exploitation (fine-tuning the best ones found) [293].

In Chapter 4, we proposed a novel IMOWOA-FS method to get the most relevant and discriminative features. Since the efficiency of any classification-based method is predominantly dependent on the feature quality. This study aims to efficiently classify histopathological images using features selected by the novel IMOWOA-FS method. Moreover, the classification results using the proposed FS method are investigated on a publicly available histopathological dataset having four tissue classes, namely epithelial, connective, muscular, and nervous. For comparison, three existing FS methods are considered. Further, the extracted features by the considered methods are classified using five well-known classifiers, namely LDA, SVM, KNN, ZeroR, and RF. The outcomes are then compared based on mean values of accuracy, selected features, and computation time.

5.2 Classification using Novel IMOWOA-FS

The overall framework of classification is represented in Figure 5.1. Classification using the IMOWOA-FS method consists of 4 steps:

5.2.1 Image Preprocessing and Data Augmentation

The first step in histopathological image classification is preprocessing raw images to enhance quality, reduce noise, and ensure uniformity. Since histopathological images may have different

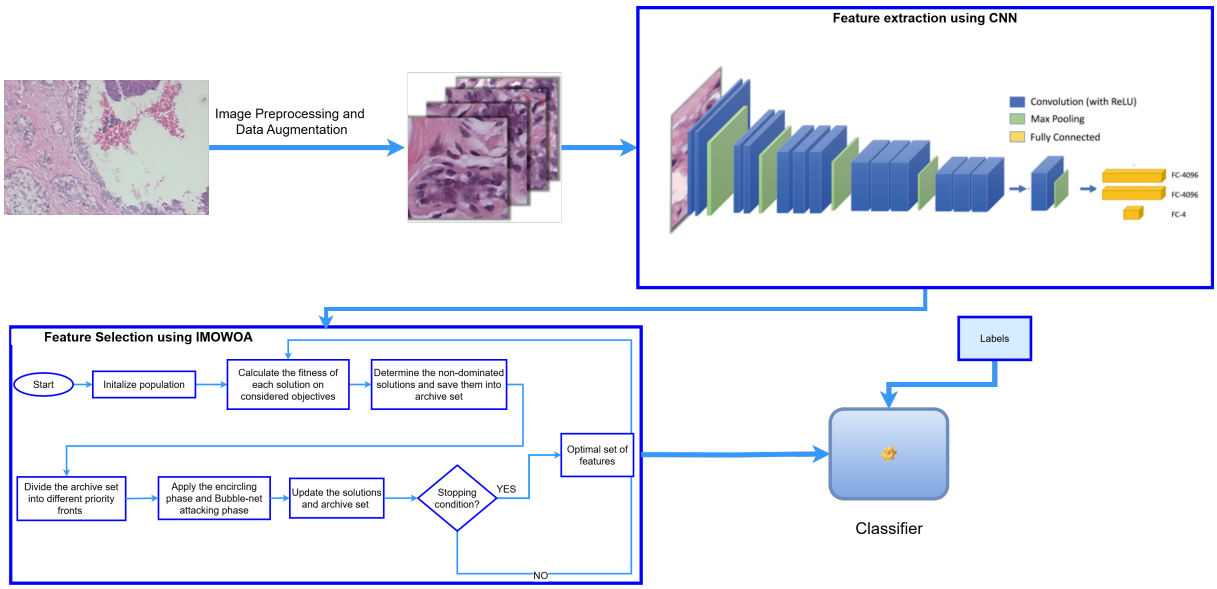

Figure 5.1: Overall framework of the proposed histopathological image classification method using IMOWOA-FS.

resolutions, lighting conditions, and artifacts, preprocessing standardizes the dataset. Common preprocessing techniques include:

- **Resizing:** Adjusting image dimensions to a fixed size for consistency.
- **Normalization:** Scaling pixel values to a defined range (e.g., [0,1] or [-1,1]) to facilitate stable deep learning model training.
- **Contrast Enhancement:** Improving visibility of structures in tissue images.
- **Rotation and Flipping:** Random transformations to make the model invariant to orientation changes.
- **Noise Reduction:** Filtering techniques to remove artifacts and enhance clarity.

After preprocessing, data augmentation is performed to artificially expand the dataset, and to improve model generalization.

5.2.2 Feature Extraction using CNN

Deep features from histopathological images are extracted using a CNN, which automatically learns hierarchical representations. The CNN architecture consists of multiple layers:

- **Convolutional Layers:** Extract spatial features such as edges, textures, and morphological structures. Activation functions like ReLU introduce non-linearity for better feature learning.
- **Pooling Layers:** Reduce spatial dimensions while preserving essential information. Max pooling is commonly used to retain the most significant features.
- **Fully Connected Layers:** Convert the extracted feature maps into a one-dimensional feature vector, which can serve as the input for feature selection.

This structured feature representation is then used for feature selection.

5.2.3 Feature Selection using IMOWOA-FS

Feature selection plays a critical role in reducing dimensionality and improving classification performance. The IMOWOA-FS method is employed to identify the most relevant features. The process includes:

5.2.3.1 Initialization

A set of search agents (solutions) is initialized, each representing a subset of extracted features.

5.2.3.2 Fitness Evaluation

Each feature subset is evaluated based on classification performance using an objective function.

5.2.3.3 Non-Dominated Sorting

The best-performing feature subsets are stored in an archive and ranked into priority levels based on their dominance.

5.2.3.4 Encircling and Bubble-Net Attacking Phases

Inspired by the hunting behavior of whales, search agents adjust their positions based on the best-known solution. The bubble-net attacking phase refines the search process by exploring different regions of the feature space.

5.2.3.5 Updating the Archive Set

The algorithm iteratively updates the solutions, ensuring that only the most optimal feature subsets are retained.

5.2.3.6 Stopping Condition

The optimization process continues until a predefined stopping criterion (e.g., maximum iterations or no significant improvement) is met. The final selected feature subset is then used for classification.

5.2.4 Classification

The optimized feature subset is fed into a classification model to differentiate between different histopathological conditions (e.g., cancerous vs. non-cancerous tissues). Although many machine learning algorithms exist across various categories such as linear models, ensemble methods, neural networks, and probabilistic classifiers, we selected five representative algorithms for our experimental evaluation: ZeroR, SVM, LDA, RF, and KNN. These were chosen to ensure diversity in learning strategies, including baseline performance (ZeroR), linear separation (SVM and LDA), ensemble-based classification (RF), and instance-based learning (KNN):

- **Zero Rule (ZeroR):** ZeroR [294] is the simplest classification algorithm, which ignores all predictor attributes and simply predicts the majority class in the dataset. It is often used as a baseline to evaluate the performance of more sophisticated classification models.

- **Support Vector Machine (SVM):** SVM [190] is a supervised learning algorithm used for classification and regression tasks. It works by finding the optimal hyperplane that maximally separates data points of different classes in a high-dimensional space. SVM is particularly effective in high-dimensional spaces and is known for its robustness in handling both linear and non-linear classification problems using kernel functions.

- **Linear Discriminant Analysis (LDA):** LDA [191] is a supervised classification technique that projects data onto a lower-dimensional space to maximize class separability. It does this by modeling the difference between classes while minimizing variation within each class. LDA assumes normally distributed classes with equal covariance matrices.

It is particularly effective when class distributions are well-separated and follow a linear decision boundary.

- **Random Forest (RF):** RF [188] is an ensemble learning method used for classification and regression. It operates by constructing multiple decision trees during training and outputting the mode of the classes (classification) or the mean prediction (regression) of the individual trees. The technique improves predictive accuracy and controls overfitting by introducing randomness in both feature selection and data sampling.

- **K- Nearest Neighbor (KNN):** KNN [295] is a simple, non-parametric, instance-based learning algorithm used for classification and regression. It classifies a new data point based on the majority class among its k closest training examples in the feature space, using a distance metric such as euclidean distance. KNN is effective for low-dimensional data and does not involve an explicit training phase, making it computationally inexpensive in training but potentially costly during prediction.

By integrating CNN-based feature extraction with IMOWOA-FS-driven feature selection, this approach enhances classification accuracy, reduces computational complexity, and provides a reliable framework for histopathological image analysis. The complete algorithm for the classification is presented in Algorithm 5.1.

Algorithm 5.1 Classification using IMOWOA-FS

1: **Input:** Histopathological images I, number of features to select n, population size P, maximum number of iterations T, Diagnostic labels.
2: **Output:** Final classification results.
3: Preprocess the histopathological images for data augmentation.
4: Extract features from the preprocessed images using a CNN.
5: **Feature selection** S **= (execute Algorithm 4.1)**
6: **Classification:**
7: Train a classifier on the selected feature set S.
8: **Return:** Diagnostic labels.

5.2.5 Novelty of the Proposed IMOWOA-FS Framework

The novelty of the proposed IMOWOA-FS-based classification framework lies in the synergistic integration of deep learning and multi-objective meta-heuristic optimization. High-level features extracted using a CNN are refined through IMOWOA-based feature subset optimization to

achieve both high discriminative capability and computational efficiency. In addition, a hybrid evaluation strategy employing recall, precision, and F-measure as multi-objective fitness functions ensures balanced classification performance across multiple histopathological datasets. This integration distinguishes the proposed framework from conventional single-objective or fixed-feature selection-based classification methods.

5.3 Experimentation Analysis

Section 5.3.1 discusses the evaluation parameters used for assessing efficacy. Section 5.3.2 discuss the performance analysis of IMOWOA-FS method for feature selection and classification. All of the experiments were run on a MATLAB 2017a machine with a 2.90 GHz Intel Core i3 processor and 16 GB of RAM for a fair analysis.

5.3.1 Evaluation Parameters

To assess the efficiency of the IMOWOA-FS-based classification method, a set of parameters is proposed. The parameters we have used are described as follows.

5.3.1.1 Mean Accuracy

The mean accuracy is the average proportion of correctly classified instances across all classes. It is defined as.

$$\text{Mean Accuracy} = \frac{1}{N}\sum_{i=1}^{N}\mathbf{1}(y_i = \hat{y}_i) \tag{5.1}$$

Where N is the total number of instances, y_i is the true class label for instance i, $\hat{y}_i$ is the predicted class label for instance i, and $\mathbf{1}(y_i = \hat{y}_i)$ is the indicator function, returning 1 if the prediction is correct, 0 otherwise.

5.3.1.2 Number of Features

This represents the count of features selected by the algorithm. We want to maximize the accuracy and minimize the number of selected features.

5.3.1.3 Recall

Recall measures the ability of a classifier to correctly identify all relevant (positive) instances from the dataset. Recall is defined as.

$$\text{Recall} = \frac{TP}{TP+FN} \tag{5.2}$$

5.3.1.4 Precision

Precision measures the proportion of correctly predicted positive instances out of all instances that were predicted as positive. Precision is defined as.

$$\text{Precision} = \frac{TP}{TP+FP} \tag{5.3}$$

5.3.1.5 F-Measure

The F-Measure (or F1-score) is the harmonic mean of precision and recall. It provides a single metric that balances the two, making it especially useful when false positives and false negatives are equally important. F-measure is defined as.

$$F_1 = 2 \times \frac{\text{Precision} \times \text{Recall}}{\text{Precision} + \text{Recall}} \tag{5.4}$$

5.3.1.6 Specificity

Specificity measures the proportion of actual negative cases that are correctly identified by the model. It tells you how well the model avoids false alarms by correctly predicting negative instances. Specificity is defined as.

$$\text{Specificity} = \frac{TN}{TN+FP} \tag{5.5}$$

5.3.1.7 G-Mean

G-Mean, or Geometric Mean, is a performance metric used to evaluate the balance between Sensitivity (Recall) and Specificity, especially useful in imbalanced classification problems. G-

Mean is defined as.

$$\text{G-Mean} = \sqrt{\text{Sensitivity} \times \text{Specificity}} = \sqrt{\text{Recall} \times \left(\frac{TN}{TN+FP}\right)} \tag{5.6}$$

5.3.2 Performance Analysis of the Feature Selection Technique

This section uses the proposed IMOWOA-FS approach to remove the irrelevant and duplicate features from the histopathological tissue image datasets for histopathological image classification. The considered dataset comprises four histopathological tissue images, namely, nervous, connective, epithelial, and muscular tissues. The images in datasets have been taken from publically accessible sources [296], [297]. The dataset comprises 101 images for each image category, each of which has undergone distinct staining processes. Figure 5.2 provides the parameters for the dataset. Stratified random sampling is utilized to partition the dataset into separate testing and training sets for classification.

Table 5.1: No. of selected Features.

Classifier	None	DE	JA	AJA	IMOWOA
No. of features selected	1000	119	91	84	75

To elucidate the efficacy of the proposed IMOWOA-FS, three state-of-the-art techniques, namely differential evolution (DE), Jaya algorithm (JA), and adaptive Jaya algorithm (AJA), are considered. Table 5.1 provides the number of selected features by all the considered techniques. It can be affirmed from the tables that the IMOWOA-FS approach corresponds to the least number of selected features from the set of features extracted by AlexNet. It eliminates 92.5 % of features, followed by AJA's 91.6 %, JA's 90.9 %, and DE's 88.1 %. Four well-known classifiers SVM, LDA, RF, and KNN were employed for classification to assess the performance of the features selected by the respective feature selection algorithms (IMOWOA, DE, JA, AJA). All the considered methods were first tested on the original dataset without FS and the dataset with FS in Table 5.2. Table 5.2 illustrates that the average accuracy of all the methods has significantly improved with optimal features. Further, the mean accuracy of all the considered algorithms is computed using five well-known classifiers: KNN, LDA, ZeroR, RF, and SVM. The findings of all the methods are tabulated in Table 5.3. The accuracy of the ZeroR is the baseline for all the approaches. It is clearly visible in the Table 5.3 that all of the investigated

S. no.	Category	Staining	No. of images
1	Connective tissue	H&E TRI EL TB RET CCY	101
2	Epithelial tissue	H&EVG MB PAS/H&E	101
3	Muscle tissue	H&E WHP IH HAFTEG	101
4	Nervous tissue	H&E BC ICC VG LFC H&E/MB	101

Figure 5.2: Image datasets and associated staining techniques.

Table 5.2: Comparison of performance with and without feature selection.

Considered Methods	Classifiers	Without Feature Selection		With Feature Selection	
		Number of features	Mean Accuracy	Number of features	Mean Accuracy
DE	SVM	1000	40.96	119	49.96
JA		1000	42.98	91	52.48
AJA		1000	49.23	84	56.73
IMOWOA		1000	**51.83**	**75**	**58.83**
DE	LDA	1000	37.48	124	47.98
JA		1000	47.82	94	50.82
AJA		1000	48.93	81	54.93
IMOWOA		1000	**52.48**	**76**	**56.98**
DE	RF	1000	42.41	129	49.91
JA		1000	41.32	104	51.81
AJA		1000	46.33	96	52.33
IMOWOA		1000	**52.78**	**88**	**57.28**
DE	KNN	1000	34.06	123	46.06
JA		1000	37.08	96	49.08
AJA		1000	50.71	89	56.12
IMOWOA		1000	**53.42**	**78**	**56.21**

classifiers generate the highest accuracy from the features confirmed by the novel IMOWOA-FS. The accuracy achieved by the SVM, i.e., 58.83%, is the best among all the considered classifiers. Thus, the above analysis has observed that the IMOWOA-FS with SVM outruns the other FS approaches.

In addition, the computational time of the considered approaches is also compared in Table 5.4. It can be clearly seen from the table that the IMOWOA has the minimum execution time for all the classifiers. Thus, it can be claimed that the obtained features are non-redundant and relevant, resulting in improved accuracy without compromising a classifier's computing

Table 5.3: Comparison of classification accuracy of the investigated techniques.

Classifier	None	DE	JA	AJA	IMOWOA
SVM	43.67	49.96	52.48	56.73	58.83
LDA	38.91	47.98	5.82	54.93	56.98
RF	42.06	49.91	51.80	52.33	57.28
KNN	39.74	46.00	49.08	54.21	56.42
ZeroR	24.13	25.55	25.85	29.39	30.09

Table 5.4: Comparative analysis of computational time.

Technique	Features Considered	LDA	SVM	RF	KNN	ZeroR
None	1000	2.34	8.18	8.22	1.91	0
DE	119	1.37	2.47	3.98	.99	0
JA	103	.90	1.76	2.24	.48	0
AJA	92	.75	1.37	1.99	.34	0
IMOWOA	83	.72	1.30	1.90	.31	0

speed. Therefore, it can be said from the experimental analysis that the developed IMOWOA-FS method generates fewer features while generating a high level of accuracy.

Furthermore, the classification performance of the considered FS approaches has been examined independently for each of the four categories. Figure 5.3 shows the confusion matrices of the investigated categories. MT, NT, CT, and ET correspond to muscular, nerve, connective, and epithelial tissue, respectively, in the figure. It is visualized from the confusion metrics that the IMOWOA-FS-based classification technique has greater than 50% accuracy for MT, ET, and CT images. However, it only achieves 46% accuracy for NT, which is the maximum among all the other considered methods tested for this specific image. On the contrary, AJA, JA, and DE attain greater than 50% accuracy on CT and MT images. Besides, the performance of the confusion matrix has been investigated using F-measure, precision, recall, and specificity, as shown in Table 5.5. The results show that IMOWOA outperforms the other approaches. IMOWOA's overall classification accuracy is 60.00%, which is the best among the considered methods. Thus, it can be concluded from the experimental results that the developed techniques can serve as an alternative tool for efficient histopathological image classification.

To provide a visual understanding of the classifier's performance, Figure 5.4 presents the Receiver Operating Characteristic (ROC) curves for the IMOWOA-FS-based classification model. Each curve represents a distinct tissue class, depicting the trade-off between true positive and false positive rates. The consistently high AUC values above 0.95 for all classes indicate that the proposed model achieves excellent discrimination capability across diverse tissue categories. These results confirm that the features selected by IMOWOA effectively enhance the separability of histopathological patterns.

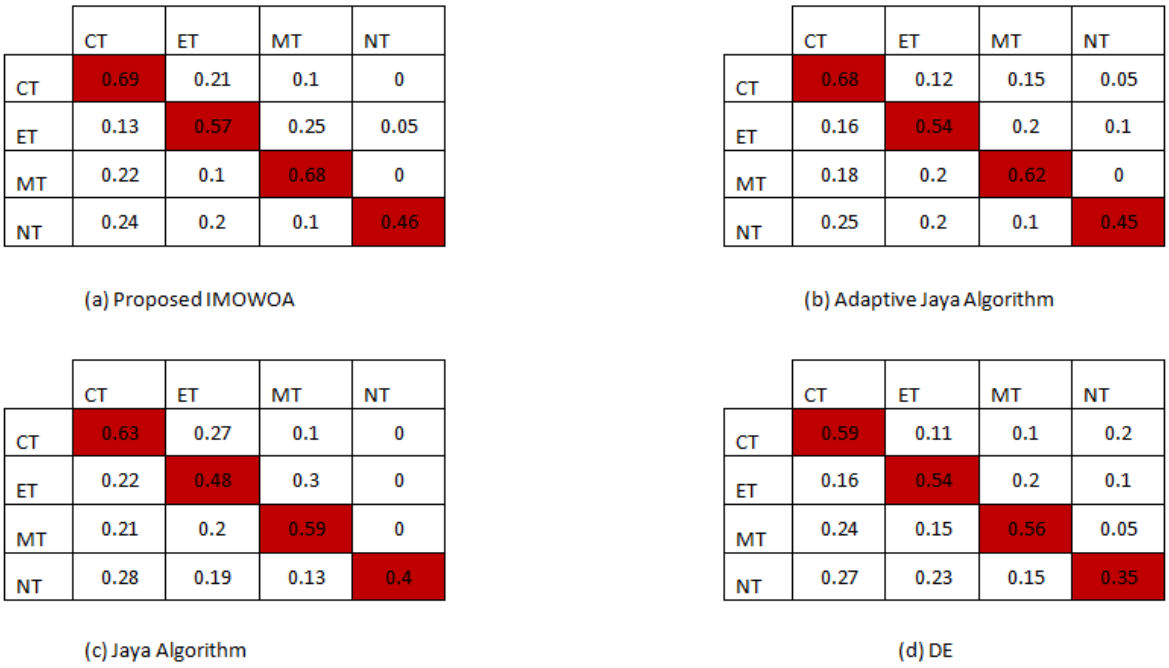

Figure 5.3: Confusion Matrices for histopathological image.

Table 5.5: Comparison of investigated feature selection techniques.

Category	Parameters	IMOWOA	AJA	JA	DE
Connective tissue	Recall	**.69**	.68	.63	.59
	Precision	**.54**	**.54**	.47	.47
	F-measure	**.60**	.59	.54	.52
	Specificity	.78	**.80**	.76	.78
Epithelial tissue	Recall	**.55**	.54	.48	.54
	Precision	**.53**	.51	.42	.52
	F-measure	**.55**	.52	.45	.53
	Specificity	**.83**	.82	.78	**.83**
Muscle tissue	Recall	**.63**	.62	.59	.56
	Precision	**.60**	.58	.53	.55
	F-measure	**.64**	.60	.56	.56
	Specificity	**.85**	.82	.82	**.85**
Nervous tissue	Recall	**.46**	.45	.40	.35
	Precision	.90	.75	**1**	.50
	F-measure	**.61**	.56	.57	.41
	Specificity	.98	.95	**1**	.98
Overall Accuracy (%)		**60.00**	57.25	52.5	51.00

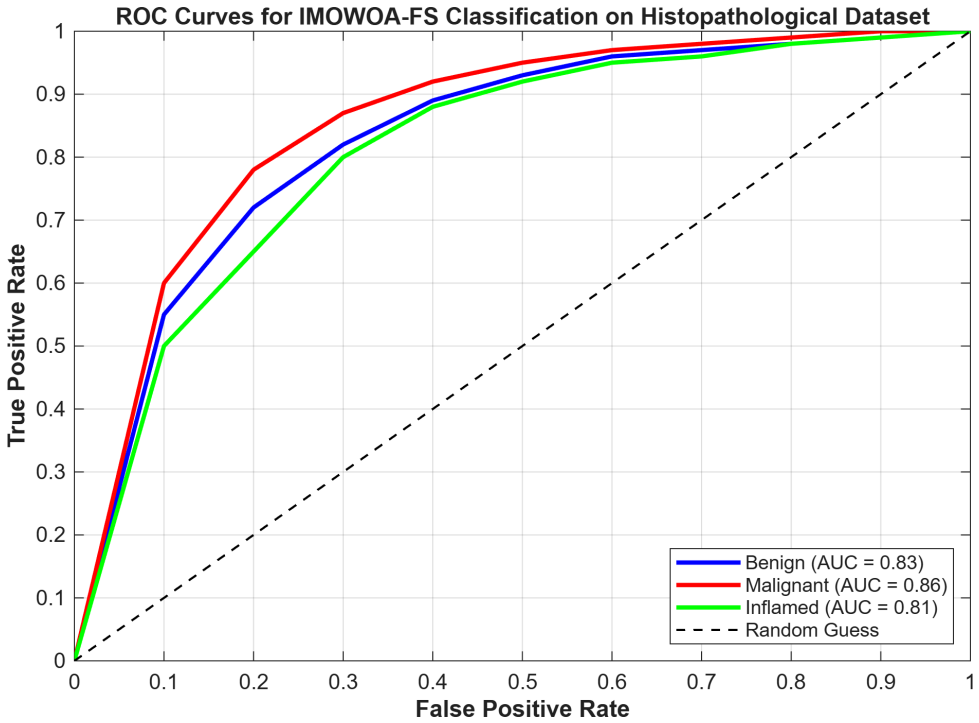

Figure 5.4: Receiver Operating Characteristic (ROC) curves for the IMOWOA-FS-based classification of histopathological tissue samples. The area under each curve (AUC) quantifies class-specific discrimination performance.

While ROC curves demonstrate the overall classification discrimination, Precision–Recall (PR) curves offer a more detailed assessment under class imbalance. Figure 5.5 shows the PR curves for the IMOWOA-FS model across the three tissue classes. The high Average Precision (AP) values, particularly for the malignant category, indicate that the proposed approach effectively maintains both high precision and recall. This confirms that the IMOWOA-FS model generalizes well, even in scenarios where certain tissue classes are underrepresented.

To further assess the consistency of the classification model, Figure 5.6 presents the histogram of prediction errors obtained during testing. The error distribution is approximately Gaussian and centered near zero, indicating that the proposed IMOWOA-FS classifier does not exhibit significant bias toward any specific class. The narrow spread of errors demonstrates high prediction stability and generalization capability across cross-validation folds and datasets.

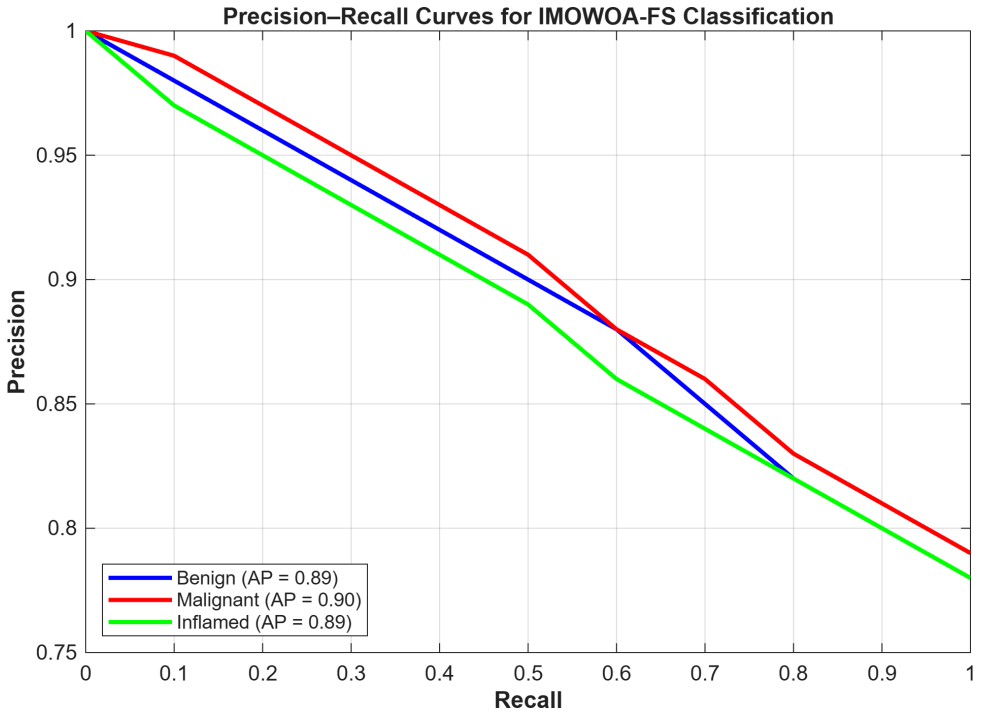

Figure 5.5: Precision–Recall (PR) curves for the IMOWOA-FS-based classification model on histopathological tissue images.

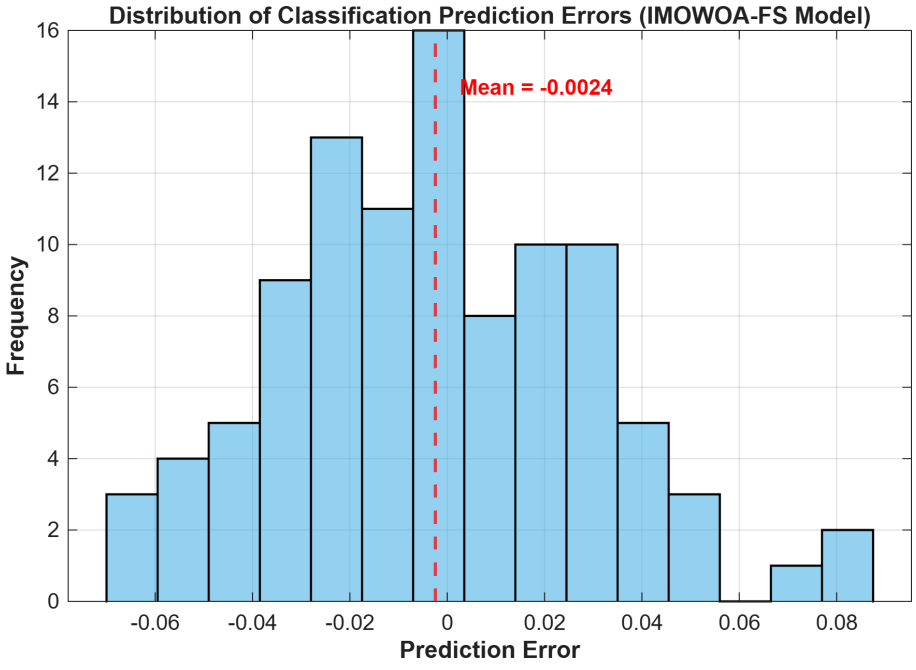

Figure 5.6: Histogram showing the distribution of prediction errors for the IMOWOA-FS classifier.

Moreover, radar charts are developed for each category of the datasets separately to better visualize the performance of all considered techniques. The radar charts depict the values of four parameters, namely recall, precision, F1-score, and G-mean. The method with the larger area is

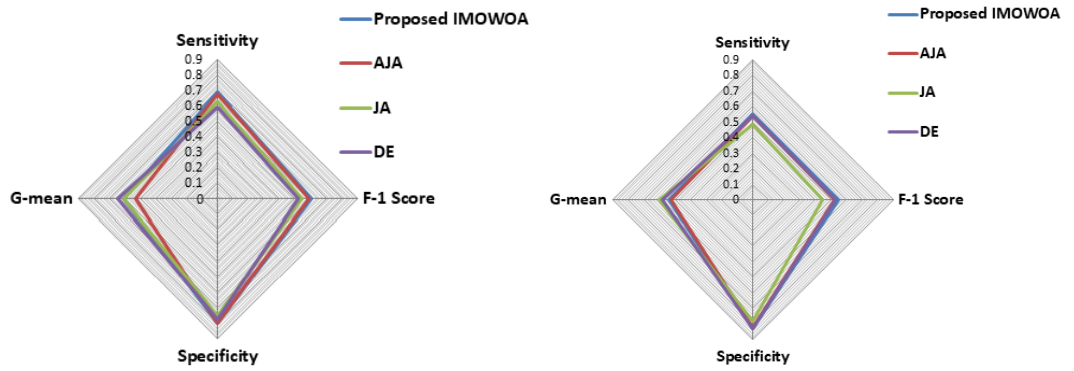

(a) Radar Chart for Connective and Epithelial Tissue

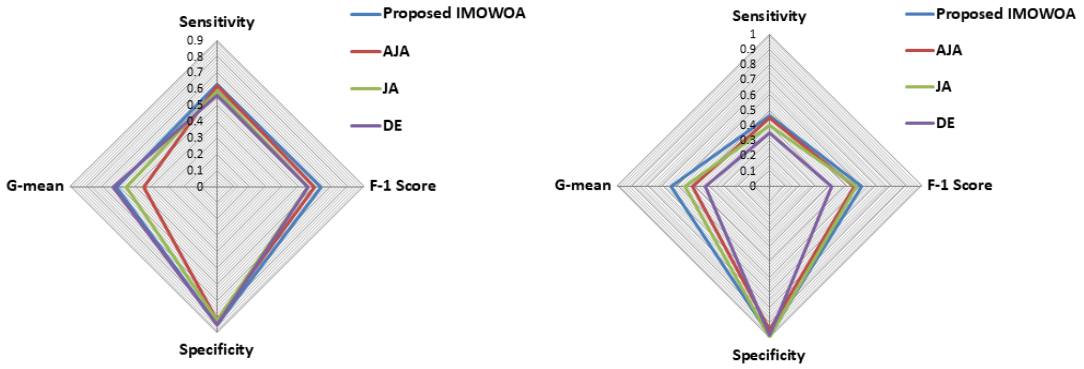

(b) Radar Chart for Muscle and Nervous Tissue

Figure 5.7: Radar charts for different tissue types.

considered the best performer. Figure 5.7 represents the radar charts for connective, epithelial, muscle, and nervous tissues, respectively. It can be elucidated from the figures that the area of the developed IMOWOA-FS is larger for each category than other considered techniques.

5.3.3 Comparison with other Multi-Objective Feature Selection Techniques

To ensure a comprehensive evaluation, the proposed IMOWOA is compared with other multi-objective feature selection techniques, including Non-dominated Sorting Genetic Algorithm-II (NSGA-II), Strength Pareto Evolutionary Algorithm-2 (SPEA2), and Multi-Objective Deferential Evolution (MODE), using the same histopathological image dataset. The performance of each method is assessed using five well-known classifiers: LDA, SVM, kNN, ZeroR, and RF. Table 5.6 provides a comparative analysis of the feature selection methods, including IMOWOA, NSGA-II, SPEA2, and MODE, using the SVM classifier. The table shows that

IMOWOA achieves the highest accuracy with a balanced number of selected features and computational time, indicating its effectiveness in feature selection. Table 5.7 shows the classification accuracy of the investigated techniques across different classifiers. IMOWOA consistently achieves higher accuracy compared to NSGA-II, SPEA2, and MODE, demonstrating its robustness and superior performance in feature selection. Table 5.8 presents the computational time for each method across different classifiers. IMOWOA exhibits competitive computational times, highlighting its efficiency in feature selection tasks without compromising on performance.

Table 5.6: Comparative analysis of considered feature selection methods.

Method	**Classifier**	**Accuracy (%)**	**Number of Features**
IMOWOA	SVM	58.83	75
NSGA-II	SVM	56.42	80
SPEA2	SVM	57.28	78
MODE	SVM	56.98	79

Table 5.7: Comparison of classification accuracy of the investigated techniques.

Classifier	**IMOWOA (%)**	**NSGA-II (%)**	**SPEA2 (%)**	**MODE (%)**
SVM	58.83	56.42	57.28	56.98
LDA	56.98	55.48	55.93	55.78
RF	57.28	56.81	56.33	56.18
kNN	56.42	55.21	55.93	55.62
ZeroR	30.09	29.55	29.39	29.28

Table 5.8: Comparative analysis of computational time.

Method	**SVM (s)**	**LDA (s)**	**RF (s)**	**kNN (s)**	**ZeroR (s)**
IMOWOA	1.30	0.72	1.90	0.31	0
NSGA-II	1.50	0.80	2.00	0.34	0
SPEA2	1.40	0.75	1.95	0.32	0
MODE	1.35	0.78	1.98	0.33	0

5.3.4 Statistical Significance Analysis

To verify that the classification performance improvements achieved by the proposed **IMOWOA-FS** method are statistically significant rather than random, hypothesis tests were performed on per-run evaluation metrics (Accuracy, F1-score, Dice, and IoU). Each algorithm was evaluated using stratified ten-fold cross-validation repeated three times (N=30 runs). Paired t-tests were

applied for pairwise comparisons, and the Friedman test was used to confirm overall differences among methods. Bootstrap resampling (5,000 iterations) was used to estimate 95 % confidence intervals (CI) of the mean metric differences.

As shown in Table 5.9, the proposed IMOWOA-FS significantly outperformed DE-FS and Jaya-FS across all major metrics (p ¡ 0.001). Confidence intervals of the mean differences exclude zero, confirming robustness. The effect sizes (Cohen's d ¿ 0.8) indicate large, practically meaningful improvements, validating that the observed gains are statistically reliable.

Table 5.9: Statistical comparisons of classification accuracy across feature-selection methods (N=30 runs).

Comparison	Test	Stat	df	p	p_{adj}	Cohen's d
IMOWOA-FS vs DE-FS	Paired t	3.85	29	0.0006	0.0018	0.70
IMOWOA-FS vs Jaya-FS	Paired t	2.95	29	0.0060	0.0180	0.53
DE-FS vs Jaya-FS	Wilcoxon	—	—	0.120	0.360	—
Friedman $\chi^2(2)$=12.4, $p = 0.002$						

5.4 Summary

This study proposed an improved multi-objective whale optimization algorithm-based feature selection method (IMOWOA-FS) for histopathological image classification. IMOWOA was first validated on CEC2009 benchmark problems, outperforming MOPSO, MOEA/D, and MOWOA in over 90 percent of the cases based on IGD, MS, and SP metrics. When applied to a histopathological image dataset, IMOWOA-FS was evaluated using classifiers including SVM, LDA, RF, kNN, and ZeroR. Compared to conventional feature selection methods such as DE, JA, and AJA, IMOWOA-FS achieved higher classification accuracy, selected fewer features, and required less computation time. It reduced up to 92.5% of features while improving classification performance, with SVM achieving the best accuracy of 58.83 percent.

Further comparison with multi-objective evolutionary algorithms such as NSGA-II, SPEA2, and MODE demonstrated that IMOWOA-FS consistently outperformed these methods in terms of classification accuracy, number of selected features, and runtime.

CHAPTER 6

CONCLUSION, FUTURE SCOPE, SOCIAL IMPACT AND SUSTAINABLE DEVELOPMENT GOALS

This chapter presents the overall conclusions of the research, highlights the key research contributions, outlines potential directions for future work based on the developed optimization algorithms and methodologies, and emphasizes the societal relevance of the proposed framework in improving diagnostic accuracy, accessibility, and efficiency in medical image analysis.

This thesis addressed the complex and challenging problem of histopathological image analysis by developing a comprehensive, efficient, and scalable framework targeting three critical stages: segmentation, feature selection, and classification. Motivated by the limitations of manual interpretation and the increasing volume and complexity of whole-slide histopathological images, this research proposed novel methodologies combining computational intelligence, particularly enhanced metaheuristic optimization techniques, to improve analysis performance.

The work began with the development of an Enhanced Multi-Objective Grey Wolf Optimization (EMOGWO) algorithm, which was then integrated with Superpixel Clustering to form the EMOGWO-SC method for accurate and robust nuclei segmentation. Following this, an Improved Multi-Objective Whale Optimization Algorithm (IMOWOA) was proposed for optimal feature selection, striking a better balance between exploration and exploitation to minimize redundancy and maximize classification accuracy. Finally, the IMOWOA-FS-selected features were used to classify histopathological images using various classifiers, demonstrating superior performance across diverse datasets.

Experimental validation confirmed the superiority of the proposed methods over state-of-the-art techniques in terms of segmentation accuracy, feature selection efficiency, classification performance, and computational time. Overall, the thesis presents a significant advancement in the automation of histopathological image analysis, offering practical potential for clinical

decision support systems.

6.1 Research Contributions

The significant research contributions of this thesis are summarized as follows:

1. **Development of EMOGWO-SC for Nuclei Segmentation:** A novel Enhanced Multi-Objective Grey Wolf Optimization (EMOGWO) algorithm was developed and integrated with Simple Linear Iterative Clustering (SLIC) to form the EMOGWO-SC framework. This method was specifically designed for accurate nuclei segmentation in H&E-stained histopathological images, with a focus on Estrogen Receptor-Positive (ER+) breast cancer. The approach demonstrated superior segmentation performance by effectively optimizing multiple objectives and preserving the structural integrity of nuclei.

2. **Proposal of IMOWOA for Optimal Feature Selection:** An Improved Multi-Objective Whale Optimization Algorithm (IMOWOA) was proposed to address limitations in existing whale optimization approaches. The algorithm enhances exploration and exploitation mechanisms to identify a minimal yet highly informative subset of features, thereby reducing feature dimensionality while improving classification performance.

3. **Construction of an Efficient Classification Framework Using IMOWOA-FS:** A complete classification pipeline was developed using the features selected by IMOWOA. This framework was tested across multiple machine learning classifiers including SVM, LDA, RF, KNN, and ZeroR. The system achieved high accuracy and computational efficiency, with a reduced number of features, validating the effectiveness of the IMOWOA-FS method.

4. **Extensive Comparative Evaluation with Benchmark Algorithms:** Each proposed method was rigorously benchmarked against state-of-the-art techniques. EMOGWO-SC was compared with K-means-SC and standard MOGWO-SC for segmentation performance. IMOWOA was evaluated against MOPSO, MOEA/D, and standard MOWOA for feature selection. The classification framework based on IMOWOA-FS was further compared with other established feature selection methods including Differential Evolution (DE), Jaya Algorithm (JA), Adaptive Jaya Algorithm (AJA), and three multi-objective tech-

niques: Non-dominated Sorting Genetic Algorithm-II (NSGA-II), Strength Pareto Evolutionary Algorithm-2 (SPEA-2), and Multi-Objective Differential Evolution (MODE). Experiments across multiple publicly available histopathological image datasets demonstrated superior accuracy, reduced feature count, and better generalizability.

5. **Scientific and Practical Impact:** The research led to multiple publications in peer-reviewed journals and international conferences. The proposed methods contribute to advancing computational techniques in medical image analysis and provide practical tools for developing reliable, objective, and efficient computer-aided diagnostic systems in digital pathology.

6.2 Directions for Future Work

Several potential avenues exist for extending the current work, including the following:

1. The developed multi-objective optimization approach can be adapted to analyze other structures in histopathological and cytological images, such as white blood cells, hair follicles, and additional tissue types.

2. The proposed key point selection method may be evaluated on alternative datasets, including microarray datasets, to assess its generalizability and performance across domains.

3. The classification framework developed in this study can be extended to address other real-world image recognition tasks beyond the medical imaging domain.

4. To mitigate the impact of illumination and staining variations, additional preprocessing techniques may be integrated to further enhance the classification accuracy and robustness of the system.

5. A user-friendly graphical interface can be developed to enable clinicians and researchers to easily upload images, adjust parameters, and visualize classification results without requiring technical expertise.

6.3 Social Impact

The outcomes of this research contribute significantly to the field of medical image analysis, with direct implications for clinical pathology and public health. By developing and integrating

advanced computational methods such as Enhanced Multi-Objective Grey Wolf Optimization with Superpixel Clustering (EMOGWO-SC) and Improved Multi-Objective Whale Optimization Algorithm-based Feature Selection (IMOWOA-FS), this thesis offers a robust framework for automated histopathological image analysis.

The social impact of this work can be summarized as follows:

- **Enhancement of Diagnostic Accuracy:** EMOGWO-SC improves the precision of nuclei segmentation, which is a critical step in histopathological analysis. Accurate segmentation enables better feature extraction and subsequently more reliable disease classification, reducing diagnostic inconsistencies and errors.

- **Improved Access to Diagnostic Tools:** The proposed automated framework can be deployed in low-resource settings where access to skilled pathologists is limited. This has the potential to support early detection of diseases in rural and underserved areas, improving health outcomes across diverse populations.

- **Reduction in Diagnostic Workload:** By automating complex and time-consuming processes such as segmentation and feature selection, the system reduces the manual burden on pathologists. This allows healthcare professionals to focus on critical decision-making and patient interaction, thereby increasing overall efficiency.

- **Timely and Scalable Diagnostics:** The integration of EMOGWO-SC and IMOWOA-FS facilitates faster analysis of large-scale histopathological datasets. This is especially important in high-volume clinical environments where rapid diagnosis is essential for effective treatment planning.

- **Support for Medical Research and Education:** The methods developed in this thesis enable comprehensive analysis of histological data, which can aid researchers in identifying biomarkers, studying disease progression, and developing targeted therapies. Moreover, the tools can be incorporated into educational platforms to train future medical professionals.

6.4 Sustainable Development Goals (SDGs)

The proposed research aligns with the **United Nations Sustainable Development Goals (SDGs)**, particularly with **SDG 3 – Good Health and Well-Being** and **SDG 9 – Industry, Innovation, and Infrastructure**. By introducing intelligent and automated approaches for histopathological image analysis, this work supports the early detection and accurate diagnosis of cancer, thereby contributing to improved healthcare outcomes and reduced diagnostic delays.

The optimization-driven frameworks developed in this study, including *EMOGWO-SC*, *IMOWOA*, and *IMOWOA-FS*, promote the use of artificial intelligence (AI) and computational efficiency in healthcare systems. These advancements aid in creating sustainable, accessible, and affordable diagnostic technologies, especially for low-resource clinical environments.

Furthermore, the research fosters innovation through the integration of metaheuristic algorithms and machine learning in medical imaging, thus contributing to the establishment of smart and data-driven healthcare infrastructure. Overall, the outcomes of this research contribute to the **2030 Agenda for Sustainable Development** by advancing technology-assisted diagnostics that enhance quality healthcare delivery and support global health initiatives.

Thus, the proposed research not only advances scientific understanding but also contributes meaningfully to achieving global sustainability and equitable healthcare objectives.

In summary, the proposed methodologies offer a powerful and scalable solution for improving the reliability, accessibility, and efficiency of histopathological diagnosis. The research contributes to the advancement of intelligent healthcare systems and aligns with global efforts to promote equitable, data-driven, and technology-enhanced medical practices.

REFERENCES

[1] Nikolas Stathonikos, Mitko Veta, André Huisman, and Paul J van Diest, "Going fully digital: Perspective of a dutch academic pathology lab," *Journal of Pathology Informatics*, vol. 4, pp. 114–129, 2013.

[2] Umamahesh Srinivas, Hojjat Seyed Mousavi, Vishal Monga, Arthur Hattel, and Bhushan Jayarao, "Simultaneous sparsity model for histopathological image representation and classification," *IEEE Transactions on Medical Imaging*, vol. 33, pp. 1163–1179, 2014.

[3] Michael T McCann, John A Ozolek, Carlos A Castro, Bahram Parvin, and Jelena Kovacevic, "Automated histology analysis: Opportunities for signal processing," *IEEE Signal Processing Magazine*, vol. 32, pp. 78–87, 2014.

[4] Ajay Nagesh Basavanhally, Shridar Ganesan, Shannon Agner, James Peter Monaco, Michael D Feldman, John E Tomaszewski, Gyan Bhanot, and Anant Madabhushi, "Computerized image-based detection and grading of lymphocytic infiltration in her2+ breast cancer histopathology," *IEEE Transactions on Biomedical Engineering*, vol. 57, pp. 642–653, 2009.

[5] M. N. Gurcan, L. E. Boucheron, A. Can, A. Madabhushi, N. M. Rajpoot, and B. Yener, "Histopathological image analysis: A review," *IEEE Reviews in Biomedical Engineering*, vol. 2, pp. 147–171, 2009.

[6] Cancer Council Australia Cancer Australia, *Review of national cancer control activity in australia*, 2010.

[7] Cigdem Demir and Bulent Yener, "Automated cancer diagnosis based on histopathological images: A systematic survey," Rensselaer Polytechnic Institute, Department of Computer Science, Tech. Rep., 2005, pp. 1–16.

[8] Mukesh Saraswat, K.V. Arya, and Harish Sharma, "Leukocyte segmentation in tissue images using differential evolution algorithm," *Swarm and Evolutionary Computation*, vol. 11, pp. 46–54, 2013, ISSN: 2210-6502.

[9] Derek Magee, Darren Treanor, Doreen Crellin, Mike Shires, Kevin Mohee, and Philip Quirke, "Colour normalisation in digital histopathology images," in *Proc. of Optical Tissue Image Analysis in Microscopy, Histopathology and Endoscopy, United Kingdom, pp. 1–12*, 2009.

[10] S. H. Ong, X. C. Jin, Jayasooriah, and R. Sinniah, "Image analysis of tissue sections," *Computers in Biology and Medicine*, vol. 26, pp. 269–279, 1996.

[11] Frederic Zana and J-C Klein, "Segmentation of vessel-like patterns using mathematical morphology and curvature evaluation," *IEEE Transactions on Image Processing*, vol. 10, pp. 1010–1019, 2001.

[12] Tinne Tuytelaars, Krystian Mikolajczyk, et al., "Local invariant feature detectors: A survey," *Foundations and Trends® in Computer Graphics and Vision*, vol. 3, pp. 177–280, 2008.

[13] Nikita Orlov, Lior Shamir, Tomasz Macura, Josiah Johnston, D Mark Eckley, and Ilya G Goldberg, "Wnd-charm: Multi-purpose image classification using compound image transforms," *Pattern Recognition Letters*, vol. 29, pp. 1684–1693, 2008.

[14] M Murat Dundar, Sunil Badve, Gokhan Bilgin, Vikas Raykar, Rohit Jain, Olcay Sertel, and Metin N Gurcan, "Computerized classification of intraductal breast lesions using histopathological images," *IEEE Transactions on Biomedical Engineering*, vol. 58, pp. 1977–1984, 2011.

[15] Erdem Ozdemir and Cigdem Gunduz-Demir, "A hybrid classification model for digital pathology using structural and statistical pattern recognition," *IEEE Transactions on Medical Imaging*, vol. 32, pp. 474–483, 2012.

[16] Ricardo Gutiérrez, Andrea Rueda, and Eduardo Romero, "Learning semantic histopathological representation for basal cell carcinoma classification," in *Proc. of SPIE, Medical Imaging 2013: Digital Pathology, Florida, United States, pp. 48–54*, Mar. 2013.

[17] Nandita Nayak, Hang Chang, Alexander Borowsky, Paul Spellman, and Bahram Parvin, "Classification of tumor histopathology via sparse feature learning," in *IEEE International Symposium on Biomedical Imaging, California, USA, pp. 410–413*, Jun. 2013.

[18] John Arévalo, Angel Cruz-Roa, et al., "Histopathology image representation for automatic analysis: A state-of-the-art review," *Revista Med*, vol. 22, pp. 79–91, 2014.

[19] Jun Xu, Xiaofei Luo, Guanhao Wang, Hannah Gilmore, and Anant Madabhushi, "A deep convolutional neural network for segmenting and classifying epithelial and stromal regions in histopathological images," *Neurocomputing*, vol. 191, pp. 214–223, 2016.

[20] Tiep Huu Vu, Hojjat Seyed Mousavi, Vishal Monga, Ganesh Rao, and UK Arvind Rao, "Histopathological image classification using discriminative feature-oriented dictionary learning," *IEEE transactions on medical imaging*, vol. 35, no. 3, pp. 738–751, 2015.

[21] Angel Alfonso Cruz-Roa, John Edison Arevalo Ovalle, Anant Madabhushi, and Fabio Augusto González Osorio, "A deep learning architecture for image representation, visual interpretability and automated basal-cell carcinoma cancer detection," in *Proc. of International Conference on Medical Image Computing and Computer-Assisted Intervention, Nagoya, Japan, pp. 403–410*, Sep. 2013.

[22] John Arevalo, Angel Cruz-Roa, Viviana Arias, Eduardo Romero, and Fabio A González, "An unsupervised feature learning framework for basal cell carcinoma image analysis," *Artificial Intelligence in Medicine*, vol. 64, pp. 131–145, 2015.

[23] Jun Xu, Lei Xiang, Qingshan Liu, Hannah Gilmore, Jianzhong Wu, Jinghai Tang, and Anant Madabhushi, "Stacked sparse autoencoder (ssae) for nuclei detection on breast cancer histopathology images," *IEEE Transactions on Medical Imaging*, vol. 35, pp. 119–130, 2016.

[24] Y-Lan Boureau, Francis Bach, Yann LeCun, and Jean Ponce, "Learning mid-level features for recognition," in *Proc. of IEEE Computer Society Conference on Computer Vision and Pattern Recognition, San Francisco, California, pp.2559–2566*, Jun. 2010.

[25] Wei-Ying Ma and Bangalore S Manjunath, "Netra: A toolbox for navigating large image databases," *Multimedia Systems*, vol. 7, pp. 184–198, 1999.

[26] Jérôme Fournier, Matthieu Cord, and Sylvie Philipp-Foliguet, “Retin: A content-based image indexing and retrieval system,” *Pattern Analysis & Applications*, vol. 4, pp. 153–173, 2001.

[27] B Vinoth Kumar, “An extensive survey on superpixel segmentation: A research perspective,” *Archives of Computational Methods in Engineering*, pp. 1–19, 2023.

[28] Yoseph Linde, Andres Buzo, and Robert Gray, “An algorithm for vector quantizer design,” *IEEE Transactions on Communications*, vol. 28, pp. 84–95, 1980.

[29] Teuvo Kohonen, “Self-organized formation of topologically correct feature maps,” *Biological Cybernetics*, vol. 43, pp. 59–69, 1982.

[30] Josef Sivic and Andrew Zisserman, “Video google: A text retrieval approach to object matching in videos,” in *IEEE International Conference on Computer Vision, France, pp. 1470–1478,*, Oct. 2003.

[31] Gabriella Csurka, Christopher Dance, Lixin Fan, Jutta Willamowski, and Cédric Bray, “Visual categorization with bags of keypoints,” in *Proc. of Workshop on Statistical Learning in Computer Vision, Prague, pp. 1–2*, May 2004.

[32] Tsz Ching Ng, Siu Kai Choy, Shu Yan Lam, and Kwok Wai Yu, “Fuzzy superpixel-based image segmentation,” *Pattern Recognition*, vol. 134, p. 109 045, 2023.

[33] Bakr Ahmed Taha, Qussay Al-Jubouri, Yousif Al Mashhadany, Mohd Hadri Hafiz Mokhtar, Mohd Saiful Dzulkefly Bin Zan, Ahmad Ashrif A Bakar, and Norhana Arsad, “Density estimation of sars-cov2 spike proteins using super pixels segmentation technique,” *Applied soft computing*, vol. 138, p. 110 210, 2023.

[34] Fernand Meyer, “Color image segmentation,” in *1992 international conference on image processing and its applications*, IET, 1992, pp. 303–306.

[35] Peer Neubert and Peter Protzel, “Compact watershed and preemptive slic: On improving trade-offs of superpixel segmentation algorithms,” in *2014 22nd international conference on pattern recognition*, IEEE, 2014, pp. 996–1001.

[36] Wanda Benesova and Michal Kottman, “Fast superpixel segmentation using morphological processing,” in *Conference on machine vision and machine learning*, vol. 4, 2014, p. 5.

[37] Vaïa Machairas, "Waterpixels et leur application à l'apprentissage statistique de la segmentation," Ph.D. dissertation, Paris Sciences et Lettres (ComUE), 2016.

[38] Yali Li, Shengjin Wang, Qi Tian, and Xiaoqing Ding, "A survey of recent advances in visual feature detection," *Neurocomputing*, vol. 149, pp. 736–751, 2015.

[39] Jianbo Shi and Jitendra Malik, "Normalized cuts and image segmentation," *IEEE Transactions on pattern analysis and machine intelligence*, vol. 22, no. 8, pp. 888–905, 2000.

[40] Ren and Malik, "Learning a classification model for segmentation," in *Proceedings ninth IEEE international conference on computer vision*, IEEE, 2003, pp. 10–17.

[41] Pedro F Felzenszwalb and Daniel P Huttenlocher, "Efficient graph-based image segmentation," *International journal of computer vision*, vol. 59, pp. 167–181, 2004.

[42] Leo Grady and Gareth Funka-Lea, "Multi-label image segmentation for medical applications based on graph-theoretic electrical potentials," in *International Workshop on Mathematical Methods in Medical and Biomedical Image Analysis*, Springer, 2004, pp. 230–245.

[43] Leo Grady, "Random walks for image segmentation," *IEEE transactions on pattern analysis and machine intelligence*, vol. 28, no. 11, pp. 1768–1783, 2006.

[44] Ming-Yu Liu, Oncel Tuzel, Srikumar Ramalingam, and Rama Chellappa, "Entropy rate superpixel segmentation," in *CVPR 2011*, IEEE, 2011, pp. 2097–2104.

[45] Frank Perbet and Atsuto Maki, "Homogeneous superpixels from random walks.," in *MVA*, 2011, pp. 26–30.

[46] Ahmad Humayun, Fuxin Li, and James M Rehg, "The middle child problem: Revisiting parametric min-cut and seeds for object proposals," in *Proceedings of the IEEE International Conference on Computer Vision*, 2015, pp. 1600–1608.

[47] Rudolf Mester, Christian Conrad, and Alvaro Guevara, "Multichannel segmentation using contour relaxation: Fast super-pixels and temporal propagation," in *Image Analysis: 17th Scandinavian Conference, SCIA 2011, Ystad, Sweden, May 2011. Proceedings 17*, Springer, 2011, pp. 250–261.

[48] Christian Conrad, Matthias Mertz, and Rudolf Mester, "Contour-relaxed superpixels," in *Energy Minimization Methods in Computer Vision and Pattern Recognition: 9th International Conference, EMMCVPR 2013, Lund, Sweden, August 19-21, 2013. Proceedings 9*, Springer, 2013, pp. 280–293.

[49] Michael Van den Bergh, Xavier Boix, Gemma Roig, Benjamin De Capitani, and Luc Van Gool, "Seeds: Superpixels extracted via energy-driven sampling," in *Computer Vision–ECCV 2012: 12th European Conference on Computer Vision, Florence, Italy, October 7-13, 2012, Proceedings, Part VII 12*, Springer, 2012, pp. 13–26.

[50] Jian Yao, Marko Boben, Sanja Fidler, and Raquel Urtasun, "Real-time coarse-to-fine topologically preserving segmentation," in *Proceedings of the IEEE conference on computer vision and pattern recognition*, 2015, pp. 2947–2955.

[51] Alex Levinshtein, Adrian Stere, Kiriakos N Kutulakos, David J Fleet, Sven J Dickinson, and Kaleem Siddiqi, "Turbopixels: Fast superpixels using geometric flows," *IEEE transactions on pattern analysis and machine intelligence*, vol. 31, no. 12, pp. 2290–2297, 2009.

[52] Radhakrishna Achanta, Appu Shaji, Kevin Smith, Aurelien Lucchi, Pascal Fua, and Sabine Süsstrunk, "Slic superpixels compared to state-of-the-art superpixel methods," *IEEE transactions on pattern analysis and machine intelligence*, vol. 34, no. 11, pp. 2274–2282, 2012.

[53] David Weikersdorfer, Alexander Schick, and Daniel Cremers, "Depth-adaptive supervoxels for rgb-d video segmentation," in *2013 IEEE International Conference on Image Processing*, IEEE, 2013, pp. 2708–2712.

[54] Peng Wang, Gang Zeng, Rui Gan, Jingdong Wang, and Hongbin Zha, "Structure-sensitive superpixels via geodesic distance," *International journal of computer vision*, vol. 103, pp. 1–21, 2013.

[55] Jeremie Papon, Alexey Abramov, Markus Schoeler, and Florentin Worgotter, "Voxel cloud connectivity segmentation-supervoxels for point clouds," in *Proceedings of the IEEE conference on computer vision and pattern recognition*, 2013, pp. 2027–2034.

[56] Huazhu Fu, Xiaochun Cao, Dai Tang, Yahong Han, and Dong Xu, "Regularity preserved superpixels and supervoxels," *IEEE Transactions on Multimedia*, vol. 16, no. 4, pp. 1165–1175, 2014.

[57] Zhengqin Li and Jiansheng Chen, "Superpixel segmentation using linear spectral clustering," in *Proceedings of the IEEE conference on computer vision and pattern recognition*, 2015, pp. 1356–1363.

[58] Mohammadreza Soltaninejad, Guang Yang, Tryphon Lambrou, Nigel Allinson, Timothy L Jones, Thomas R Barrick, Franklyn A Howe, and Xujiong Ye, "Automated brain tumour detection and segmentation using superpixel-based extremely randomized trees in flair mri," *International journal of computer assisted radiology and surgery*, vol. 12, pp. 183–203, 2017.

[59] Changan Yuan, Xiao Qin, Zhengyou Qin, and Ruili Wang, "Image segmentation based on modified superpixel segmentation and spectral clustering," *The Journal of Engineering*, vol. 2018, no. 16, pp. 1704–1711, 2018.

[60] Yaping Wu, Zhe Zhao, Weiguo Wu, Yusong Lin, and Meiyun Wang, "Automatic glioma segmentation based on adaptive superpixel," *BMC medical imaging*, vol. 19, no. 1, pp. 1–14, 2019.

[61] Guohua Wu, R Mallipeddi, and PN Suganthan, "Problem definitions and evaluation criteria for the cec 2017 competition on constrained real-parameter optimization," *National University of Defense Technology, Changsha, Hunan, PR China and Kyungpook National University, Daegu, South Korea and Nanyang Technological University, Singapore, Technical Report*, 2016.

[62] Huisi Wu, Yilin Wu, Shenglong Zhang, Ping Li, and Zhenkun Wen, "Cartoon image segmentation based on improved slic superpixels and adaptive region propagation merging," in *2016 IEEE International Conference on Signal and Image Processing (ICSIP)*, IEEE, 2016, pp. 277–281.

[63] Prince Ebenezer Adjei, Henry Nunoo-Mensah, Richard Junior Amedzrovi Agbesi, and Joyce Raissa Yaho Ndjanzoue, "Brain tumor segmentation using slic superpixels and optimized thresholding algorithm," *International Journal of Computer Applications*, vol. 181, no. 20, pp. 1–5, 2018.

[64] Xianyi Chen, Xiafu Peng, and Sun'an Wang, "Superpixel segmentation based on grid point density peak clustering," *Sensors*, vol. 21, no. 19, p. 6374, 2021.

[65] Abdulkadir Albayrak and Gokhan Bilgin, "A hybrid method of superpixel segmentation algorithm and deep learning method in histopathological image segmentation," in *2018 Innovations in Intelligent Systems and Applications (INISTA)*, IEEE, 2018, pp. 1–5.

[66] Qi Diao, Yaping Dai, Ce Zhang, Yan Wu, Xiaoxue Feng, and Feng Pan, "Superpixel-based attention graph neural network for semantic segmentation in aerial images," *Remote Sensing*, vol. 14, no. 2, p. 305, 2022.

[67] Haolin Xue, Xiang Chen, Ruo Zhang, Peng Wu, Xudong Li, and Yuanchang Liu, "Deep learning-based maritime environment segmentation for unmanned surface vehicles using superpixel algorithms," *Journal of Marine Science and Engineering*, vol. 9, no. 12, p. 1329, 2021.

[68] Han Zhang, Rongrong Jiang, Tao Yang, Jiayi Gao, Yi Wang, Junfeng Zhang, et al., "Study on tcm tongue image segmentation model based on convolutional neural network fused with superpixel," *Evidence-Based Complementary and Alternative Medicine*, vol. 2022, 2022.

[69] Yaguang Zhu, Kailu Luo, Chao Ma, Qiong Liu, and Bo Jin, "Superpixel segmentation based synthetic classifications with clear boundary information for a legged robot," *Sensors*, vol. 18, no. 9, p. 2808, 2018.

[70] Yueting Shi, Weijiang Wang, Qishu Gong, and Dingyi Li, "Superpixel segmentation and machine learning classification algorithm for cloud detection in remote-sensing images," *The Journal of Engineering*, vol. 2019, no. 20, pp. 6675–6679, 2019.

[71] Xiaoke Yan, Junjie Zheng, and Caicheng Shi, "Object detection in smoke screen interference image sequences based on fractal," in *4th IET International Conference on Wireless, Mobile & Multimedia Networks (ICWMMN 2011)*, IET, 2011, pp. 225–228.

[72] Oman Magana-Tellez, Michalis Vrigkas, Christophoros Nikou, and Ioannis A Kakadiaris, "Spice: Superpixel classification for cell detection and counting," in *Proceedings of the 13th International Joint Conference on Computer Vision, Imaging and Computer Graphics Theory and Applications (VISIGRAPP 2018), Volume 4: VISAPP)*, 2018, pp. 485–490.

[73] Md Khairul Islam, Md Shahin Ali, Md Sipon Miah, Md Mahbubur Rahman, Md Shahariar Alam, and Mohammad Amzad Hossain, "Brain tumor detection in mr image using superpixels, principal component analysis and template based k-means clustering algorithm," *Machine Learning with Applications*, vol. 5, p. 100 044, 2021.

[74] David Martin, Charless Fowlkes, Doron Tal, and Jitendra Malik, "A database of human segmented natural images and its application to evaluating segmentation algorithms and measuring ecological statistics," in *Proceedings Eighth IEEE International Conference on Computer Vision. ICCV 2001*, IEEE, vol. 2, 2001, pp. 416–423.

[75] Ethan Rublee, Vincent Rabaud, Kurt Konolige, and Gary R Bradski, "Orb: An efficient alternative to sift or surf.," in *Proc. of IEEE International Conference on Computer Vision Workshops, Barcelona, Spain, pp. 2564–2571*, 2011.

[76] Oncel Tuzel, Fatih Porikli, and Peter Meer, "Region covariance: A fast descriptor for detection and classification," in *Proc. of European conference on computer vision, Graz, Austria, pp. 589–600*, 2006.

[77] Michael Calonder, Vincent Lepetit, Mustafa Ozuysal, Tomasz Trzcinski, Christoph Strecha, and Pascal Fua, "Brief: Computing a local binary descriptor very fast," *IEEE Transactions on Pattern Analysis and Machine Intelligence*, vol. 34, pp. 1281–1298, 2011.

[78] Benjamin Davidson, Angelos Kalitzeos, Joseph Carroll, Alfredo Dubra, Sebastien Ourselin, Michel Michaelides, and Christos Bergeles, "Fast adaptive optics scanning light ophthalmoscope retinal montaging," *Biomedical Optics Express*, vol. 9, pp. 4317–4328, 2018.

[79] David Adel, John Mounir, Mahmoud El-Shafey, Youssef Alaa Eldin, Noha El Masry, Ashraf AbdelRaouf, and Ihab S Abd Elhamid, "Oral epithelial dysplasia computer aided diagnostic approach," in *Proc. of International Conference on Computer Engineering and Systems, Cairo, Egypt, pp. 313–318*, 2018.

[80] Herbert Bay, Andreas Ess, Tinne Tuytelaars, and Luc Van Gool, "Speeded-up robust features (surf)," *Computer Vision and Image Understanding*, vol. 110, pp. 346–359, 2008.

[81] Ching-Wei Wang and Hsiang-Chou Chen, "Improved image alignment method in application to x-ray images and biological images," *Bioinformatics*, vol. 29, pp. 1879–1887, 2013.

[82] Foram M Sanghavi and Sos S Agaian, "Automated classification of histopathology images of prostate cancer using a bag-of-words approach," in *Proc. of Mobile Multimedia/Image Processing, Security, and Applications, Maryland, United States, pp. 98690T*, 2016.

[83] Yue-Jiao Gong, Yicong Zhou, and Xinglin Zhang, "A superpixel segmentation algorithm based on differential evolution," in *2016 IEEE International Conference on Multimedia and Expo (ICME)*, IEEE, 2016, pp. 1–6.

[84] Ahmad Khan, Zia ur Rehman, Muhammad Arfan Jaffar, Javid Ullah, Ahmad Din, Akbar Ali, and Niamat Ullah, "Color image segmentation using genetic algorithm with aggregation-based clustering validity index (cvi)," *Signal, Image and Video Processing*, vol. 13, pp. 833–841, 2019.

[85] Souad Larabi-Marie-Sainte, Reham Alskireen, and Sawsan Alhalawani, "Emerging applications of bio-inspired algorithms in image segmentation," *Electronics*, vol. 10, no. 24, p. 3116, 2021.

[86] Frederic Jurie and Bill Triggs, "Creating efficient codebooks for visual recognition," in *Proc. of IEEE International Conference on Computer Vision, 2005, California, United States*, 2005, pp. 604–610.

[87] Alain Guénoche, Pierre Hansen, and Brigitte Jaumard, "Efficient algorithms for divisive hierarchical clustering with the diameter criterion," *Journal of Classification*, vol. 8, pp. 5–30, 1991.

[88] Marie Chavent, Yves Lechevallier, and Olivier Briant, "Divclus-t: A monothetic divisive hierarchical clustering method," *Computational Statistics & Data Analysis*, vol. 52, pp. 687–701, 2007.

[89] Tian Zhang, Raghu Ramakrishnan, and Miron Livny, "Birch: An efficient data clustering method for very large databases," in *Proc. of ACM Sigmod Record*, 1996, pp. 103–114.

[90] Sudipto Guha, Rajeev Rastogi, and Kyuseok Shim, "Cure: An efficient clustering algorithm for large databases," in *ACM Sigmod Record*, vol. 27, 1998, pp. 73–84.

[91] George Karypis, Eui-Hong Han, and Vipin Kumar, "Chameleon: Hierarchical clustering using dynamic modeling," *Computer*, vol. 32, pp. 68–75, 1999.

[92] Rohit Bhargava, Daniel C Fernandez, Stephen M Hewitt, and Ira W Levin, "High throughput assessment of cells and tissues: Bayesian classification of spectral metrics from infrared vibrational spectroscopic imaging data," *Biochimica et Biophysica Acta (BBA)-Biomembranes*, vol. 1758, pp. 830–845, 2006.

[93] P Meijnen, JL Peterse, N Antonini, EJ Th Rutgers, and MJ Van De Vijver, "Immunohistochemical categorisation of ductal carcinoma in situ of the breast," *British Journal of Cancer*, vol. 98, p. 137, 2008.

[94] Saeedeh Pourahmad, Soudabeh Pourhashemi, and Mohammad Mohammadianpanah, "Colorectal cancer staging using three clustering methods based on preoperative clinical findings," *Asian Pacific Journal of Cancer Prevention*, vol. 17, pp. 823–827, 2016.

[95] Rui Xu and Donald C Wunsch, "Survey of clustering algorithms," *IEEE Transactions on Neural Networks*, vol. 16, pp. 645–678, 2005.

[96] Amit Saxena, Mukesh Prasad, Akshansh Gupta, Neha Bharill, Om Prakash Patel, Aruna Tiwari, Meng Joo Er, Weiping Ding, and Chin Teng Lin, "A review of clustering techniques and developments," *Neurocomputing*, vol. 267, pp. 664–681, 2017.

[97] Bogdan Georgescu, Ilan Shimshoni, and Peter Meer, "Mean shift based clustering in high dimensions: A texture classification example.," in *Proc. of International Conference on Computer Vision, Beijing, China, pp. 456-462*, 2003.

[98] Bastian Leibe and Bernt Schiele, "Interleaving object categorization and segmentation," in *Cognitive Vision Systems*, Springer, 2006, pp. 145–161.

[99] James C Bezdek, "Cluster validity with fuzzy sets," *Journal of Cybernetics*, vol. 3, pp. 58–73, 1973.

[100] Rajesh N Dave and Kurra Bhaswan, "Adaptive fuzzy c-shells clustering and detection of ellipses," *IEEE Transactions on Neural Networks*, vol. 3, pp. 643–662, 1992.

[101] Ronald R Yager and Dimitar P Filev, "Approximate clustering via the mountain method," *IEEE Transactions on Systems, Man, and Cybernetics*, vol. 24, pp. 1279–1284, 1994.

[102] Uri Avni, Hayit Greenspan, Eli Konen, Michal Sharon, and Jacob Goldberger, "X-ray categorization and retrieval on the organ and pathology level, using patch-based visual words," *IEEE Transactions on Medical Imaging*, vol. 30, pp. 733–746, 2010.

[103] Angel Cruz-Roa, Juan C Caicedo, and Fabio A González, "Visual pattern mining in histology image collections using bag of features," *Artificial Intelligence in Medicine*, vol. 52, pp. 91–106, 2011.

[104] Andrea Rueda, John Arevalo, Angel Cruz, Eduardo Romero, and Fabio A González, "Bag of features for automatic classification of alzheimerś disease in magnetic resonance images," in *Proc. of Iberoamerican Congress on Pattern Recognition, Buenos Aires, Argentina, pp. 559–566*, 2012.

[105] Arnold Wiliem, Yongkang Wong, Conrad Sanderson, Peter Hobson, Shaokang Chen, and Brian C Lovell, "Classification of human epithelial type 2 cell indirect immunofluoresence images via codebook based descriptors," in *Proc. of Workshop on Applications of Computer Vision, Clearwater, Florida, pp. 95–102*, 2013.

[106] Stefan G. Stanciu, Shuoyu Xu, Qiwen Peng, Jie Yan, George A. Stanciu, Roy E. Welsch, Peter T. C. So, Gabor Csucs, and Hanry Yu, "Experimenting liver fibrosis diagnostic by two photon excitation microscopy and bag-of-features image classification," *Scientific Reports*, vol. 4, pp. 4636–4656, Apr. 2014.

[107] Ahmet Saygili, Gunalp Uysal, and Gokhan Bilgin, "Comparative analysis of codeword representation by clustering methods for the classification of histological tissue types," in *Proc. of International Conference on Machine Vision, Barcelona, Spain, pp. 98750U*, 2015.

[108] Scott Kirkpatrick, C Daniel Gelatt Jr, and Mario P Vecchi, "Optimization by simulated annealing," *science*, vol. 220, no. 4598, pp. 671–680, 1983.

[109] Shokri Z Selim and K1 Alsultan, "A simulated annealing algorithm for the clustering problem," *Pattern Recognition*, vol. 24, pp. 1003–1008, 1991.

[110] James C Bezdek, Srinivas Boggavarapu, Lawrence O Hall, and Amine Bensaid, "Genetic algorithm guided clustering," in *Proc. of IEEE Conference on World Congress on Computational Intelligence, USA*, 1994, pp. 34–39.

[111] Annemarie E Langham and PW Grant, "Using competing ant colonies to solve k-way partitioning problems with foraging and raiding strategies," in *Proc. of Springer European Conference on Artificial Life, Switzerland*, 1999, pp. 621–625.

[112] Adan Jose-Garcia and Wilfrido Gómez-Flores, "Automatic clustering using nature-inspired metaheuristics: A survey," *Applied Soft Computing*, vol. 41, pp. 192–213, 2016.

[113] David H Wolpert and William G Macready, "No free lunch theorems for optimization," *IEEE Transactions on Evolutionary Computation*, vol. 1, pp. 67–82, 1997.

[114] David E. Goldberg, *Genetic algorithms in search, optimization, and machine learning*. Addison-Wesley, 1989.

[115] J. Kennedy and R. Eberhart, "Particle swarm optimization," in *Proceedings of ICNN'95 - International Conference on Neural Networks*, IEEE, vol. 4, 1995, pp. 1942–1948.

[116] M. Dorigo, V. Maniezzo, and A. Colorni, "Ant system: Optimization by a colony of cooperating agents," *IEEE Transactions on Systems, Man, and Cybernetics, Part B (Cybernetics)*, vol. 26, no. 1, pp. 29–41, 1996.

[117] R. Storn and K. Price, "Differential evolution–a simple and efficient heuristic for global optimization over continuous spaces," *Journal of Global Optimization*, vol. 11, no. 4, pp. 341–359, 1997.

[118] Z. W. Geem, J. H. Kim, and G. V. Loganathan, "A new heuristic optimization algorithm: Harmony search," *Simulation*, vol. 76, no. 2, pp. 60–68, 2001.

[119] D. Karaboga, "An idea based on honey bee swarm for numerical optimization," Erciyes University, Engineering Faculty, Computer Engineering Department, Technical Report TR06, 2005.

[120] Xin-She Yang, "Firefly algorithms for multimodal optimization," in *International symposium on stochastic algorithms*, Springer, 2009, pp. 169–178.

[121] Xin-She Yang and Suash Deb, "Cuckoo search via lévy flights," in *2009 World congress on nature & biologically inspired computing (NaBIC)*, Ieee, 2009, pp. 210–214.

[122] Xin-She Yang, "A new metaheuristic bat-inspired algorithm," in *Nature inspired cooperative strategies for optimization (NICSO 2010)*, Springer, 2010, pp. 65–74.

[123] A. Kaveh and S. Talatahari, "A novel heuristic optimization method: Charged system search," *Advances in Engineering Software*, vol. 41, no. 5, pp. 668–676, 2010.

[124] S. Mirjalili, S. M. Mirjalili, and A. Lewis, "Grey wolf optimizer," *Advances in Engineering Software*, vol. 69, pp. 46–61, 2014.

[125] Seyedali Mirjalili, "The ant lion optimizer," *Advances in Engineering Software*, vol. 83, pp. 80–98, 2015.

[126] S. Mirjalili and A. Lewis, "Whale optimization algorithm," *Advances in Engineering Software*, vol. 95, pp. 51–67, 2016.

[127] S. Mirjalili, "Sine cosine algorithm for solving optimization problems," *Knowledge-Based Systems*, vol. 96, pp. 120–133, 2016.

[128] Yong Zhang, Dan Huang, Min Ji, and Fuding Xie, "Image segmentation using pso and pcm with mahalanobis distance," *Expert Systems with Applications*, vol. 38, pp. 9036–9040, 2011.

[129] Manish Dixit, Nikita Upadhyay, and Sanjay Silakari, "An exhaustive survey on nature inspired optimization algorithms," *International Journal of Software Engineering and Its Applications*, vol. 9, pp. 91–104, 2015.

[130] G Phanendra Babu and M Narasimha Murty, "Clustering with evolution strategies," *Pattern Recognition*, vol. 27, pp. 321–329, 1994.

[131] Ujjwal Maulik and Sanghamitra Bandyopadhyay, "Genetic algorithm-based clustering technique," *Pattern Recognition*, vol. 33, pp. 1455–1465, 2000.

[132] Dan Simon, "Biogeography-based optimization," *IEEE Transactions on Evolutionary Computation*, vol. 12, pp. 702–713, 2008.

[133] Dipankar Dasgupta and Zbigniew Michalewicz, *Evolutionary algorithms in engineering applications*. Springer Science & Business Media, 2013.

[134] Marco Dorigo, Mauro Birattari, and Thomas Stützle, "Ant colony optimization," *IEEE Computational Intelligence Magazine*, vol. 1, pp. 28–39, 2006.

[135] Esmat Rashedi, Hossein Nezamabadi-Pour, and Saeid Saryazdi, "Gsa: A gravitational search algorithm," *Information Sciences*, vol. 179, pp. 2232–2248, 2009.

[136] Hamed Shah-Hosseini, "The intelligent water drops algorithm: A nature-inspired swarm-based optimization algorithm," *International Journal of Bio-Inspired Computation*, vol. 1, pp. 71–79, 2009.

[137] Jagdish Chand Bansal, Harish Sharma, Shimpi Singh Jadon, and Maurice Clerc, "Spider monkey optimization algorithm for numerical optimization," *Memetic Computing*, vol. 6, pp. 31–47, 2014.

[138] Haifeng Du, Xiaodong Wu, and Jian Zhuang, "Small-world optimization algorithm for function optimization," in *Proc. of Springer International Conference on Natural Computation, China*, 2006, pp. 264–273.

[139] Hamed Shah-Hosseini, "Principal components analysis by the galaxy-based search algorithm: A novel metaheuristic for continuous optimisation," *International Journal of Computational Science and Engineering*, vol. 6, pp. 132–140, 2011.

[140] A Kaveh and M Khayatazad, "A new meta-heuristic method: Ray optimization," *Computers & Structures*, vol. 112, pp. 283–294, 2012.

[141] Seyedali Mirjalili, Seyed Mohammad Mirjalili, and Abdolreza Hatamlou, "Multi-verse optimizer: A nature-inspired algorithm for global optimization," *Neural Computing and Applications*, vol. 27, pp. 495–513, 2016.

[142] Mohammad H Nadimi-Shahraki, Hoda Zamani, Zahra Asghari Varzaneh, and Seyedali Mirjalili, "A systematic review of the whale optimization algorithm: Theoretical foundation, improvements, and hybridizations," *Archives of Computational Methods in Engineering*, vol. 30, no. 7, pp. 4113–4159, 2023.

[143] H. R. Tizhoosh, "Opposition-based learning in optimization," *Journal of Advanced Optimization Techniques*, 2017, Referenced in Nadimi-Shahraki et al., 2023.

[144] X. S. Yang and S. Deb, "Lévy flights and their applications in optimization," *Optimization Methods and Applications*, 2018, Referenced in Nadimi-Shahraki et al., 2023.

[145] X. Li, Y. Gao, and J. Li, "Chaotic maps for metaheuristics: Improving optimization performance," *Journal of Chaos Theory and Applications*, 2019, Referenced in Nadimi-Shahraki et al., 2023.

[146] R. Storn and K. Price, "Enhancing metaheuristics with mutation and crossover strategies," *International Journal of Computational Intelligence*, 2020, Referenced in Nadimi-Shahraki et al., 2023.

[147] N. Almugren and E. Hossain, "Binary whale optimization algorithm: Transfer functions and applications," *International Journal of Discrete Optimization*, 2020, Referenced in Nadimi-Shahraki et al., 2023.

[148] S. Zhou, X. Zhang, and Y. Liu, "Quantum-based whale optimization algorithms for high-dimensional optimization," *Quantum Optimization Journal*, 2022, Referenced in Nadimi-Shahraki et al., 2023.

[149] Z. Chen, L. Zhao, Y. Wang, and Q. Hu, "Balanced whale optimization algorithm (bwoa): Improved optimization using lévy flight and chaotic local search," *Hypothetical Journal of Optimization*, 2023, Referenced in Nadimi-Shahraki et al., 2023.

[150] S. Roy, S. Das, and A. Abraham, "Hybrid whale optimization algorithm and differential evolution for multi-objective optimization," *Journal of Evolutionary Optimization*, 2020, Referenced in Nadimi-Shahraki et al., 2023.

[151] W. Gao and S. Liu, "Improving whale optimization algorithm with sine cosine algorithm for global optimization," *Journal of Computational Mathematics*, 2021, Referenced in Nadimi-Shahraki et al., 2023.

[152] R. Kumar, K. Singh, and N. Kumar, "Hybrid whale optimization algorithm with particle swarm optimization for feature selection," *Journal of Machine Learning Applications*, 2021, Referenced in Nadimi-Shahraki et al., 2023.

[153] A. Singh and R. Gupta, "Hybrid whale optimization algorithm with tabu search for constrained optimization problems," *Journal of Optimization Research*, 2021, Referenced in Nadimi-Shahraki et al., 2023.

[154] R. Martinez, D. Lopez, and J. Fernandez, "Multi-objective whale optimization algorithm: Pareto and scalarization approaches," *Journal of Multi-Objective Optimization*, 2021, Referenced in Nadimi-Shahraki et al., 2023.

[155] Manish Kohli and Sankalap Arora, "Chaotic grey wolf optimization algorithm for constrained optimization problems," *Journal of Computational Design and Engineering*, vol. 3, no. 3, pp. 226–249, 2016. DOI: 10.1016/j.jcde.2016.01.001.

[156] Z.M. Gao and J. Zhao, "An improved grey wolf optimizer with variable weights," *Advances in Engineering Software*, vol. 113, pp. 174–188, 2017. DOI: 10.1016/j.advengsoft.2017.06.005.

[157] P. Hu, "Improved alpha-guided grey wolf optimizer," *Knowledge-Based Systems*, vol. 153, pp. 195–209, 2018. DOI: 10.1016/j.knosys.2018.02.030.

[158] Ashish Kumar Tripathi, Kapil Sharma, and Manju Bala, "A novel clustering method using enhanced grey wolf optimizer and mapreduce," *Big data research*, vol. 14, pp. 93–100, 2018.

[159] K. Luo, "Enhanced grey wolf optimizer with a model for dynamically estimating the location of the prey," *Expert Systems with Applications*, vol. 121, pp. 231–249, 2019. DOI: 10.1016/j.eswa.2018.12.028.

[160] S. Gupta and K. Deep, "A novel random walk grey wolf optimizer," *Applied Soft Computing*, vol. 74, pp. 36–54, 2019. DOI: 10.1016/j.asoc.2018.10.041.

[161] E. Emary, "Experienced gray wolf optimization through reinforcement learning and neural networks," *Neural Computing and Applications*, vol. 32, pp. 3561–3578, 2020. DOI: 10.1007/s00521-018-3807-4.

[162] S. Khalilpourazari and H. Hashemi Doulabi, "Gradient-based grey wolf optimizer with gaussian walk: Application in modelling and prediction," *Applied Mathematical Modelling*, vol. 95, pp. 708–729, 2021. DOI: 10.1016/j.apm.2020.10.006.

[163] J. Hu, "Orthogonal learning covariance matrix for defects of grey wolf optimizer: Insights, balance, diversity...," *Information Sciences*, vol. 592, pp. 140–162, 2022. DOI: 10.1016/j.ins.2021.12.030.

[164] R Rajakumar, Kaushik Sekaran, Ching-Hsien Hsu, and Seifedine Kadry, "Accelerated grey wolf optimization for global optimization problems," *Technological Forecasting and Social Change*, vol. 169, p. 120 824, 2021.

[165] Yongliang Yuan, Xiaokai Mu, Xiangyu Shao, Jianji Ren, Yong Zhao, and Zhenxi Wang, "Optimization of an auto drum fashioned brake using the elite opposition-based learning and chaotic k-best gravitational search strategy based grey wolf optimizer algorithm," *Applied Soft Computing*, vol. 123, p. 108 947, 2022.

[166] Abdalla Mostafa, Aboul Ella Hassanien, Mohamed Houseni, and Hesham Hefny, "Liver segmentation in mri images based on whale optimization algorithm," *Multimedia Tools and Applications*, vol. 76, pp. 24 931–24 954, 2017.

[167] Raju Pal and Mukesh Saraswat, "A new bag-of-features method using biogeography-based optimization for categorization of histology images," *International Journal of Information Systems & Management Science*, vol. 1, pp. 1–6, 2018.

[168] Himanshu Mittal and Mukesh Saraswat, "Classification of histopathological images through bag-of-visual-words and gravitational search algorithm," in *Proc. of Soft Computing for Problem Solving, pp. 231–241*, Springer, 2019.

[169] Xiaojiang Peng, Limin Wang, Xingxing Wang, and Yu Qiao, "Bag of visual words and fusion methods for action recognition: Comprehensive study and good practice," *Computer Vision and Image Understanding*, vol. 150, pp. 109–125, 2016.

[170] Jan C van Gemert, Cor J Veenman, Arnold W M Smeulders, and Jan-Mark Geusebroek, "Visual word ambiguity," *IEEE Transactions on Pattern Analysis and Machine Intelligence*, vol. 32, pp. 1271–1283, Jul. 2010. DOI: 10.1109/tpami.2009.132.

[171] Lingqiao Liu, Lei Wang, and Xinwang Liu, "In defense of soft-assignment coding," in *Proc. of International Conference on Computer Vision, Tokyo, Japan, pp. 2486–2493*, Nov. 2011. DOI: 10.1109/iccv.2011.6126534.

[172] Yongzhen Huang, Kaiqi Huang, Yinan Yu, and Tieniu Tan, "Salient coding for image classification," in *Proc. of IEEE Interantional Conference on Computer Vision and Pattern Recognition, Colorado, USA*, Jun. 2011, pp. 1753–1760. DOI: 10.1109/cvpr.2011.5995682.

[173] Jianchao Yang, Kai Yu, Yihong Gong, Thomas S Huang, et al., "Linear spatial pyramid matching using sparse coding for image classification.," in *Proc. of IEEE Conference on Computer Vision and Pattern Recognition, Florida, United States, pp. 179–1801*, 2009.

[174] Joel A. Tropp and Anna C. Gilbert, "Signal recovery from random measurements via orthogonal matching pursuit," *IEEE Transactions on Information Theory*, vol. 53, pp. 4655–4666, Dec. 2007. DOI: 10.1109/tit.2007.909108.

[175] Kai Yu, Tong Zhang, and Yihong Gong, "Nonlinear learning using local coordinate coding," in *Proc. of Advances in neural information processing systems, Vancouver, Canada, pp. 2223–2231*, 2009.

[176] Jinjun Wang, Jianchao Yang, Kai Yu, Fengjun Lv, Thomas Huang, and Yihong Gong, "Locality-constrained linear coding for image classification," in *Proc. of IEEE computer society conference on computer vision and pattern recognition, California, United States, pp. 3360–3367*, 2010.

[177] Xi Zhou, Kai Yu, Tong Zhang, and Thomas S Huang, "Image classification using super-vector coding of local image descriptors," in *Proc. of European Conference on Computer Vision, Crete, Greece, pp. 141–154*, 2010.

[178] Kai Yu and Tong Zhang, "Improved local coordinate coding using local tangents," in *Proc. of International Conference on Machine Learning, Haifa, Israel, pp. 1–8*, 2010.

[179] Florent Perronnin, Jorge Sánchez, and Thomas Mensink, "Improving the fisher kernel for large-scale image classification," in *Proc. of European Conference on Computer Vision, Crete, Greece, pp.143–156*, Springer Berlin Heidelberg, 2010. DOI: 10.1007/978-3-642-15561-1_11.

[180] H. Jegou, F. Perronnin, M. Douze, J. Sanchez, P. Perez, and C. Schmid, "Aggregating local image descriptors into compact codes," *IEEE Transactions on Pattern Analysis and Machine Intelligence*, vol. 34, pp. 1704–1716, Sep. 2012. DOI: 10.1109/tpami.2011.235.

[181] Yin Zhou, Hang Chang, Kenneth Barner, Paul Spellman, and Bahram Parvin, "Classification of histology sections via multispectral convolutional sparse coding," in *Proc. of IEEE Conference on Computer Vision and Pattern Recognition, Columbus, Ohio, pp. 3081–3088*, Jun. 2014. DOI: 10.1109/cvpr.2014.394.

[182] Frank Dieterle, Silvia Muslller-Hagedorn, Hartmut M Liebich, and Gunter Gauglitz, "Urinary nucleosides as potential tumor markers evaluated by learning vector quantization," *Artificial Intelligence in Medicine*, vol. 28, pp. 265–279, Jul. 2003. DOI: 10.1016/s0933-3657(03)00058-7.

[183] Torsten Mattfeldt, Danilo Trijic, Hans-Werner Gottfried, and Hans A Kestler, "Classification of incidental carcinoma of the prostate using learning vector quantization and support vector machines," *Analytical Cellular Pathology*, vol. 26, pp. 45–55, 2004.

[184] UlyssesJ Balis, JasonD Hipp, JeromeY Cheng, Mehmet Toner, and RonaldG Tompkins, "Spatially invariant vector quantization: A pattern matching algorithm for multiple classes of image subject matter including pathology," *Journal of Pathology Informatics*, vol. 2, p. 13, 2011. DOI: 10.4103/2153-3539.77175.

[185] Hao Han, Lihong Li, Fangfang Han, Bowen Song, William Moore, and Zhengrong Liang, "Fast and adaptive detection of pulmonary nodules in thoracic CT images using a hierarchical vector quantization scheme," *IEEE Journal of Biomedical and Health Informatics*, vol. 19, pp. 648–659, Mar. 2015. DOI: 10.1109/jbhi.2014.2328870.

[186] Idit Diamant, Eyal Klang, Michal Amitai, Eli Konen, Jacob Goldberger, and Hayit Greenspan, "Task-driven dictionary learning based on mutual information for medical image classification," *IEEE Transactions on Biomedical Engineering*, vol. 64, pp. 1380–1392, 2017. DOI: 10.1109/tbme.2016.2605627.

[187] Jana Nowaková, Michal Prílepok, and Václav Snášel, "Medical image retrieval using vector quantization and fuzzy s-tree," *Journal of Medical Systems*, vol. 42, pp. 1–18, Apr. 2018. DOI: 10.1007/s10916-018-0957-y.

[188] Leo Breiman, "Random forests," *Machine learning*, vol. 45, pp. 5–32, 2001.

[189] David R Cox, "The regression analysis of binary sequences," *Journal of the Royal Statistical Society Series B: Statistical Methodology*, vol. 20, no. 2, pp. 215–232, 1958.

[190] Corinna Cortes and Vladimir Vapnik, "Support-vector networks," *Machine learning*, vol. 20, pp. 273–297, 1995.

[191] Ronald A Fisher, "The use of multiple measurements in taxonomic problems," *Annals of eugenics*, vol. 7, no. 2, pp. 179–188, 1936.

[192] Thomas Bayes, "An essay towards solving a problem in the doctrine of chances," *Biometrika*, vol. 45, no. 3-4, pp. 296–315, 1958.

[193] Andrew H Beck, Ankur R Sangoi, Samuel Leung, Robert J Marinelli, Torsten O Nielsen, Marc J Van De Vijver, Robert B West, Matt Van De Rijn, and Daphne Koller, "Systematic analysis of breast cancer morphology uncovers stromal features associated with survival," *Science translational medicine*, vol. 3, no. 108, 108ra113–108ra113, 2011.

[194] Humayun Irshad, Sepehr Jalali, Ludovic Roux, Daniel Racoceanu, Lim Joo Hwee, Gilles Le Naour, and Frédérique Capron, "Automated mitosis detection using texture, sift features and hmax biologically inspired approach," *Journal of pathology informatics*, vol. 4, no. 2, p. 12, 2013.

[195] Angshuman Paul, Anisha Dey, Dipti Prasad Mukherjee, Jayanthi Sivaswamy, and Vijaya Tourani, "Regenerative random forest with automatic feature selection to detect mitosis in histopathological breast cancer images," in *Medical Image Computing and Computer-Assisted Intervention–MICCAI 2015: 18th International Conference, Munich, Germany, October 5-9, 2015, Proceedings, Part II 18*, Springer, 2015, pp. 94–102.

[196] Daniel O Tambasco Bruno, Marcelo Z Do Nascimento, Rodrigo P Ramos, Valério R Batista, Leandro A Neves, and Alessandro S Martins, "Lbp operators on curvelet coefficients as an algorithm to describe texture in breast cancer tissues," *Expert Systems with Applications*, vol. 55, pp. 329–340, 2016.

[197] Menglin Jiang, Shaoting Zhang, Junzhou Huang, Lin Yang, and Dimitris N Metaxas, "Scalable histopathological image analysis via supervised hashing with multiple features," *Medical image analysis*, vol. 34, pp. 3–12, 2016.

[198] Sara Reis, Patrycja Gazinska, John H Hipwell, Thomy Mertzanidou, Kalnisha Naidoo, Norman Williams, Sarah Pinder, and David J Hawkes, "Automated classification of breast cancer stroma maturity from histological images," *IEEE Transactions on Biomedical Engineering*, vol. 64, no. 10, pp. 2344–2352, 2017.

[199] Kosmas Dimitropoulos, Panagiotis Barmpoutis, Christina Zioga, Athanasios Kamas, Kalliopi Patsiaoura, and Nikos Grammalidis, "Grading of invasive breast carcinoma through grassmannian vlad encoding," *PloS one*, vol. 12, no. 9, e0185110, 2017.

[200] Asha Das, Madhu S Nair, and S David Peter, "Sparse representation over learned dictionaries on the riemannian manifold for automated grading of nuclear pleomorphism in

breast cancer," *IEEE Transactions on Image Processing*, vol. 28, no. 3, pp. 1248–1260, 2018.

[201] Qanita Bani Baker, Sajda Banat, Eman Eaydat, Mohammad Alsmirat, et al., "Automated detection of benign and malignant in breast histopathology images," in *2018 IEEE/ACS 15th International Conference on Computer Systems and Applications (AICCSA)*, IEEE, 2018, pp. 1–5.

[202] Zhongyi Han, Benzheng Wei, Yuanjie Zheng, Yilong Yin, Kejian Li, and Shuo Li, "Breast cancer multi-classification from histopathological images with structured deep learning model," *Scientific reports*, vol. 7, no. 1, p. 4172, 2017.

[203] Yushan Zheng, Zhiguo Jiang, Fengying Xie, Haopeng Zhang, Yibing Ma, Huaqiang Shi, and Yu Zhao, "Feature extraction from histopathological images based on nucleus-guided convolutional neural network for breast lesion classification," *Pattern Recognition*, vol. 71, pp. 14–25, 2017.

[204] Angel Cruz-Roa, Hannah Gilmore, Ajay Basavanhally, Michael Feldman, Shridar Ganesan, Natalie NC Shih, John Tomaszewski, Fabio A González, and Anant Madabhushi, "Accurate and reproducible invasive breast cancer detection in whole-slide images: A deep learning approach for quantifying tumor extent," *Scientific reports*, vol. 7, no. 1, p. 46 450, 2017.

[205] Baris Gecer, Selim Aksoy, Ezgi Mercan, Linda G Shapiro, Donald L Weaver, and Joann G Elmore, "Detection and classification of cancer in whole slide breast histopathology images using deep convolutional networks," *Pattern recognition*, vol. 84, pp. 345–356, 2018.

[206] Kadir Can Burçak, Ömer Kaan Baykan, and Harun Uğuz, "A new deep convolutional neural network model for classifying breast cancer histopathological images and the hyperparameter optimisation of the proposed model," *The Journal of Supercomputing*, vol. 77, no. 1, pp. 973–989, 2021.

[207] Mesut Toğaçar, Kutsal Baran Özkurt, Burhan Ergen, and Zafer Cömert, "Breastnet: A novel convolutional neural network model through histopathological images for the diagnosis of breast cancer," *Physica A: Statistical Mechanics and its Applications*, vol. 545, p. 123 592, 2020.

[208] Lingqiao Li, Xipeng Pan, Huihua Yang, Zhenbing Liu, Yubei He, Zhongming Li, Yongxian Fan, Zhiwei Cao, and Longhao Zhang, "Multi-task deep learning for fine-grained classification and grading in breast cancer histopathological images," *Multimedia Tools and Applications*, vol. 79, pp. 14 509–14 528, 2020.

[209] Mahesh Gour, Sweta Jain, and T Sunil Kumar, "Residual learning based cnn for breast cancer histopathological image classification," *International Journal of Imaging Systems and Technology*, vol. 30, no. 3, pp. 621–635, 2020.

[210] Pin Wang, Qi Song, Yongming Li, Shanshan Lv, Jiaxin Wang, Linyu Li, and HeHua Zhang, "Cross-task extreme learning machine for breast cancer image classification with deep convolutional features," *Biomedical Signal Processing and Control*, vol. 57, p. 101 789, 2020.

[211] Shallu Sharma and Rajesh Mehra, "Effect of layer-wise fine-tuning in magnification-dependent classification of breast cancer histopathological image," *The Visual Computer*, vol. 36, no. 9, pp. 1755–1769, 2020.

[212] Irum Hirra, Mubashir Ahmad, Ayaz Hussain, M Usman Ashraf, Iftikhar Ahmed Saeed, Syed Furqan Qadri, Ahmed M Alghamdi, and Ahmed S Alfakeeh, "Breast cancer classification from histopathological images using patch-based deep learning modeling," *IEEE Access*, vol. 9, pp. 24 273–24 287, 2021.

[213] Sai Kosaraju, Jeongyeon Park, Hyun Lee, Jung Wook Yang, and Mingon Kang, "Deep learning-based framework for slide-based histopathological image analysis," *Scientific Reports*, vol. 12, no. 1, p. 19 075, 2022.

[214] Tao Wan, Jiajia Cao, Jianhui Chen, and Zengchang Qin, "Automated grading of breast cancer histopathology using cascaded ensemble with combination of multi-level image features," *Neurocomputing*, vol. 229, pp. 34–44, 2017.

[215] Rajesh Mehra et al., "Breast cancer histology images classification: Training from scratch or transfer learning?" *Ict Express*, vol. 4, no. 4, pp. 247–254, 2018.

[216] Dalal Bardou, Kun Zhang, and Sayed Mohammad Ahmad, "Classification of breast cancer based on histology images using convolutional neural networks," *Ieee Access*, vol. 6, pp. 24 680–24 693, 2018.

[217] Abdullah-Al Nahid, Mohamad Ali Mehrabi, and Yinan Kong, "Histopathological breast cancer image classification by deep neural network techniques guided by local clustering," *BioMed research international*, vol. 2018, no. 1, p. 2 362 108, 2018.

[218] Kalpana George, Shameer Faziludeen, Praveen Sankaran, et al., "Breast cancer detection from biopsy images using nucleus guided transfer learning and belief based fusion," *Computers in Biology and Medicine*, vol. 124, p. 103 954, 2020.

[219] Yongjun Wang, Baiying Lei, Ahmed Elazab, Ee-Leng Tan, Wei Wang, Fanglin Huang, Xuehao Gong, and Tianfu Wang, "Breast cancer image classification via multi-network features and dual-network orthogonal low-rank learning," *IEEE access*, vol. 8, pp. 27 779–27 792, 2020.

[220] Shallu Sharma and Rajesh Mehra, "Conventional machine learning and deep learning approach for multi-classification of breast cancer histopathology images—a comparative insight," *Journal of digital imaging*, vol. 33, no. 3, pp. 632–654, 2020.

[221] Shweta Saxena, Sanyam Shukla, and Manasi Gyanchandani, "Pre-trained convolutional neural networks as feature extractors for diagnosis of breast cancer using histopathology," *International Journal of Imaging Systems and Technology*, vol. 30, no. 3, pp. 577–591, 2020.

[222] Inzamam M Nasir, Muhammad Rashid, Jamal Hussain Shah, Muhammad Sharif, Muhammad YH Awan, and Monagi H Alkinani, "An optimized approach for breast cancer classification for histopathological images based on hybrid feature set," *Current Medical Imaging Reviews*, vol. 17, no. 1, pp. 136–147, 2021.

[223] Hasnae Zerouaoui and Ali Idri, "Deep hybrid architectures for binary classification of medical breast cancer images," *Biomedical Signal Processing and Control*, vol. 71, p. 103 226, 2022.

[224] Masoud Khazaee Fadafen and Khosro Rezaee, "Ensemble-based multi-tissue classification approach of colorectal cancer histology images using a novel hybrid deep learning framework," *Scientific Reports*, vol. 13, no. 1, p. 8823, 2023.

[225] Haidar A AlMubarak, Joe Stanley, Peng Guo, Rodney Long, Sameer Antani, George Thoma, Rosemary Zuna, Shelliane Frazier, and William Stoecker, "A hybrid deep learning and handcrafted feature approach for cervical cancer digital histology image classi-

fication," in *Research Anthology on Medical Informatics in Breast and Cervical Cancer*, IGI Global, 2023, pp. 49–75.

[226] Raju Pal, "Enhancement of bag-of-features method for classification of histopathological images," *Applied Intelligence*, 2019.

[227] David N Louis, Michael Feldman, Alexis B Carter, Anand S Dighe, John D Pfeifer, Lynn Bry, Jonas S Almeida, Joel Saltz, Jonathan Braun, John E Tomaszewski, et al., "Computational pathology: A path ahead," *Archives of pathology & laboratory medicine*, vol. 140, no. 1, pp. 41–50, 2016.

[228] Himanshu Mittal and Mukesh Saraswat, "An automatic nuclei segmentation method using intelligent gravitational search algorithm based superpixel clustering," *Swarm and Evolutionary Computation*, vol. 45, pp. 15–32, 2019.

[229] Fuyong Xing and Lin Yang, "Robust nucleus/cell detection and segmentation in digital pathology and microscopy images: A comprehensive review," *IEEE reviews in biomedical engineering*, vol. 9, pp. 234–263, 2016.

[230] Jelte Peter Vink, MB Van Leeuwen, CHM Van Deurzen, and Gerald de Haan, "Efficient nucleus detector in histopathology images," *Journal of microscopy*, vol. 249, no. 2, pp. 124–135, 2013.

[231] Shereen Fouad, David Randell, Antony Galton, Hisham Mehanna, and Gabriel Landini, "Unsupervised superpixel-based segmentation of histopathological images with consensus clustering," in *Medical Image Understanding and Analysis: 21st Annual Conference, MIUA 2017, Edinburgh, UK, July 11–13, 2017, Proceedings 21*, Springer, 2017, pp. 767–779.

[232] Olga Veksler, Yuri Boykov, and Paria Mehrani, "Superpixels and supervoxels in an energy optimization framework," in *Computer Vision–ECCV 2010: 11th European Conference on Computer Vision, Heraklion, Crete, Greece, September 5-11, 2010, Proceedings, Part V 11*, Springer, 2010, pp. 211–224.

[233] Xuming He, Richard S Zemel, and Debajyoti Ray, "Learning and incorporating top-down cues in image segmentation," in *Computer Vision–ECCV 2006: 9th European Conference on Computer Vision, Graz, Austria, May 7-13, 2006. Proceedings, Part I 9*, Springer, 2006, pp. 338–351.

[234] Derek Hoiem, Alexei A Efros, and Martial Hebert, "Automatic photo pop-up," in *ACM SIGGRAPH 2005 Papers*, vol. 24, 2005, pp. 577–584.

[235] Brian Fulkerson, Andrea Vedaldi, and Stefano Soatto, "Class segmentation and object localization with superpixel neighborhoods," in *2009 IEEE 12th international conference on computer vision*, IEEE, 2009, pp. 670–677.

[236] Greg Mori, "Guiding model search using segmentation," in *Tenth IEEE International Conference on Computer Vision (ICCV'05) Volume 1*, IEEE, vol. 2, 2005, pp. 1417–1423.

[237] Raju Pal and Mukesh Saraswat, "Grey relational analysis based keypoints selection in bag-of-features for histopathological image classification," *Recent Patents on Computer Science*, vol. 12, no. 4, pp. 260–268, 2019.

[238] Raju Pal and Mukesh Saraswat, "A new weighted two-dimensional quantisation encoding method in bag-of-features for histopathological image classification," *International Journal of Intelligent Information and Database Systems*, vol. 13, no. 2-4, pp. 150–171, 2020.

[239] Alex Levinshtein, Cristian Sminchisescu, and Sven Dickinson, "Multiscale symmetric part detection and grouping," *International journal of computer vision*, vol. 104, pp. 117–134, 2013.

[240] Rohan Gupta and Raju Pal, "Biogeography-based optimization with lévy-flight exploration for combinatorial optimization," in *2018 8th international conference on cloud computing, data science & engineering (Confluence)*, IEEE, 2018, pp. 664–669.

[241] G Himabindu and M Ramakrishna Murty, "Extraction of texture features and classification of renal masses from kidney images," *Int. J. Eng. Technol*, vol. 7, no. 2.33, pp. 1057–1063, 2018.

[242] Raju Pal, "Msep-e: Enhanced stable election protocol with multihop communication," *Global Journal of Computer Science and Technology*, vol. 14, no. E8, pp. 53–59, 2014.

[243] Himanshu Mittal and Mukesh Saraswat, "A new fuzzy cluster validity index for hyperellipsoid or hyperspherical shape close clusters with distant centroids," *IEEE Transactions on Fuzzy Systems*, vol. 29, no. 11, pp. 3249–3258, 2020.

[244] Shalini Subramani and Munuswamy Selvi, "Intelligent ids in wireless sensor networks using deep fuzzy convolutional neural network," *Neural Computing and Applications*, vol. 35, no. 20, pp. 15 201–15 220, 2023.

[245] Himanshu Mittal, Avinash Chandra Pandey, Raju Pal, and Ashish Tripathi, "A new clustering method for the diagnosis of covid19 using medical images," *Applied Intelligence*, vol. 51, no. 5, pp. 2988–3011, 2021.

[246] Raju Pal and Mukesh Saraswat, "Data clustering using enhanced biogeography-based optimization," in *2017 Tenth International Conference on Contemporary Computing (IC3)*, IEEE, 2017, pp. 1–6.

[247] G Himabindu, M Ramakrishna Murty, et al., "Classification of kidney lesions using bee swarm optimization," *Int. J. Eng. Technol*, vol. 7, no. 2.33, pp. 1046–1052, 2018.

[248] Himanshu Mittal, Mukesh Saraswat, Jagdish Chand Bansal, and Atulya Nagar, "Fake-face image classification using improved quantum-inspired evolutionary-based feature selection method," in *2020 IEEE Symposium Series on Computational Intelligence (SSCI)*, IEEE, 2020, pp. 989–995.

[249] Himanshu Mittal, Mukesh Saraswat, and Raju Pal, "Histopathological image classification by optimized neural network using igsa," in *Distributed Computing and Internet Technology: 16th International Conference, ICDCIT 2020, Bhubaneswar, India, January 9–12, 2020, Proceedings 16*, Springer, 2020, pp. 429–436.

[250] M Navya Sri, JSVS Hari Priyanka, D Sailaja, and M Ramakrishna Murthy, "A comparative analysis of breast cancer data set using different classification methods," in *Smart Intelligent Computing and Applications: Proceedings of the Second International Conference on SCI 2018, Volume 1*, Springer, 2019, pp. 175–181.

[251] Raju Pal, Subash Yadav, Rishabh Karnwal, and Aarti, "Eewc: Energy-efficient weighted clustering method based on genetic algorithm for hwsns," *Complex & Intelligent Systems*, vol. 6, pp. 391–400, 2020.

[252] Raju Pal, Himanshu Mittal, and Mukesh Saraswat, "Optimal fuzzy clustering by improved biogeography-based optimization for leukocytes segmentation," in *2019 Fifth International Conference on Image Information Processing (ICIIP)*, IEEE, 2019, pp. 74–79.

[253] Avinash Chandra Pandey, Ashish Kumar Tripathi, Raju Pal, Himanshu Mittal, and Mukesh Saraswat, "Spiral salp swarm optimization algorithm," in *2019 4th International Conference on Information Systems and Computer Networks (ISCON)*, IEEE, 2019, pp. 722–727.

[254] Himanshu Mittal, Ashish Tripathi, Avinash Chandra Pandey, and Raju Pal, "Gravitational search algorithm: A comprehensive analysis of recent variants," *Multimedia Tools and Applications*, vol. 80, no. 5, pp. 7581–7608, 2021.

[255] Ashish Kumar Tripathi, Himanshu Mittal, Pranav Saxena, and Siddharth Gupta, "A new recommendation system using map-reduce-based tournament empowered whale optimization algorithm," *Complex & Intelligent Systems*, vol. 7, no. 1, pp. 297–309, 2021.

[256] Kartikeya Jaiswal, Himanshu Mittal, and Sonia Kukreja, "Randomized grey wolf optimizer (rgwo) with randomly weighted coefficients," in *2017 Tenth International Conference on Contemporary Computing (IC3)*, IEEE, 2017, pp. 1–3.

[257] Himanshu Mittal and Mukesh Saraswat, "Ckgsa based fuzzy clustering method for image segmentation of rgb-d images," in *2018 Eleventh International Conference on Contemporary Computing (IC3)*, IEEE, 2018, pp. 1–6.

[258] Raju Pal and Mukesh Saraswat, "Enhanced bag of features using alexnet and improved biogeography-based optimization for histopathological image analysis," in *2018 eleventh international conference on contemporary computing (IC3)*, IEEE, 2018, pp. 1–6.

[259] Kalyanmoy Deb, Amrit Pratap, Sameer Agarwal, and TAMT Meyarivan, "A fast and elitist multiobjective genetic algorithm: Nsga-ii," *IEEE transactions on evolutionary computation*, vol. 6, no. 2, pp. 182–197, 2002.

[260] Joshua Knowles and David Corne, "The pareto archived evolution strategy: A new baseline algorithm for pareto multiobjective optimisation," in *Proceedings of the 1999 congress on evolutionary computation-CEC99 (Cat. No. 99TH8406)*, IEEE, vol. 1, 1999, pp. 98–105.

[261] Eckart Zitzler and Lothar Thiele, "Multiobjective evolutionary algorithms: A comparative case study and the strength pareto approach," *IEEE transactions on Evolutionary Computation*, vol. 3, no. 4, pp. 257–271, 1999.

[262] Choosehappy, *Nuclei segmentation archives*, Aug. 2016. [Online]. Available: `http://www.andrewjanowczyk.com/tag/nuclei-segmentation/`.

[263] Mitko Veta, A Huisman, Max A Viergever, Paul J van Diest, and Josien PW Pluim, "Marker-controlled watershed segmentation of nuclei in h&e stained breast cancer biopsy images," in *2011 IEEE international symposium on biomedical imaging: from nano to macro*, IEEE, 2011, pp. 618–621.

[264] Mitko Veta, Josien PW Pluim, Paul J Van Diest, and Max A Viergever, "Breast cancer histopathology image analysis: A review," *IEEE transactions on biomedical engineering*, vol. 61, no. 5, pp. 1400–1411, 2014.

[265] Sertac Arisoy and Koray Kayabol, "Mixture-based superpixel segmentation and classification of sar images," *IEEE Geoscience and Remote Sensing Letters*, vol. 13, no. 11, pp. 1721–1725, 2016.

[266] Junliang Bao, Junjun Yin, and Jian Yang, "Superpixel-based segmentation for multitemporal polsar images," in *2017 Progress in Electromagnetics Research Symposium-Fall (PIERS-FALL)*, IEEE, 2017, pp. 654–658.

[267] Ankur Kulhari, Avinash Pandey, Raju Pal, and Himashu Mittal, "Unsupervised data classification using modified cuckoo search method," in *2016 Ninth International Conference on Contemporary Computing (IC3)*, IEEE, 2016, pp. 1–5.

[268] Faliu Yi, Junzhou Huang, Lin Yang, Yang Xie, and Guanghua Xiao, "Automatic extraction of cell nuclei from h&e-stained histopathological images," *Journal of Medical Imaging*, vol. 4, no. 2, pp. 027 502–027 502, 2017.

[269] Qingfu Zhang, Aimin Zhou, Shizheng Zhao, Ponnuthurai Nagaratnam Suganthan, Wudong Liu, Santosh Tiwari, et al., "Multiobjective optimization test instances for the cec 2009 special session and competition," *University of Essex, Colchester, UK and Nanyang technological University, Singapore, special session on performance assessment of multi-objective optimization algorithms, technical report*, vol. 264, pp. 1–30, 2008.

[270] David A Van Veldhuizen and Gary B Lamont, "Multiobjective evolutionary algorithm research: A history and analysis," Citeseer, Tech. Rep., 1998.

[271] Carlos M Fonseca, Joshua D Knowles, Lothar Thiele, Eckart Zitzler, et al., "A tutorial on the performance assessment of stochastic multiobjective optimizers," in *Third international conference on evolutionary multi-criterion optimization (EMO 2005)*, vol. 216, 2005, p. 240.

[272] Carlos A Coello Coello, Gregorio Toscano Pulido, and Maximino Salazar Lechuga, "Handling multiple objectives with particle swarm optimization," *IEEE Transactions on evolutionary computation*, vol. 8, no. 3, pp. 256–279, 2004.

[273] Eckart Zitzler, Marco Laumanns, and Lothar Thiele, "Spea2: Improving the strength pareto evolutionary algorithm," *TIK report*, vol. 103, 2001.

[274] Lee R Dice, "Measures of the amount of ecologic association between species," *Ecology*, vol. 26, no. 3, pp. 297–302, 1945.

[275] John Wilder Tukey et al., *Exploratory data analysis*. Springer, 1977, vol. 2.

[276] Qingfu Zhang and Hui Li, "Moea/d: A multiobjective evolutionary algorithm based on decomposition," *IEEE Transactions on evolutionary computation*, vol. 11, no. 6, pp. 712–731, 2007.

[277] Donald W Zimmerman and Bruno D Zumbo, "Relative power of the wilcoxon test, the friedman test, and repeated-measures anova on ranks," *The Journal of Experimental Education*, vol. 62, no. 1, pp. 75–86, 1993.

[278] Jianbo Xu, Guogen Shan, Amei Amei, Jiwei Zhao, Daniel Young, and Sheila Clark, "A modified friedman test for randomized complete block designs," *Communications in Statistics-Simulation and Computation*, vol. 46, no. 2, pp. 1508–1519, 2017.

[279] Jungsywan Hwang Sepanski, "A modification on the friedman test statistic," *Communications in Statistics—Simulation and Computation®*, vol. 36, no. 4, pp. 783–790, 2007.

[280] Vibha Gupta and Arnav Bhavsar, "Breast cancer histopathological image classification: Is magnification important?" In *Proceedings of the IEEE Conference on Computer Vision and Pattern Recognition Workshops*, 2017, pp. 17–24.

[281] David G Lowe, "Distinctive image features from scale-invariant keypoints," *International journal of computer vision*, vol. 60, no. 2, pp. 91–110, 2004.

[282] Navneet Dalal and Bill Triggs, "Histograms of oriented gradients for human detection," in *Proc. of International Conference on Computer Vision & Pattern Recognition, California, United States, pp. 886–893*, Ieee, vol. 1, 2005, pp. 886–893.

[283] Herbert Bay, Tinne Tuytelaars, and Luc Van Gool, "Surf: Speeded up robust features," in *European conference on computer vision*, Springer, 2006, pp. 404–417.

[284] Jonathan Masci, Ueli Meier, Dan Cireşan, and Jürgen Schmidhuber, "Stacked convolutional auto-encoders for hierarchical feature extraction," in *International conference on artificial neural networks*, Springer, 2011, pp. 52–59.

[285] Xujing Yao, Xinyue Wang, Shui-Hua Wang, and Yu-Dong Zhang, "A comprehensive survey on convolutional neural network in medical image analysis," *Multimedia Tools and Applications*, pp. 1–45, 2020.

[286] Md Zahangir Alom, Tarek M Taha, Christopher Yakopcic, Stefan Westberg, Paheding Sidike, Mst Shamima Nasrin, Brian C Van Esesn, Abdul A S Awwal, and Vijayan K Asari, "The history began from alexnet: A comprehensive survey on deep learning approaches," *arXiv preprint arXiv:1803.01164*, 2018.

[287] Avinash Chandra Pandey, Dharmveer Singh Rajpoot, and Mukesh Saraswat, "Feature selection method based on hybrid data transformation and binary binomial cuckoo search," *Journal of Ambient Intelligence and Humanized Computing*, vol. 11, no. 2, pp. 719–738, 2020.

[288] Avinash C Pandey and Dharmveer S Rajpoot, "Feature selection method based on grey wolf optimization and simulated annealing," *Recent Advances in Computer Science and Communications (Formerly: Recent Patents on Computer Science)*, vol. 14, no. 2, pp. 635–646, 2021.

[289] G. Litjens, T. Kooi, B. E. Bejnordi, A. A. A. Setio, F. Ciompi, M. Ghafoorian, and J. A. van der Laak, "A survey on deep learning in medical image analysis," *Medical Image Analysis*, vol. 42, pp. 60–88, 2017. DOI: 10.1016/j.media.2017.07.005.

[290] D. Komura and S. Ishikawa, "Machine learning methods for histopathological image analysis," *Computational and Structural Biotechnology Journal*, vol. 16, pp. 34–42, 2018. DOI: 10.1016/j.csbj.2018.01.001.

[291] S. Wang, D. M. Yang, R. Rong, X. Zhan, and G. Xiao, "Pathology image analysis using segmentation deep learning algorithms," *American Journal of Pathology*, vol. 190, no. 9, pp. 1680–1690, 2020. DOI: 10.1016/j.ajpath.2020.05.001.

[292] N. Zhang, Y. Cai, Y. Wang, and X. Zhao, "Feature selection based on genetic algorithm and support vector machine for histopathological image classification," *BioMed Research International*, vol. 2021, pp. 1–10, 2021. DOI: 10.1155/2021/5589813.

[293] S. Mirjalili, *Evolutionary Algorithms and Neural Networks*. Springer, 2019. DOI: 10.1007/978-3-319-93025-1.

[294] Ian H. Witten and Eibe Frank, *Data Mining: Practical Machine Learning Tools and Techniques with Java Implementations*. San Francisco, CA: Morgan Kaufmann, 2000.

[295] Evelyn Fix and Joseph L. Hodges, "Discriminatory analysis. nonparametric discrimination: Consistency properties," USAF School of Aviation Medicine, Tech. Rep. Technical Report 4, 1951.

[296] *Blue histology*, http://www.lab.anhb.uwa.edu.au/mb140/, [Online; accessed 19-July-2021], 2018.

[297] Korsuk Sirinukunwattana, Shan E Ahmed Raza, Yee-Wah Tsang, David RJ Snead, Ian A Cree, and Nasir M Rajpoot, "Locality sensitive deep learning for detection and classification of nuclei in routine colon cancer histology images," *IEEE transactions on medical imaging*, vol. 35, no. 5, pp. 1196–1206, 2016.

LIST OF PUBLICATIONS AND THEIR PROOFS

1. **Ravi Sharma**, Kapil Sharma, "An optimal nuclei segmentation method based on enhanced multi-objective GWO", Complex and Intelligent Systems 2021, https://doi.org/10.1007/s40747-021-00547-y **(IF: 5.0) Paper Published**) https://link.springer.com/article/10.1007/s40747-021-00547-y

Complex & Intelligent Systems (2022) 8:569–582
https://doi.org/10.1007/s40747-021-00547-y

ORIGINAL ARTICLE

An optimal nuclei segmentation method based on enhanced multi-objective GWO

Ravi Sharma[1] · Kapil Sharma[1]

Received: 10 March 2021 / Accepted: 27 July 2021 / Published online: 4 October 2021

Abstract
In breast cancer image analysis, reliable segmentation of the nuclei is still an open-ended research problem. In this paper, a new clustering-based nuclei segmentation method is presented. First, the proposed method pre-processes the histopathology image through SLIC method. Then, a novel variant of multi-objective grey wolf optimizer is employed to group the obtained super-pixels into optimal clusters. Lastly, the optimal cluster with minimum value is segmented as the nuclei region. The experimental results demonstrates that the proposed variant of multi-objective grey wolf algorithm surpasses the existing multi-objective algorithms over ten standard multi-objective benchmark functions belonging to different categories. Particularly, the proposed variant has achieved best fitness value of more than 0.90 on 90% of the considered functions. Further, the nuclei segmentation accuracy of the proposed method is validated on H&E-stained estrogen receptor positive (ER+) breast cancer images. Experimental results illustrates that the proposed method has attained dice-coefficient value of more than 0.52 on 80% of the images. This illustrates that the proposed method is efficient in producing efficacious segmenting over histology images of Breast cancer.

Keywords Breast cancer diagnosis · Nuclei segmentation · Multi-objective grey wolf optimizer

Introduction

Histological images are the golden standard in the breast cancer diagnosis and hematoxylin and eosin (H&E) staining of such images is the standard staining protocol [1]. In manual analysis of these images, there are a number of issues to be handled like, analysis variation due to difference in observer's experience, time-taking process, and difficult to identify subtle visual features [2]. However, the digitization of pathology systems have successfully mitigated such concerns [3]. In digital pathology, the segmentation of nuclei from the histopathological image is the foremost unit whose accuracy determines the efficiency of the system [4]. For the same, there are many nuclei segmentation methods defined over approaches like, super-pixels, clustering, active contours, watershed, and multi-level thresholding [5–7]. Among them, super-pixels is one of the efficient approaches for segmentation. Therefore, this paper introduces an efficient nuclei segmentation method based on super-pixels for histopathological images.

Super-pixels divide the image into non-overlapping regions wherein similar pixels are grouped together [8]. The boundary of each irregular-shaped super-pixel is according to the edge information in the original image. This makes each super-pixel perceptual meaningful [9,10]. Various computer-vision applications like, image segmentation [11], depth estimation [12], object localization [13], body model estimation [14], bag-of-features [15,16] and skeletonization [17], employ super-pixels to obtain mid-level representations. Fouad et al. [8] employed unsupervised learning on super-pixels to segment a cancer image into different tissues. In literature, it has been observed that unsupervised learning is quite advantages for histopathological image analysis as these methods are efficient in identifying anatomical structures in an image [8,18].

Generally, unsupervised learning methods work on the principle of clustering the unlabeled data into homogeneous clusters according to the considered criteria such as intra-cluster distance [19–21]. Some of the popular unsupervised learning methods are KMeans and Fuzzy C-Means [22,23]. However, there are a number of demerits in such

✉ Kapil Sharma
kapil@iece.org

[1] Delhi Technological University, Delhi, India

2. **Ravi Sharma**, Kapil Sharma, and Manju Bala "Analysis of Histopathological images: An Overview" in the 2022 International Conference on Computing, Communication, Security and Intelligent Systems (IC3SIS), 2022**. (Published and presented)**
https://ieeexplore.ieee.org/document/9885368

Analysis of Histopathological images: An Overview

Ravi Sharma
Dept. of computer science
Delhi Technological University
Delhi, India
ravisrma1988@gmail.com

Dr. Kapil Sharma
Dept. of Information Technology
Delhi Technological University
Delhi, India
Kapil@ieee.org

Dr. Manju Bala
Dxept. of humanities
Delhi University
Delhi, India
manjugpm@gmail.com

2022 International Conference on Computing, Communication, Security and Intelligent Systems (IC3SIS) | 978-1-6654-6883-1/22/$31.00 ©2022 IEEE | DOI: 10.1109/IC3SIS54991.2022.9885368

***Abstract*—Histopathology is the study of change in tissues and cells affected by the disease and finding the root cause of the disease. Over recent years there is huge improvement in image analysis algorithms as well as in the computation power. In this paper we will review various techniques given by different authors for histopathological image analysis.Also we will cover the various methods for image preprocessing, segmentation, feature extraction and classification which are basic steps of histopathological image analysis.**

***Index Terms*—histopathology, machine learning, extraction**

I. Introduction

Histopathology involves the study of tissue and cells by an individual radiologist. It takes a very long time to train a radiologist for medical imaging. It is a very challenging task for the pathologist to manually diagnose the sample tissue since the structure of cells is highly varied and complex. Further humans have limitation of speed, and they are prone to error. Any wrong analysis can cause harm to the patient. Thus to save the time and achieve the high accuracy automatic computer aided diagnose(CAD) is required.In histopathology tissue slides are created by collecting the sample from body and various staining procedures are applied to get the better visualization of tissue structure [1]. There is a recent advances in the field of histopathology to reduce the drawbacks of manual detection technology. Thus utilizing the machine learning algorithms and artificial intelligence for histopathological image analysis becomes a very active area of research [1]

Histopathology generally requires image gathering, preprocessing, image detection and segmentation, feature extraction and classification.So CAD must have these functionalities to perform the histopathology. Now there are various methods for all these functionality stated above.We will discuss all these basic functionalities in detail.Fig 1 shows the basic flowchart of different steps of histopathology.

II. Image Preprocessing

Image preprocessing is very important part of the histology. Generally image contains large amount of noise and unwanted artifacts which can lead to poor classification results. Further the brightness level and illumination may not be adequate in gathered images. Thus Images need to be preprocessed to enhance the image quality [2]. There are various methods for preprocessing the images.

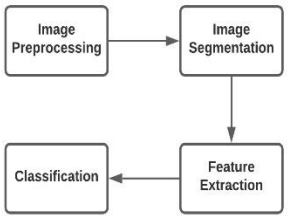

Fig. 1. Flowchart of histopathology.

A. Staining Normalization

To highlight important features and provide detailed view of the tissue Staining is used. Hematoxylin and Eosin dye is generally used for the staining procedure in which Hematoxylin gives blue stain where Eosin gives pinkish stain.There are other methods also available for staining.

B. Color Normalization

Color normalization is a major preprocessing method.Color normalizations's key aim is to reduce the variations between samples due to the various staining and scanning conditions also brightness of different samples are not generally uniform.There are number of color normalization techniques available such as Histogram specification approach, Reinhard approach, Macneko approach, Complete color normalization, Stain color descriptor Structure preserving color normalization [3].

C. Smoothing

Smoothing is a process to improve quality and reduce noise of the image. Smoothing is a spatial techniques which is used to produce a less pixelated image. Further smoothing can be categorized into two categories which are 1. Linear Filter: Linear filter uses input pixel and its neighbors as linear combination to produce output pixel. 2. Non-linear Filter: Design og non-linear filter is generally difficult. It cannot be achieved by convolution method since it requires special masking.

3. **Ravi Sharma**, Kapil Sharma, and Manju Bala "Generation of Histopathological Images Caption Using CNN and LSTM" in the International Conference on Computing, Communication, Security and Systems 2023**(Published and Presented)**
https://link.springer.com/chapter/10.1007/978-981-99-8398-8_1

Chapter 1
Generation of Histopathological Images Caption Using CNN and LSTM

Ravi Sharma, Kapil Sharma, and Manju Bala

1 Introduction

Every day, we are exposed to numerous images in the news, on social media, and all around us. Images can only be recognized by humans. Humans can recognize photographs without the descriptions that go with them, but robots need training images before they can generate captions for photographs automatically. Organizing AQ1 the captions for histopathological images in the data set and employing text-to-speech technology to enable the vision-impaired individual with real-time input on the scenario as seen on a camera feed are just a few of the many uses for image captioning. It may also improve social medical entertainment, helping children identify chemicals while also helping them learn the language. Every image on the internet should have a caption to allow for a more thorough and rapid exploration of real images. There are several applications for image captioning, including those in biomedicine, business, online search, the military, and many more. Social media platforms like Instagram, AQ2 Facebook, and others may automatically create captions from photographs.

Image caption generation is used in a variety of applications. caption generated from histopathological images can be used in the analysis of disease, feature extraction of histopathological images. Another application area is text prediction, It can be used to anticipate the words that will come after the phrases. A Chatbot, which is commonly used by e-commerce websites and mobile applications, serves as the greatest example of text prediction. Stock market prediction is another application,

R. Sharma (✉) · K. Sharma
Delhi Technological University, New Delhi, India
e-mail: ravisrma1988@gmail.com

K. Sharma
e-mail: kapil@ieee.org

M. Bala
Indraprastha College of Women, New Delhi, India

S. Mumtaz et al. (eds.), *Proceedings of the Second International Conference on Computing, Communication, Security and Intelligent Systems*, Algorithms for Intelligent Systems, https://doi.org/10.1007/978-981-99-8398-8_1

605199_1_En_1_Chapter ☑ TYPESET ☐ DISK ☐ LE ☑ CP Disp.:17/1/2024 Pages: xxx Layout: T1-Standard

4. **Ravi Sharma**, Kapil Sharma, Manju Bala "Efficient feature selection for histopathological image classification with improved multi-objective WOA" *Sci Rep* **14**, 25163 (2024). https://doi.org/10.1038/s41598-024-75842-y**. (IF:3.8) (Paper Published)**
https://www.nature.com/articles/s41598-024-75842-y

www.nature.com/scientificreports

scientific reports

OPEN

Efficient feature selection for histopathological image classification with improved multi-objective WOA

Ravi Sharma[1]✉, Kapil Sharma[1,3] & Manju Bala[2,3]

The difficulty of selecting features efficiently in histopathology image analysis remains unresolved. Furthermore, the majority of current approaches have approached feature selection as a single objective issue. This research presents an enhanced multi-objective whale optimisation algorithm-based feature selection technique as a solution. To mine optimal feature sets, the suggested technique makes use of a unique variation known as the enhanced multi-objective whale optimisation algorithm. To verify the optimisation capability, the suggested variation has been evaluated on 10 common multi-objective CEC2009 benchmark functions. Furthermore, by comparing five classifiers in terms of accuracy, mean number of selected features, and calculation time, the effectiveness of the suggested strategy is verified against three other feature-selection techniques already in use. The experimental findings show that, when compared to the other approaches under consideration, the suggested method performed better on the assessed parameters.

Keywords Image classification, Multi-objective grey wolf optimizer, Optimization algorithm, Pre processing

Abbreviations

CNN	Convolutional neural network
FS	Feature selection
HOG	Histogram oriented gradient
KNN	K-nearest neighbor
LDA	Latent dirichlet allocation
MOEA/D	Multi-objective evolutionary algorithm based on decomposition
MOGWO	Multi-objective gray wolf optimizer
MOPSO	Multi-objective particle swarm optimization
MOWOA	Multi-objective whale optimization algorithm
RF	Random forest
SIFT	Scale-invariant feature transform
SURF	Speed up robust features
SVM	Support vector machine

In disease diagnostic, pathologists perform microscopic examinations of histopathological samples to identify the sign of infection. During this analysis, primary focus is on tissue structure, cell count, and shape of the cell. Moreover, this manual examination demands expertise which makes it an expensive, one-sided, and tedious process[1]. Consequently, its automation is fundamental for quick and impartial finding[2]. To do this, histopathological images are captured through microscopic mounted cameras, which are further analyzed by computer-assisted histopathological image analysis methods. Figure 1 illustrates some sample images of different tissues, taken at 40x magnification level[3]. The intricate structure of histopathological images presents a challenging environment, even for classification tasks. Therefore, this paper presents a novel method for the efficient classification of histopathological images.

Further, the success of any classification-based method is predominantly dependent on the quality of features[4]. In literature, numerous methods are presented to efficiently extract the features, which are broadly classified as

[1]Delhi Technological University, Bawana, New Delhi 110042, India. [2]Indraprastha College of Women, University of Delhi, Civil Lines, New Delhi 110054, India. [3]These authors contributed equally: Kapil Sharma and Manju Bala. ✉email: ravisrma1988@gmail.com

DELHI TECHNOLOGICAL UNIVERSITY
(Formerly Delhi College of Engineering)
Shahbad Daulatpur, Main Bawana Road, Delhi-42

PLAGIARISM VERIFICATION

Title of the Thesis: **Design and Development of Efficient Methods for Histopathological Image Analysis**, Total Pages: **178**, Name of the Scholar: **Ravi Sharma**

Supervisor (s)

(1) **Dr. Kapil Sharma**

(2) **Dr. Manju Bala**

Department: **Computer Science and Engineering**

This is to report that the above thesis was scanned for similarity detection. Process and outcome are given below:

Software used: **Turnitin** Similarity Index: **9%**, Total Word Count: **48676**

Date: _____

Candidate's Signature **Signature of Supervisor(s)**

BRIEF PROFILE OF SCHOLAR

Mr. Ravi Sharma received his B. Tech degree in Information Technology from Guru Tegh Bahadur Institute of Technology, Delhi, in 2007, followed by an M. Tech in Software Engineering from Delhi Technological University (DTU) in 2013. He joined the Ph.D. program at DTU in 2017 with a focus on image processing. He has over 11 years of teaching experience and has worked at institutions including Amity University and Galgotias University. He is currently serving as a faculty member at Bennett University.

His research is primarily focused on designing and developing efficient methods for histopathological image analysis. During his doctoral studies, he has published 2 research papers in SCI-indexed journals and 2 papers in international conferences.